

University of Nevada, Reno

**Evaluation of the IDEAL-CT for Hveem-Designed Asphalt Mixtures in  
Nevada**

A thesis submitted in partial fulfillment of the  
requirements for the degree of Master of Science in  
Civil and Environmental Engineering

by

Buveenthiran Mahenthiran

Dr. Elie Y. Hajj / Thesis Advisor

August 2025



THE GRADUATE SCHOOL

We recommend that the thesis  
prepared under our supervision by

**Buveenthiran Mahenthiran**

entitled

**Evaluation of the IDEAL-CT for Hveem-Designed Asphalt  
Mixtures in Nevada**

be accepted in partial fulfillment of the  
requirements for the degree of

**MASTER OF SCIENCE**

Elie Y. Hajj, Ph.D.  
*Advisor*

Peter E. Sebaaly, Ph.D.  
*Committee Member*

Adam J.T. Hand, Ph.D.  
*Committee Member*

Anna K. Panorska, Ph.D.  
*Graduate School Representative*

Markus Kemmelmeier, Ph.D., Dean  
*Graduate School*

August, 2025

## Abstract

This study focuses on evaluating the applicability and effectiveness of the Indirect Tensile Asphalt Cracking Test (IDEAL-CT) for Hveem designed asphalt mixtures in the State of Nevada. While IDEAL-CT has traditionally been applied to Superpave Gyratory Compacted (SGC) specimens; this study investigates its use with Hveem-compacted specimens, highlighting adaptations for smaller diameters. The sensitivity of the CT Index to changes in mix design parameters, such as aggregate gradation and asphalt binder content, was evaluated, and results were compared between Hveem and SGC compaction methods.

Findings indicate that both specimen diameter and compaction method influence the IDEAL-CT test parameters, with differing effects on cracking performance. The study also explored the use of IDEAL-CT on Hveem-compacted specimens to determine the tensile strength for moisture damage evaluation in accordance with AASHTO T 283 (tensile strength ratio, TSR). In addition, the Moisture Induced Stress Tester (MiST) was examined as a potential alternative for the freeze-thaw cycle of moisture-conditioned specimens.

As an initial attempt to validate the CT Index for Nevada conditions, the LTPP SPS-10 project was used as a case study. Field core samples collected at different in-service periods within the first two years of pavement life, along with plant-produced asphalt mixtures, were tested for the CT Index. Field distress data for cracking were obtained from LTPP InfoPave and analyzed for potential correlations with the laboratory results. Limited cracking distress was observed during the early years following construction, which limited the comparison with core test results.

## Acknowledgments

To begin with, I would like to take this opportunity to express my deep gratitude and indebtedness to my graduate advisor, Dr. Elie Hajj, who has been very supportive, helpful, and a great mentor during my two years of academic life at the University of Nevada, Reno. His motivating power, trust, and belief in me have been very crucial in my educational and career growth. I appreciate his supervision as an excellent opportunity to work, and I am also grateful for the numerous opportunities that he gave me and made my learning process so effective.

My sincerest appreciation also goes out to Dr. Adam Hand and Dr. Peter Sebaaly due to their inestimable contributions to my academic development. Their courses provided me with the knowledge and the insight that became the basis of my understanding and research. Their suggestions, inspiration, and devotion towards student achievement have left a mark in my path. I want to express my sincere gratitude to both Sid and Dr. Ashraf Al Rajhi, who went above and beyond to assist me and share their knowledge. Their advice on different phases of this project, along with frequent and extensive consultations, significantly enhanced the quality of my work. Although their earlier study was incidental, it provided a stepping stone on which my study is based and added more dimensions to my research. I would also like to thank and appreciate the Nevada DOT for its guidance and support throughout the process.

Finally, I would like to thank my fellow graduate students, who have guided me through the hardship and helped me surpass the hurdles. I would also like to remember my family and friends who have supported me throughout my life and have faith in me.

## Table of Contents

Abstract.....	i
Acknowledgments.....	ii
Table of Contents.....	iii
List of Tables.....	vi
List of Figures.....	ix
Chapter 1: Introduction.....	1
1.1 Background.....	1
1.2 Research Objective.....	3
1.3 Scope of Work.....	4
Chapter 2: Literature Review.....	9
2.1 Previous Studies on Changing Diameter 150 mm to 100 mm on Cracking Performance.....	9
2.2 CT Index Correction Methods to Normalize Air Void Content and Thickness of Field Cores.....	12
2.3 CT index correlation with field performance.....	13
2.4 Implementation of IDEAL-CT by different State DOTs.....	15
2.5 Aging Effects on CT Index.....	17

Chapter 3: Selection of Materials and Characterization .....	19
3.1 NDOT Durability project Mix designs .....	19
3.2 Warm Mix Asphalt Cores and Plant Mix .....	21
Chapter 4: Experimental Plan .....	23
4.1 Compaction methods and other volumetrics.....	23
4.1.1 Hveem Compaction .....	23
4.1.2 Superpave Gyrotory Compaction (SGC) .....	24
4.1.2 Theoretical Maximum Specific Gravity ( $G_{mm}$ ).....	26
4.1.3 Asphalt Binder Extraction and Recovery.....	26
4.1.4 Sieve Analysis.....	28
4.1.5 Dynamic Shear Rheometer .....	29
4.2 Mechanical Tests of Asphalt Mixtures .....	31
4.2.1 IDEAL-CT .....	31
4.2.2 Tensile Strength Ratio.....	36
4.2.3 Moisture Induced Sensitivity Tester (MiST) .....	39
Chapter 5: Results and Analysis .....	41
5.1 Phase 1 Evaluation of the Impact of Specimen Size and Compaction Method.....	41
5.1.1 IDEAL-CT on Type 2/2C and Type 3 Gradation .....	41
5.2 Phase 2: Evaluation of Moisture Damage.....	52

5.2.1 Tensile Strength Ratio (TSR) (AASHTO T 283).....	52
5.2.2 MiST Test for the Hveem Compacted Specimens .....	53
5.2.3 Comparison of Tensile Strength Values.....	54
5.3 Phase 3: Preliminary Validation of the CT Index.....	58
5.3.1 IDEAL-CT Results for the Field Cores .....	58
5.3.2 Reheated Plant Mix Lab Compacted (RPLMC) for SPS-10 .....	61
5.3.3 Analysis of Field Distress data for SPS-10.....	62
5.3.4 Comparison of CT Index Results with Field Performance .....	65
Chapter 6: Conclusions, Findings, and Recommendations .....	71
6.1 Conclusion .....	71
6.2 Findings.....	73
6.3 Recommendation .....	74
References.....	75
Appendix.....	83

## List of Tables

Table 1: Summary of parameter changes with diameters .....	11
Table 2: NDOT Aggregate Gradation Specifications .....	20
Table 3: Volumetric Property Summary .....	20
Table 4: LTPP SPS-10 Test Section details.....	22
Table 5: Type 2/2C mixture Significance difference in population mean.....	51
Table 6: Type 3 mixture Significance difference in population mean.....	51
Table 7: Type 2/2C mixture Significance difference in population mean of tensile strength .....	56
Table 8: Type 3 mixture Significance difference in population mean of tensile strength	56
Table 9: Gmm values for Field cores and Field mixture .....	61
Table A- 1: Gradation for Gradation 1 .....	83
Table A- 2: Gradation of Gradation 04.....	84
Table A- 3: Superpave Gyratory 100 mm diameter and 63.5 mm height CT Index .....	85
Table A- 4: Superpave Gyratory 100 mm diameter and 63.5 mm height m value.....	86
Table A- 5: Superpave Gyratory 100 mm diameter and 63.5 mm height l value.....	87
Table A- 6: Superpave Gyratory 100 mm diameter and 63.5 mm height l/m value.....	88
Table A- 7: Superpave Gyratory 100 mm diameter and 63.5 mm height Peak Load.....	89

Table A- 8: Superpave Gyratory 100 mm diameter and 63.5 mm height Fracture Energy .....	90
Table A- 9: Superpave Gyratory 100 mm diameter and 63.5 mm height Tensile Strength .....	91
Table A- 10: Superpave Gyratory 150 mm diameter and 63.5 mm height CT Index .....	92
Table A- 11: Superpave Gyratory 150 mm diameter and 63.5 mm height m Value .....	93
Table A- 12: Superpave Gyratory 150 mm diameter and 63.5 mm height l Value .....	93
Table A- 13: Superpave Gyratory 150 mm diameter and 63.5 mm height l/m Value.....	94
Table A- 14: Superpave Gyratory 150 mm diameter and 63.5 mm height Peak Load.....	94
Table A- 15: Superpave Gyratory 150 mm diameter and 63.5 mm height Fracture Energy .....	95
Table A- 16: Superpave Gyratory 150 mm diameter and 63.5 mm height Tensile Strength .....	95
Table A- 17: Hveem Compacted 101.6 mm diameter and 63.5 mm height CT Index .....	96
Table A- 18: Hveem Compacted 101.6 mm diameter and 63.5 mm height m Value .....	97
Table A- 19: Hveem Compacted 101.6 mm diameter and 63.5 mm height l Value .....	97
Table A- 20: Hveem Compacted 101.6 mm diameter and 63.5 mm height l/m Value ....	98
Table A- 21: Hveem Compacted 101.6 mm diameter and 63.5 mm height Peak Load ...	98
Table A- 22: Hveem Compacted 101.6 mm diameter and 63.5 mm height Fracture Energy .....	99

Table A- 23: Hveem Compacted 101.6 mm diameter and 63.5 mm height Tensile Strength .....	100
Table A- 24: Type 2 mix summary results .....	101
Table A- 25: Type 3 mix summary results .....	102

## List of Figures

Figure 1: Phase 1 of the Project .....	6
Figure 2: Phase 2 of the project .....	7
Figure 3: Phase 3 of the project .....	8
Figure 4: California Kneading Compactor .....	24
Figure 5: Superpave Gyrotory Compactor .....	25
Figure 6: Compaction molds for 150 mm and 100 mm.....	25
Figure 7: Centrifugal extractor.....	28
Figure 8: Rotatory Evaporator .....	28
Figure 9: Mechanical Washing Apparatus.....	29
Figure 10: Dynamic Shear Rheometer.....	30
Figure 11: Loading strip modification .....	32
Figure 12: Picture of modified loading strip.....	32
Figure 13: IDEAL-CT machine .....	33
Figure 14: Load versus Displacement plot of IDEAL-CT.....	34
Figure 15: Load versus displacement plot .....	35
Figure 16: Displacement versus Time plot .....	36
Figure 17: Vacuum apparatus for T283 .....	38
Figure 18: MiST Machine.....	40

Figure 19: CT-Index values for the Type 2/2C and Type 3 mixes .....	42
Figure 20: $m_{75}$ values for the Type 2/2C and Type 3 mixtures .....	44
Figure 21: $l_{75}$ values for the Type 2/2C and Type 3 .....	45
Figure 22: $l_{75}/m_{75}$ values for the Type 2/2C and Type 3 mixtures.....	46
Figure 23: Peak Load values for the Type 2/2C and Type 3 mixture.....	47
Figure 24: Fracture Energy for the Type 2/2C and Type 3 mixture .....	48
Figure 25: Tensile Strength for the Type 2/2C and Type 3 mixtures .....	49
Figure 26: Air void percent for the Type 2/2C and Type 3 mixtures .....	50
Figure 27: TSR for Hveem compacted specimens .....	52
Figure 28: Tensile strength values of Type 2 and Type 3 mixtures.....	53
Figure 29: MiST tensile strength values of Type 2 and Type 3 mixtures.....	54
Figure 30: Comparison of tensile strength values of Type 2 and Type 3 mixtures Error bars represent the mean plus or minus the 95% confidence interval.....	55
Figure 31: Comparison of TSR.....	57
Figure 32: CT Index values Field Cores from SPS-10 .....	59
Figure 33: Air void values field cores from SPS-10.....	60
Figure 34: RPMLC CT Index for SGC and Hveem-compacted specimens .....	62
Figure 35: Longitudinal Crack NWP combination.....	63
Figure 36: Wheel path length cracks during service life .....	64

Figure 37: Alligator cracking during the service life.....	65
Figure 38: Comparison of RPMLC HV with 7% AV CT Index and NWP longitudinal crack throughout the service years .....	66
Figure 39: Comparison of RPMLC HV with In-Place AV CT Index and NWP longitudinal crack throughout service years.....	67
Figure 40: Comparison of RPMLC HV with 7% AV CT Index and Wheel path crack length throughout service years. ....	68
Figure 41: Comparison of RPMLC HV with In-place AV CT Index and Wheel path crack length throughout service years .....	68
Figure 42: Comparison of RPMLC HV with 7% AV CT Index and Alligator crack throughout service years .....	69
Figure 43: Comparison of RPMLC HV with In-Place AV CT Index and Alligator crack throughout service years .....	70
Figure A- 1: Comparison of RPMLC SP with 7% AV CT Index and NWP longitudinal crack through the service year. ....	103
Figure A- 2: Comparison of RPMLC SP with In-Place AV CT Index and NWP longitudinal crack through the service year .....	103
Figure A- 3: Comparison of PMFC 12-month field core CT Index and NWP longitudinal crack through the service year .....	104
Figure A- 4: Comparison of PMFC 23-month field core CT Index and NWP longitudinal crack through the service year .....	104

Figure A- 5: Comparison of RPMLC SP with 7% AV CT Index and Wheel path crack length throughout service years. .... 105

Figure A- 6: Comparison of RPMLC SP with In-Place AV CT Index and Wheel path crack length throughout service years. .... 105

Figure A- 7: Comparison of PMFC 12-month field core CT Index and Wheel path crack length throughout the service year ..... 106

Figure A- 8: Comparison of PMFC 23-month field core CT Index and Wheel path crack length throughout the service year ..... 106

Figure A- 9: Comparison of RPMLC SP with 7% AV CT Index and Alligator crack throughout service years. .... 107

Figure A- 10: Comparison of RPMLC SP with In-Place AV CT Index and Alligator crack throughout service years. .... 107

Figure A- 11: Comparison of PMFC 12-month field core CT Index and Alligator crack throughout the service year ..... 108

Figure A- 12: Comparison of PMFC 23-month field core CT Index and Alligator crack throughout the service year ..... 108

## **Chapter 1: Introduction**

### **1.1 Background**

By the late 1950s, the Marshall [1] and Hveem [2] methods had become the standard asphalt mix design procedures in the United States [3]. The Hveem method, which uses the California Kneading Compactor, emphasizes mixture stability and resistance to deformation, with the Hveem Stabilometer measuring stability under specific loading conditions. These methods remained dominant for decades, with most States adopting one or the other as their primary mix design approach.

In the early 1990s, the Strategic Highway Research Program (SHRP) introduced the Superpave (Superior Performing Asphalt Pavements) mix design system (REF). This volumetric mix design method incorporated the Superpave Gyrotory Compactor (SGC) to better simulate field compaction and emphasized achieving target volumetric properties [4]. Since its introduction, Superpave has been adopted by the majority of State Departments of Transportation (DOTs) in the United States [5], with 150 mm SGC-compacted specimens commonly used for performance testing.

In recent years, performance testing within the framework of Balanced Mix Design (BMD) has gained prominence as a means to produce asphalt mixtures that balance rutting resistance, cracking resistance, and durability [6]. One of the most widely used cracking tests in BMD is the Indirect Tensile Asphalt Cracking Test (IDEAL-CT) [7], which is standardized for use with 150 mm SGC-compacted specimens [8].

The Nevada Department of Transportation (NDOT) has long relied on the Hveem method and is satisfied with its ability to ensure rutting resistance through stability measurements. However, as NDOT explores the implementation of BMD at the mix design stage, the agency is seeking a reliable method to evaluate cracking resistance. The IDEAL-CT is of particular interest but adapting it to NDOT's practice poses a challenge: Hveem compaction produces 101.6 mm diameter specimens, while IDEAL-CT is based on 150 mm specimens compacted with the SGC.

This size difference is significant because specimen diameter can influence aggregate orientation, volumetric properties, and mixture behavior [9]. NDOT already uses 101.6 mm Hveem-compacted specimens for moisture damage evaluation under test method Nev T341D, *Method of Test for Resistance of Compacted Bituminous Mixture to Moisture-Induced Damage (Lottman)* [10], instead of AASHTO T 283 [45]. This raises the question of whether the IDEAL-CT can be adapted for use with the same smaller specimens, allowing NDOT to evaluate both cracking resistance and moisture susceptibility from Hveem-compacted specimens at the mix design stage.

If adopted, the smaller diameter specimens could reduce material requirements by approximately 56 percent, lowering preparation time and cost [11]. However, adjustments to test fixtures and loading protocols may be needed to account for the higher stress intensities in smaller samples, which can alter crack initiation points and fracture patterns.

## 1.2 Research Objective

The primary objective of this research is to evaluate the applicability of the IDEAL-CT [7] for 101.6 mm Hveem-compacted specimens, in comparison with the standard 150 mm Superpave (SGC) specimens, within the framework of the Nevada Department of Transportation's (NDOT) mix design practices. NDOT is satisfied with the rutting resistance provided by the Hveem stability method but seeks to incorporate a reliable cracking resistance test at the mix design stage as part of a BMD approach.

This study investigates whether Hveem-compacted specimens can provide IDEAL-CT results that are sensitive to mixture variations, such as changes in asphalt binder content, aggregate gradation, and other parameters within acceptable tolerances; and whether these results can distinguish between asphalt mixtures with different cracking performance levels. The effects of specimen diameter and compaction method on IDEAL-CT values are evaluated, with SGC-compacted specimens of comparable diameter (100 mm) prepared and tested for direct comparison. Adapting IDEAL-CT to Hveem specimens requires addressing challenges related to specimen thickness, height, and loading strip curvature; therefore, a dedicated fixture was designed and fabricated to ensure consistent testing of reduced-diameter specimens.

As an initial attempt to validate the CT Index under Nevada conditions, the LTPP SPS-10 Warm Mix Asphalt test sections was used as a case study. Field core samples collected at different in-service periods within the first two years of pavement life, along with plant-produced asphalt mixtures, were tested for the CT Index. Comparisons of plant-mixed laboratory-compacted (PMLC), and plant-mixed field-compacted (PMFC) specimens were

conducted. Field cracking distress data from LTPP InfoPave were analyzed for potential correlations with the laboratory results to establish links between IDEAL-CT performance metrics and observed field behavior.

### **1.3 Scope of Work**

This study compares SGC- and Hveem-compacted specimens to evaluate the applicability of the IDEAL-CT within NDOT's mix design process. Specimens with varying aggregate gradations were prepared to assess the sensitivity of IDEAL-CT results to mixture variations. The work also identifies potential challenges and procedural adjustments required to adapt the test for smaller-diameter specimens.

SGC-compacted specimens were produced at diameters of 150 mm and 100 mm, each with a height of 63.5 mm. Hveem-compacted specimens were prepared at 101.6 mm and 63.5 mm height, consistent with NDOT's current mix design and moisture damage testing practices. The research approaches for Phases 1 and 2 of the study are illustrated in Figures 1 and 2.

Phase 3 incorporates the SPS-10 Warm Mix Asphalt (WMA) test sections, part of the Long-Term Pavement Performance (LTPP) program [12]. Constructed in 2016 on Interstate 580 (Carson City Freeway), the SPS-10 project investigates the effects of field aging on intermediate-temperature cracking performance. As part of this phase, field cores sampled at different in-service periods within the first two years, along with plant-produced mixtures, were tested for IDEAL-CT and related properties. Cracking distress data from LTPP InfoPave [12] were analyzed to explore correlations between laboratory-measured CT Index values and early field performance.

The scope includes:

- Comparing IDEAL-CT results among 150 mm, 100 mm, and 101.6 mm specimens to evaluate the effects of specimen size and compaction method.
- Developing and implementing adaptations for testing smaller-diameter specimens.
- Using the SPS-10 project as a preliminary field reference to assess the potential of IDEAL-CT for Hveem-compacted specimens.

Figures 1 to 3 illustrate the sequence and scope of Phases 1 to 3.

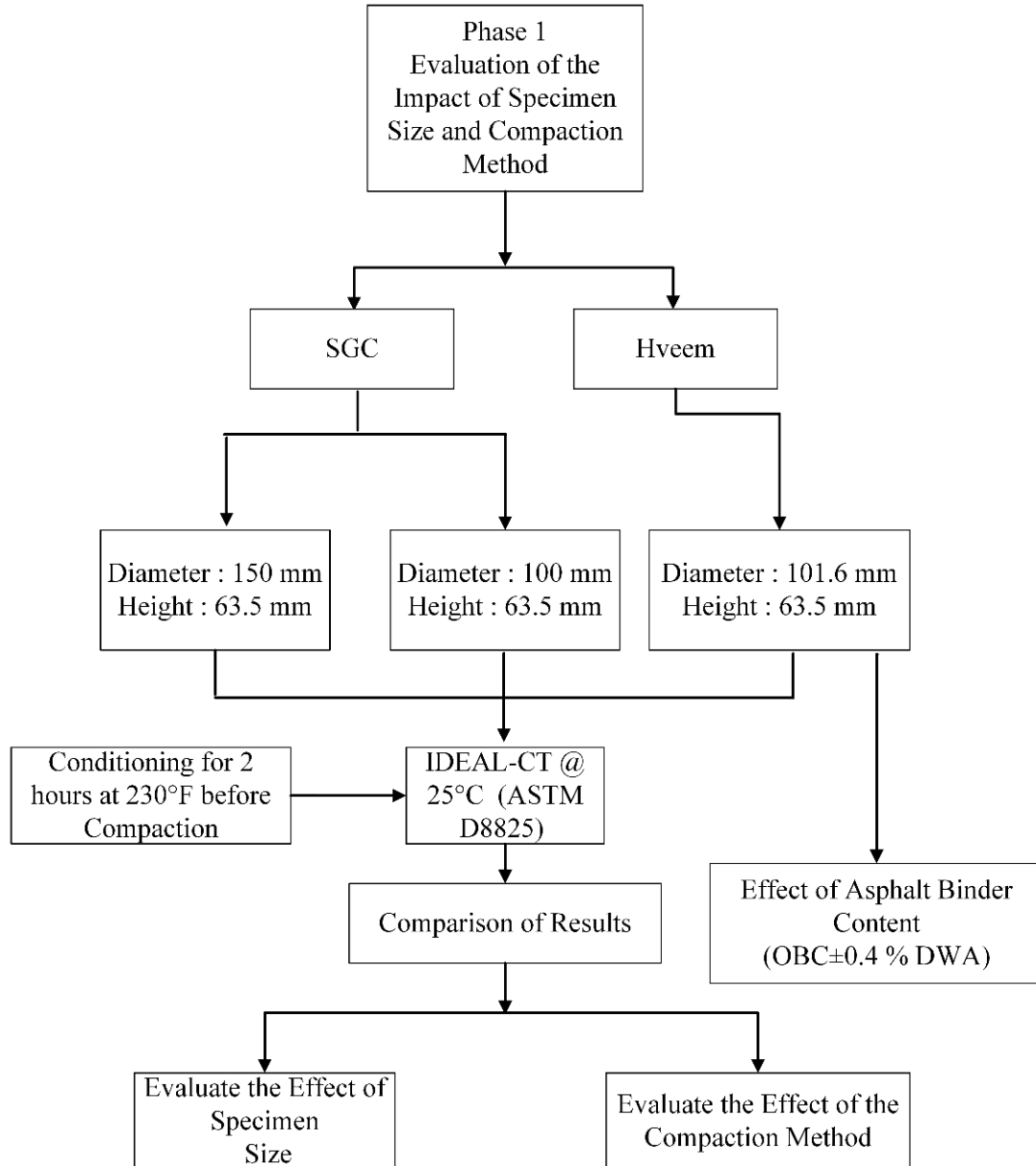


**Figure 1: Phase 1 of the Project**

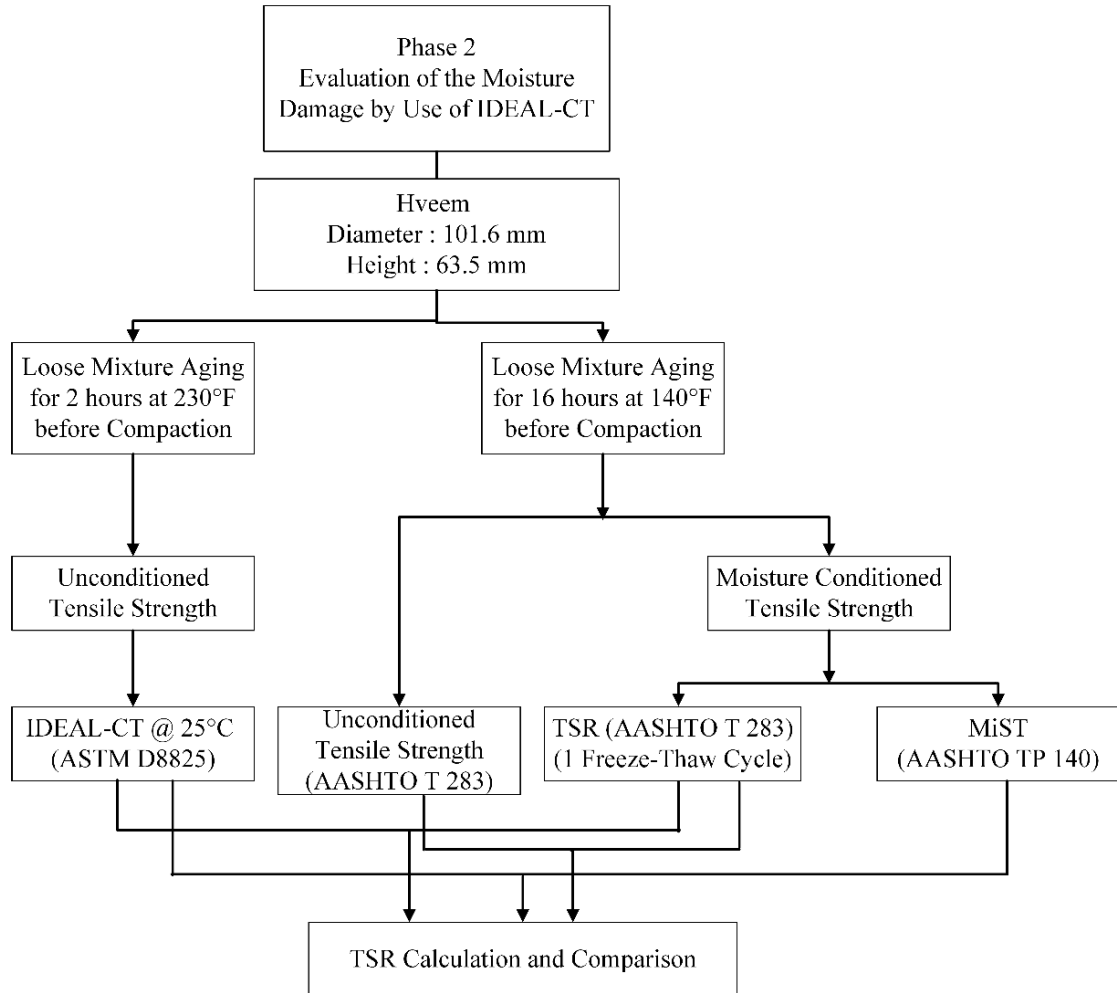


**Figure 2: Phase 2 of the project**

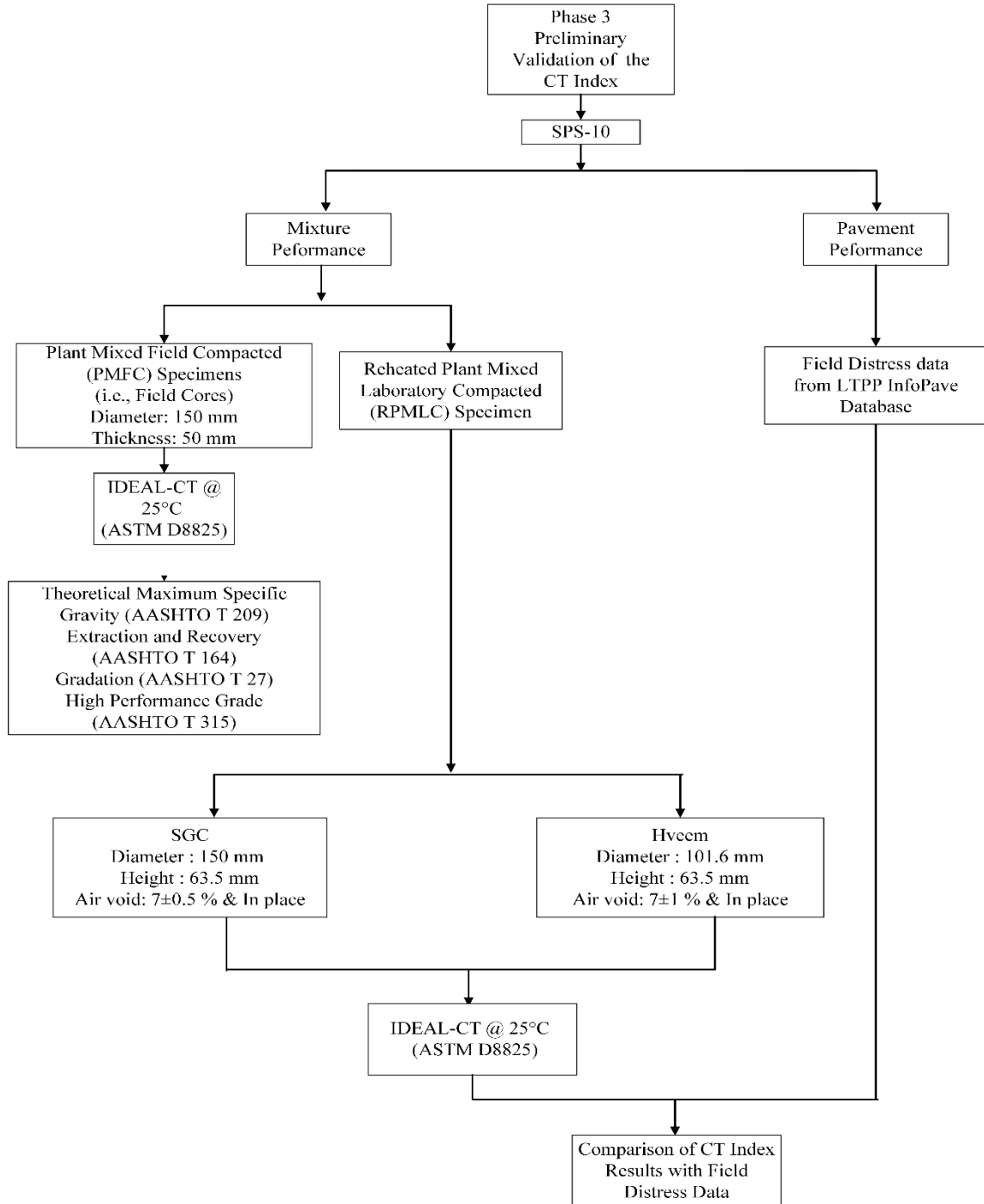


**Figure 3: Phase 3 of the project**

## **Chapter 2: Literature Review**

To improve the performance and durability of asphalt pavements, researchers have analyzed various mix design methods to achieve the target. Two of the popular methods are Superpave and Hveem. The Superpave method is more popular because it considers climate and traffic, while the Hveem method is known for its simplicity and historical use. Recently, asphalt industry researchers have been evaluating IDEAL-CT as part of BMD, which is essential because it is relatively simple and cost-effective, providing an easy measure of how asphalt mixture cracking affects pavement longevity [13]. This literature review primarily describes previous research comparing Hveem and Superpave, with a closer evaluation of IDEAL-CT performance. The diameter of the samples is 150 mm, 100 mm for SGC samples, which showed a correlation between their CT Index values. Aging of the mixture directly reduces the CT Index.

### **2.1 Previous Studies on Changing Diameter 150 mm to 100 mm on Cracking Performance**

A study conducted by Gavadakatla V. et al. provides a more in-depth review of the cracking performance of asphalt mixtures for 150 mm and 100 mm diameter samples [14]. Their main objectives were to compare IDEAL-CT (ASTM D8225-2019) [7], Indirect Tensile Strength (ITS) (ASTM D6931-2017) [15], and Indirect Tensile Asphalt Layer - Rutting Test (IDEAL-RT) (ASTM D8360-2022) [16] to the effect of diameter change for different asphalt mixtures. The study aimed to establish a threshold criterion for 100 mm samples compacted in accordance with the Marshall Mix Design method [1].

This research consists of nine dense-graded asphalt mixtures with Nominal maximum aggregate sizes (NMAS) of 25 mm, 19 mm, and 12.5 mm. Asphalt binders used for these mixtures were unmodified viscosity grade binder (VG), Crumb rubber modified binder (CRMB), Polymer modified binder (PMB), and reclaimed asphalt pavement (RAP) of 25% and 15%. They have prepared four replicate samples for each test.

The main parameters considered while calculating the CT Index are shown here

$$CT_{Index} = \frac{t}{62} \times \frac{l_{75}}{D} \times \frac{G_f}{|m_{75}|} \times 10^6 \quad \text{Equation 1}$$

*CT*- Cracking Tolerance

*l*<sub>75</sub> - displacement at 75 % the peak load after the peak (mm)

*G*<sub>*f*</sub> – Fracture Energy (Joules/m<sup>2</sup>)

|*m*<sub>75</sub>| - absolute value of the post-peak slope *m*<sub>75</sub> (N/m)

*D* – specimen diameter (mm)

*t* - specimen thickness (mm)

The results showed a correlation between the 150 mm and 100 mm, with the relationship expressed as  $CT_{100\text{ mm}} = 0.55 \times CT_{150\text{ mm}}$ . For example, a minimum CT index value of 90 for a 150 mm specimen is equivalent to a threshold value of 50 for the 100 mm sample. For different asphalt mixtures, the IDEAL-CT test parameters change with specimen diameter as shown in Table 1. Tick marks in the table depict which values increase with the specified diameter. A tick under both diameters indicates the values are closer and equal. Those tick mark differences are not based on the statistical analysis.

**Table 1: Summary of parameter changes with diameters**

Mixture	ITS		CT		L <sub>75</sub> /D		G <sub>f</sub>		m <sub>75</sub>	
	150	100	150	100	150	100	150	100	150	100
PMB, 13.2 mm,		✓	✓			✓	✓			✓
PMB, 13.2 mm, Rap 25%		✓	✓		✓	✓	✓			✓
CRMB, 13.2 mm,		✓	✓			✓	✓			✓
CRMB, 13.2 mm, Rap 15%		✓	✓			✓	✓			✓
PMB, 19.0 mm,		✓	✓			✓	✓			✓
CRMB, 19 mm,		✓	✓			✓		✓		✓
CRMB, 19 mm,		✓	✓		✓	✓		✓		✓
VG-40, 26.5mm		✓	✓			✓	✓			✓
VG-40, 26.5mm		✓	✓			✓	✓			✓

Results show that 100 mm samples show higher tensile strength than 150 mm samples. The CT Index value for the 100 mm samples is lower than the acceptance threshold. There was high repeatability of both diameter samples, with the coefficient of variation of the 150 mm diameter sample ranging from 8.3 to 25.8, and the 100 mm diameter sample ranging from 7.2 to 28.2.

A study conducted by Brown and Bassett described how the maximum aggregate size affects IDT results for samples with diameters of 101.6 mm and 150 mm [17]. Specimen preparation was conducted using a Gyrotory Testing Machine (GTM), which is calibrated to match 75 blows in Marshall compaction. A standard 101.6 mm diameter is used, and it

was proposed to use a 127 mm mold to accommodate mixtures with higher maximum size aggregates, thereby reducing variability.

Both diameter specimens were compacted to the same air voids and tested using the same loading rate of 50 mm/minute. Larger specimens deform slowly under the constant load rate, reducing the effective strain rate by 50 percent. This led to a reduction in ITS compared to the 101.6 mm specimen.

A key benefit found for the 150 mm mold specimen is reduced variability when compared to the 100 mm specimen for an aggregate size of 38 mm. Smaller specimens are affected by stress concentration and edge effect when larger aggregates are used. A study by Kandhal and Brown (1990) also explained the reduction in strain rate from 150 mm to 101.6 mm and a 50 percent decrease in variability for large aggregate mixtures [18].

## **2.2 CT Index Correction Methods to Normalize Air Void Content and Thickness of Field Cores**

Montañez (2023) [19] conducted a study to address the inconsistencies between field cores and reheated plant-mixed laboratory-compacted (RPMLC) specimens, particularly due to variations in thickness and air void content. The study aimed to develop correction factors for these variables by establishing trendline equations and quantifying the sensitivity of the CT Index to changes in thickness and air voids. Plant mixtures were sampled from three different field projects for the analysis.

Mixture A was compacted to a diameter of  $150 \pm 2$  mm and a thickness of  $62 \pm 1$  mm, with an air void content ranging from 3 to 10 percent, to evaluate the sensitivity of the CT Index to air void content. Mixture B was prepared with an air void content of  $7 \pm 1$  percent and

compacted to three different thicknesses: 35 mm, 51 mm, and 62 mm. To verify the correction factor, Mixture C was compacted to a diameter of  $150 \pm 2$  mm, with thicknesses ranging from 35 mm to 62 mm and an air void content between 5 and 8 percent.

For field core verification, data were obtained from seven projects in Texas involving 22 asphalt mixtures. In 19 out of the 22 cases, the corrected CT Index values for field cores were higher than the corresponding laboratory values. These findings suggest that the existing CT Index threshold for laboratory compacted specimens may need to be adjusted for field cores.

### **2.3 CT index correlation with field performance**

A study by Zhou et al. (2019) [20] on the development and validation of the IDEAL-CT test explored the correlation between the CT-Index and field performance. The IDEAL-CT test has consistently demonstrated a strong relationship with asphalt mixture performance across various test sections in different states and environmental conditions. Field validation studies were conducted at several sites, including the Federal Highway Administration (FHWA) Accelerated Loading Facility (ALF), Texas State Highways, and the MnRoad facility in Minnesota. These studies confirmed that asphalt mixtures with higher CT Index values exhibited improved durability and cracking resistance over their service lives.

In the FHWA ALF study, CT Index values indicated when fatigue cracking would occur, reflecting the number of loads passed before fatigue cracking initiated. Virgin asphalt mixtures with a high CT Index value of 137.2 were resistant to cracking after 368,000 load

passes; however, the highly recycled content mixtures, with respective low CT Index values (37.5 to 45.2), cracked after 36,000-42,000 load passes.

In State Highway 15 (SH 15) in Texas, side-by-side sections of pavement that varied only in binder content resulted in a higher CT Index for the section with higher binder content, with no cracking observed after two years. The lower binder content section exhibited moderate fatigue cracking. These findings suggest that even small changes in mix design, such as adjusting the CT Index, can have a prominent effect on field performance.

The CT Index predicted the reflective cracking in the overlay application. In the US 62 section in Texas, where a virgin surface mixture with a higher CT Index exhibits very low reflective cracking, a blend with 5 percent RAP (Reclaimed Asphalt Pavement) and 5 percent RAS (Reclaimed Asphalt Shingles), with a much lower CT Index, developed extensive transverse cracking.

The MnRoad project in Minnesota had three test sections with nearly the same structure but used different grade binders and types of RAPs. The section performed best in terms of thermal cracking, with the highest CT Index (235.1), and the worst performed the worst, with the lowest CT Index (128.1).

The CT Index is sensitive to substantial mixture properties, such as binder content, binder type, air voids, and recycled material content. It is beneficial for performance engineering, mix design, and correlation.

The study conducted by Golalipour et al. (2021) [21] explains how the IDEAL-CT test is used to predict the pavement performance of asphalt mixtures, using mixtures collected from the FHWA ALF, and found that the CT Index correlates well with observed field

cracking data. Test results helped differentiate mixtures with recycled content and binder type, enabling the statistical separation of four out of five sections. The study also reported that IDEAL-CT produced consistently reproducible results compared to other cracking tests, with a Coefficient of Variation (COV) of approximately 18.

#### **2.4 Implementation of IDEAL-CT by different State DOTs**

In the research study conducted by Boz et al. (2021) [22], results were evaluated in terms of accuracy, precision, and bias of the CT Index, Fracture Strain Tolerance (FST) Index, and the IDT strength from the IDT cracking test at intermediate temperature (25°C). This study supports the Virginia Department of Transportation's (VDOT) project to utilize BMD for performance-based quality control and assurance. A threshold value of 70 for the CT Index is used to screen their dense-graded mixtures. For the dense-graded mixtures, the threshold value of 70 is used.

Several studies have contributed to understanding the CT Index; some of the key limitations were equipment type, loading rate, and a limited formal precision estimate. This study was conducted through an interlaboratory survey involving 41 individual laboratories, assessing the repeatability and reproducibility of CT, FST, and IDT strength indices. This study confirmed that removing extreme data points will lead to greater consistency. Out of 41 labs, only 14 labs achieved total compliance with the standard; most labs struggled to meet the loading rate. Statistically checking all the labs with loading rate deviation did not significantly affect CT, FST, or IDT.

In the National Center for Asphalt Technology (NCAT) two-phased round-robin test, when specimens were prepared centrally among laboratories, variability was reduced from 35.3

to 20.2 percent. Rutgers University also assessed nine laboratories for the CT Index and got similar data. Zhou et al. (2017) [23] also confirmed that the CT index correlated with material properties and field cracking performance.

Study by Zhou et al. (2021) [24] about the IDEAL-CT test for asphalt mix design and quality control/quality assurance (QA/QC), which helps to optimize the asphalt mixture performance related to cracking. This goal is supported by six state DOTs in adopting the IDEAL-CT as a part of the BMD method. IDEAL-CT is used to evaluate cracking resistance, while IDEAL-RT (IDEAL Rutting test) is used to evaluate rutting resistance. The IDEAL-CT test method consists of short- and mid-term aging protocols to simulate field performance and establish thresholds, including a CT Index of  $\geq 90$  for dense-graded mixture and a CT Index of  $\geq 135$  for Stone Mastic Asphalt (SMA) following short-term aging. For the midterm, the aging CT Index is  $\geq 40$ .

In Northern Utah, a study conducted by BMD evaluated the repeatability of IDEAL-CT [25]. Three mixtures were assessed in three separate laboratories. The results indicate good repeatability, both within a single laboratory (15 percent variation) and between laboratories (20 percent variation). In specific mixtures, variability was higher than in others. Compacting samples with more than the prescribed gyration will result in greater variability. When the sample height increases, variability decreases. Specific mixtures exhibit a higher CT Index, characterized by higher air voids. The guide stated that four samples per mix should be tested, and if one result is abnormal, it should be discarded. The remaining three results must be 15 percent of each other's results; otherwise, the test is repeated.

## 2.5 Aging Effects on CT Index

In a study conducted by Leavitt et al. (2024) [26], it was found that the Asphalt Flexibility Ratio ( $AFR = I_{75}/m_{75}$ ) is more sensitive to aging than the CT Index, providing a better understanding of the brittleness of the asphalt mixture. Field aging was measured using cumulative degree days (CDD), which reflect climatic conditions. A strong correlation is found between CDD and decreasing AFR. The predictive model was constructed to estimate AFR from CDD, yielding a good fit ( $R^2 = 0.91$ ). Cracking initiates when AFR decreases to 0.48, and the worst is below 0.30. For a four-year delay in cracking, the initial AFR should be between 1.2 and 1.62, and the CT Index range is 72 to 97.

Different mixtures and test results were analyzed by NCAT [27], which includes IDEAL-CT test results from over 100 mixtures from 10 sources in the United States, focusing on Laboratory mixed Laboratory compacted (LMLC) and Plant Mixed Laboratory Compacted (PMLC) specimens. This study compared the results under various short-term oven aging (STOA) conditions: 2 hours at 275°F, 4 hours at 275°F, and 4 hours at compaction temperature. The results indicate that LMLC specimens with 4-hour STOA aging best match those of plant-produced mixtures, whether compacted hot or after reheating.

In the next part of the analysis, the CT Index change ( $\Delta$ CT Index) was related to the change in mixture components and aging binder properties. There was no noticeable correlation between the  $\Delta$ CT Index and changes in binder content ( $\Delta$ Pb) or aggregate gradation. A distinct negative correlation was found between the  $\Delta$ CT Index and the change in High Temperature Performance Grade ( $\Delta$ HPPG). The outcome finalizes aging differences; binder

hardening and oxidation during production and reheating are the main factors that cause variability.

The National Cooperative Highway Research Program (NCHRP) study by Zhou et al. (2023) [28] demonstrate the impact of aging conditions on the CT Index. The laboratory simulation, conducted through STOA and more intense critical aging (CA), was found to cause a greater reduction in the CT Index. In NCAT Test Track studies, the CT index reduces from 30.2 (LMLC-STOA) to 7.3 (LMCL-CA). Four specimen preparations are performed according to the LMLC-STOA, LMLC-CA, PMLC-RH, and PMLC-CA protocols. In all these instances, it yields the lowest CT Index, reflecting long-term pavement aging conditions. This study also includes mixtures with higher percentages of RAP and RAS. Mixtures with 5 percent RAS experienced a steep decline in CT Index. Air void content affects the CT Index; a 7 percent air void is targeted for comparison and standardization.

## **Chapter 3: Selection of Materials and Characterization**

### **3.1 NDOT Durability project Mix designs**

For this study, two aggregate gradations were selected from the NDOT Durability project [29] for comparison in the IDEAL-CT using three specimen sizes: 150 mm SGC, 100 mm SGC, and 101.6 mm Hveem-compacted specimens. The aggregates were sampled from the Spanish Spring, Nevada, quarry.

According to the NDOT 2014 Standard Specification for Road and Bridge Construction, three primary gradation types are defined: Type 2, Type 2C, and Type 3 [30]. For this research, two gradations were selected: the first consisted of meeting both Type 2 and Type 2C specifications, while the second gradation met the Type 3 specification.

Both gradations were prepared using a Hveem mix design with 15 percent RAP, a PG64-28NV asphalt binder, and 1.5 percent hydrated lime. Gradations were taken from the NDOT Durability project and were not re-verified for this study. Table 2 shows the NDOT specification bands for the Type 2, 2C, and 3.

Mix design was conducted according to the NDOT Hveem method [30]. The Optimum Binder Content (OBC) was selected according to the standard practice by NDOT [30]. Table 3 presents the volumetric properties of the mixture summary for Type 2/2C and Type 3.

**Table 2: NDOT Aggregate Gradation Specifications**

Sieve Size	Type 2		Type 2C		Type 3	
	Lower	Upper	Lower	Upper	Lower	Upper
1"	100	100	100	100	-	-
3/4"	90	100	88	95	-	-
1/2"			70	85	100	-
3/8"	63	85	60	78	85	100
#4	45	63	43	60	50	75
#10	30	44	30	44	32	52
#40	12	22	12	22	12	26
#200	3	8	3	8	3	8

**Table 3: Volumetric Property Summary**

Mix ID	Type 2	Type 3	Requirement for Type 2	Requirement for Type 3
<b>OBC (%)</b>	4.5	5.7	–	–
<b>Design Air Void (%)</b>	4	4	4	4
<b>VMA (%)</b>	13	14.8	12 to 22	–
<b>VFA (%)</b>	70	72	–	–
<b>Pbe (%)</b>	3.7	4.5	–	–
<b>DP</b>	<b>With Lime</b>	1.36	1.17	–
	<b>W/O Lime</b>	1.01	0.9	–
<b>p200 (%)</b>	5	5.3	–	–
<b>Asphalt Film Thickness (microns)</b>	7.8	8.7	–	–

For the Hveem mix designs, a stability test was performed. NDOT specifications require a minimum stability number of 35 for Type 2, 37 for Type 2C, and 30 for Type 3 mixtures [30]. In this study, the Type 2/2C blend (coarser gradation) achieved the highest stability value of 39, while Type 3 met the requirement with a stability value of 31.5.

### 3.2 Warm Mix Asphalt Cores and Plant Mix

Warm Mix Asphalt (WMA) is increasingly used as a sustainable alternative to Hot Mix Asphalt (HMA), offering reduced production temperatures, lower emissions, improved workability, and greater flexibility for compaction under cooler conditions. According to a 2023 National Asphalt Pavement Association (NAPA) survey conducted in collaboration with the Federal Highway Administration (FHWA), WMA accounted for approximately 39.1 percent of all asphalt mixtures produced in the United States, and 45.8 percent of this mix was produced with a temperature reduction of 10°F [31].

NDOT participated in the FHWA-sponsored Long-Term Pavement Performance (LTPP) Specific Pavement Study (SPS-10) project to evaluate WMA performance over time. Laboratory evaluation was conducted at the University of Nevada, Reno, using materials placed in Washoe Valley, Nevada, under NDOT Contract 3598. The SPS-10 test sections were constructed in 2016 on Interstate 580 (Carson City Freeway) to investigate the impact of field aging on intermediate-temperature cracking resistance.

The SPS-10 project included seven sections with a 2-inch overlay constructed after cold milling 1 inch of existing asphalt pavement. Table 4 summarizes the section details, mixture types, WMA technologies, and binder types. Construction was completed on June 4–5, 2016.

As part of construction monitoring, Field-Mixed Field-Compacted (FMFC) cores were obtained at four time intervals: immediately after construction ( $T_0$ ), 6 months ( $T_6$ ), 12 months ( $T_{12}$ ), and 23 months ( $T_{23}$ ). Additional cores were taken from Section 01B, which had an open-graded overlay. All cores were extracted from the centerline of the right lane.

Cores from  $T_0$  and  $T_6$  were previously tested for the Texas Overlay Test [32] and the Uniaxial Thermal Stress and Strain Test (UTSST) [33] as part of earlier research [34].

This study focuses on  $T_{12}$  and  $T_{23}$  cores, as well as plant mix samples retrieved from storage for performance verification. In total, 113 cores were obtained for  $T_{12}$  and  $T_{23}$  testing. These samples were evaluated using the IDEAL-CT alongside other relevant material characterization procedures to compare laboratory and field performance.

**Table 4: LTPP SPS-10 Test Section details**

<b>LTPP Section ID</b>	<b>Nomenclature</b>	<b>Type</b>	<b>WMA Technology</b>	<b>Binder</b>
32AA01	HMA-NV	HMA	–	PG 64-28NV
01B	HMA- NV	HMA - Open Grade Overlay	–	PG 64-28NV
32AA02	Foam-NV	WMA	Foam	PG 64-28NV
32AA03	Evotherm-NV	WMA	Evotherm	PG 64-28NV
32AA59	Sonne-NV	WMA	Sonne	PG 64-28NV
32AA60	Advera-NV	WMA	Advera	PG 64-28NV
32AA61	Advera-NVTR	WMA	Advera	PG 64-28NVTR
32AA62	HMA-NVTR	HMA	–	PG 64-28NVTR

## Chapter 4: Experimental Plan

The experimental plan evaluates the applicability of the IDEAL-CT and Indirect Tensile Strength (IDT) tests for NDOT mixtures, focusing on gradation variations and the SPS-10 Warm Mix Asphalt (WMA) project. The study aims to:

- Establish correlations between CT Index results from SGC-compacted specimens (150 mm and 100 mm) and Hveem-compacted specimens (101.6 mm).
- Compare CT Index values from field cores and plant-produced mixtures with field distress data from the SPS-10 project.

### 4.1 Compaction methods and other volumetrics

The Superpave Gyratory and Hveem compaction methods were used to compact specimens. In addition to IDEAL-CT testing, the following tests were performed: Theoretical maximum specific gravity ( $G_{mm}$ ), asphalt binder extraction and recovery, rheological properties of recovered binder, and Sieve Analysis for the extracted aggregates.

#### 4.1.1 Hveem Compaction

The California Kneading Compactor was used to prepare specimens with a diameter of 101.6 mm and a height of 63.5 mm. Compaction is performed according to the Nevada test method T303D “*Method of Test for Stabilometer Value of Bituminous Paving Mixtures*” [35]. Hveem stability on compacted specimens is conducted in accordance with AASHTO T 247 “*Standard Method of Test for Resistance to Deformation and Cohesion of Hot Mix Asphalt (HMA) by Means of the Hveem Apparatus*” [36]. The initial compaction effort is decided to be 25 tamps at 250 psi, with the mold firmly fixed in place to the mold holder and a steel shim placed under the mold temporarily. Then, by releasing the

tightening screw, allowing free movement side by side at 500 psi while tampers are set, targeting a  $7 \pm 1$  percentage air void and a 63.5 mm height. These compaction efforts were based on the Hveem mix design compaction method [35]. Figure 4 illustrates the California Kneading Compactor.



**Figure 4: California Kneading Compactor**

After compaction, the mold with the compacted sample was placed in a 140°F (60°C) oven for 1.5 hours before applying a leveling load of 2000 lbf, fixed for all specimens at a rate of 12.8 mm per minute. The sample is extracted from the mold immediately. Compaction targets both the air void and the height of the specimen simultaneously. These specimens are tested for IDEAL-CT.

#### ***4.1.2 Superpave Gyrotory Compaction (SGC)***

The SGC is essential machinery for asphalt mix design and a necessary component of Superpave mix design. The SGC applies vertical pressure to the HMA mixture while simultaneously applying gyrotory motion at an angle. Cylindrical specimen compacted to a specific height by adjusting the weight of the sample only. The SGC compactor was developed as part of the Strategic Highway Research Program (SHRP) to produce

laboratory specimens that accurately replicate field compaction [37]. ASTM D6925-15 “*Standard Test Method for Preparation and Determination of the Relative Density of Asphalt Mix Specimens by Means of the Superpave Gyrotory Compactor*” was followed for the compaction [38]. Figure 5 illustrates the picture of SGC compactors.



**Figure 5: Superpave Gyrotory Compactor**

Specimens were prepared for both 150 mm and 100 mm diameters with a height of 63.5 mm for Type 2 and Type 3 gradations. Figure 6 shows the 150 mm and 100 mm molds. Compacted specimens were tested for IDEAL-CT. The primary purpose of using specimens with both diameters is that the CT Index is significantly influenced by the diameter and size of the sample. For the two-diameter molds, different gyration angles were used.



**Figure 6: Compaction molds for 150 mm and 100 mm**

#### **4.1.2 Theoretical Maximum Specific Gravity ( $G_{mm}$ )**

The theoretical maximum specific gravity of the mixture was determined following the AASHTO T 209 “*Theoretical Maximum Specific Gravity ( $G_{mm}$ ) and Density of Asphalt Mixtures*” [39]. The weight of the sample used was decided by the Nominal Maximum Aggregate Size (NMAS). For the field cores, three tested samples were loosened up and mixed. Then, the cut aggregate particles were removed, and a sample was created according to the quartering technique. The quartering was done according to AASHTO R 47 “*Standard Practice for Reducing Samples of Hot Mix Asphalt (HMA) to Testing Size by Means of Mechanical Splitting and Quartering*” [40]. The sample was conditioned for 2 hours at compaction temperature.  $G_{mm}$  was calculated based on Equation 2 below.

$$G_{mm} = \frac{A}{A-C} \quad \text{Equation 2}$$

A – mass of the oven-dry specimen in air, g

C- mass of the sample in the water at 77°F (25°C)

#### **4.1.3 Asphalt Binder Extraction and Recovery**

Extraction and recovery of asphalt binder are essential processes used to characterize the properties of asphalt mixtures when working with Reclaimed Asphalt Pavement (RAP) or Recycled Asphalt Shingles (RAS). This is done according to AASHTO T 164 “*Quantitative Extraction of Asphalt Binder from Asphalt Mixtures*” [41] and AASHTO T 319 “*Quantitative Extraction and Recovery of Asphalt Binder from Asphalt Mixtures*” [42]. Splitting loose mixtures and field cores was done according to

AASHTO R 47 [40]. The minimum mass of asphalt mixture to be placed on the bowl is determined according to the NMAAS of the mixture.

A solution of n-propyl bromide (nPb) was used as a chemical solvent to extract the asphalt from the mixture. The mixture was placed in the extraction bowl and soaked for about 45 to 60 minutes. The top edge of the extraction bowl was fitted with a dried filter ring to reduce the loss of fines. The centrifuge rotator rotated slowly, increasing the revolutions per minute to a maximum of 3600 until the solvent coming from the drain stops. The procedure was repeated until the liquid became darker than the color of light straw. The extracted solution obtained from the centrifuge is introduced into a centrifugal screen to collect additional fines that escape. This setup includes a No. 200 sieve on top, with a rotatory tube inside to collect fine particles that pass through the No. 200 sieve. In the end, the bowl containing the aggregate, filter, No. 200 sieve, and rotatory tube is dried in the oven until a constant mass is achieved at  $110 \pm 5^{\circ}\text{C}$  ( $230^{\circ}\text{F} \pm 9^{\circ}\text{F}$ ). The weight of each instrument mentioned above was recorded to calculate the binder content of the asphalt mixture.

Recovery of binder is done according to AASHTO T 319 [42]. A rotatory evaporation device is used to recover the binder from the extracted solution mixed with nPb. Recovery flask, oil bath, vacuum, and pressure controller. Nitrogen gas is used for vacuuming and reduces oxidation of the binder while heating. Figures 7 and 8 state the extraction and recovery setup.



**Figure 7: Centrifugal extractor**



**Figure 8: Rotatory Evaporator**

The recovered binder can be obtained in a small can and used to check the Performance Grade (PG) and Carbonyl properties. Extracted aggregates are used to check the binder content and aggregate gradation.

#### ***4.1.4 Sieve Analysis***

Sieve analysis is a standard laboratory method used by civil engineers and materials scientists to determine the particle size distribution and gradation of aggregates. Sieve analyses consist of multiple sieves from 1” to pan openings that progressively measure the passing and retaining of dry aggregates. This test is done according to AASHTO T 27

*“Standard method of test for sieve analysis of fine and coarse aggregates”* [43] and AASHTO T 30 *“Mechanical Analysis of Extracted Aggregate”* [44].

The weight of aggregate is decided according to the NMAS of stockpiles and the blend of aggregate. Extracted field core aggregates were dried, and washing was done using a mechanical washing apparatus. Sieve sizes used were No. 8 and No. 200 to prevent clogging during the washing of the aggregates. An adequate amount of wetting agent is used to ensure the thorough separation of material passing through the No. 200 sieve. This operation was continued until reasonably clear water was obtained from the washing. Figure 9 illustrates the mechanical washing apparatus used for the wash sieve analysis.



**Figure 9: Mechanical Washing Apparatus**

Aggregates were carefully transferred into the tray and dried until a constant mass. Aggregates are sieved according to the required sieves, and the weight of the retained mass is carefully measured. This gradation is compared with the actual mixture gradation.

#### ***4.1.5 Dynamic Shear Rheometer***

As part of the Superpave specification, the Dynamic Shear Rheometer (DSR) test is a standard test used to determine the rheological properties of asphalt binders. Binder tested under shear loading in relation to several temperatures and loading frequencies. This test

is done according to the AASHTO T 315-24 “*Determining the Rheological Properties of Asphalt Binder Using a Dynamic Shear Rheometer (DSR)*” [45]. DSR is used to evaluate the performance properties of both aged, unaged, and modified binders, which represent pavement performance. Asphalt binder is subjected to oscillatory shear loading in a parallel plate, which allows finding the viscoelastic properties like Complex Shear Modulus ( $G^*$ ) and Phase Angle ( $\delta$ ).

For the project, tested field cores were loosened and extracted. The extracted binder is tested for its PG high grade and Intermediate temperature. There is no Rolling Thin Film Oven Test (RTFO) and Pressure Aging Vessel (PAV) aging done because the field cores are already exposed to a certain extent of aging. These PG grades were checked with the original binder grade of the field mix. This will give an idea about how field aging occurs for T<sub>0</sub>, T<sub>6</sub>, T<sub>12</sub>, and T<sub>23</sub> months. Figure 10 shows the picture of DSR.



**Figure 10: Dynamic Shear Rheometer**

## 4.2 Mechanical Tests of Asphalt Mixtures

Mechanical testing of asphalt mixtures is crucial for evaluating how the mixture performs mechanically under the loading and environmental conditions of field simulation. Designers can understand pavement performance by examining cracking susceptibility, moisture sensitivity, and tensile strength in relation to pavement failure. These tests provide meaningful results for long-term pavement durability. The IDEAL-CT, TSR, and Moisture-Induced Stress Test (MiST) are the primary tests used for this project.

### 4.2.1 IDEAL-CT

The IDEAL-CT is a part of ASTM D8225-19 “*Standard Test Method for Determination of Cracking Tolerance Index of Asphalt Mixture Using the Indirect Tensile Cracking Test at Intermediate Temperature*” [7]. It is a well-established method for assessing the cracking resistance of asphalt mixtures at intermediate temperatures. This method is effective and applicable to practical service life conditions where asphalt pavement can be subjected to cracking. IDEAL-CT is a simple process for checking cracking. This test can be completed on mixtures with modified binder, aggregate gradations, fibers, additives, and recycled material.

In this test method, a monotonic compressive load is applied at a constant rate of  $50 \pm 2$  mm/min. The load is applied on a cylindrical asphalt specimen in the indirect tensile mode until the specimen fails. The test begins when the loading strip makes contact with the sample. Load, displacement, and time are measured to create a load displacement curve. The test finished when the load was reduced to 0.1 kN.

The specimen for the IDEAL-CT is a cylinder with a diameter of  $150 \pm 2$  mm and a thickness of  $62 \pm 1$  mm, and a second specimen with a diameter of 100 mm and a thickness of 63.5 mm. This is decided according to the Nominal Maximum Aggregate Size (NMAS). The target air void is  $7 \pm 0.5$  percent. For Hveem compacted specimen, the air void range is  $7 \pm 1$  percent. This test can be performed to accommodate both lab- and field-compacted samples. The testing temperature is typically  $25^{\circ}\text{C}$ . This project is based on SP (150 mm), SP (100 mm), HV (101.6 mm), and filed (150 mm) compact specimen. IDEAL-CT is mainly designed for testing the 150 mm diameter specimen. For testing the small-diameter samples, modifications were made to the thickness and height of the loading strip. Figures 11 and 12 illustrate the modification of loading strips from 150 mm to 100 mm.

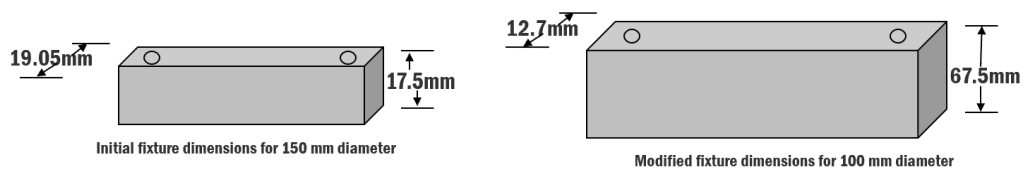


**Figure 11: Loading strip modification**



**Figure 12: Picture of modified loading strip**

For the 150 mm loading strip, the radius of curvature is 75 mm, and for the 100 mm loading strip, it is 50 mm. This method maintains the top position of the specimens and increases the height of the bottom loading strip to match. When the load is applied to the sample radially. The tension zone occurred in the vertical plane that cuts horizontally through the center of the specimens. Maximum tension occurs horizontally through the center of the specimen; cracking occurs when the tensile stress exceeds the tensile strength of the asphalt mixture.

The compression zone is concentrated at the top and bottom of the loading contact area, where the specimens interact with the loading strips. The transition zone is between the top, bottom, and middle of the sample, where stress changes gradually. Figure 13 shows a picture of an IDEAL-CT machine.

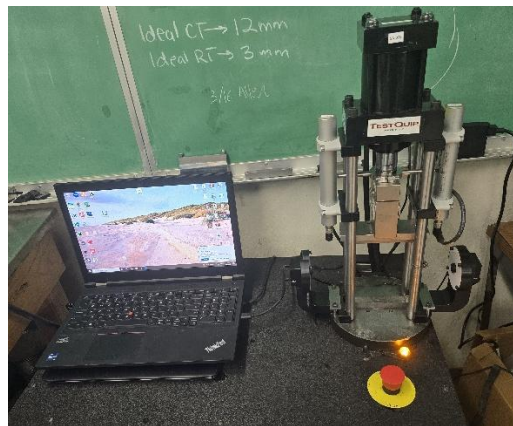


**Figure 13: IDEAL-CT machine**

Load and displacement curves can be plotted using raw data obtained from the machine. Figure 14 states the plot of the load versus displacement. The plot displays key parameters for calculating the CT Index.  $P_{100}$  is the maximum peak load of the test.  $P_{85}$ ,  $P_{75}$ , and  $P_{65}$  are 85 percent, 75 percent, and 65 percent of the maximum peak load, respectively.  $l_{85}$ ,  $l_{75}$ ,

and  $l_{65}$  represent the displacement of the loading strip for the load mentioned above. The final displacement is measured at a load of 0.1 kN. Work done during the test is the area under the curve of load versus displacement.

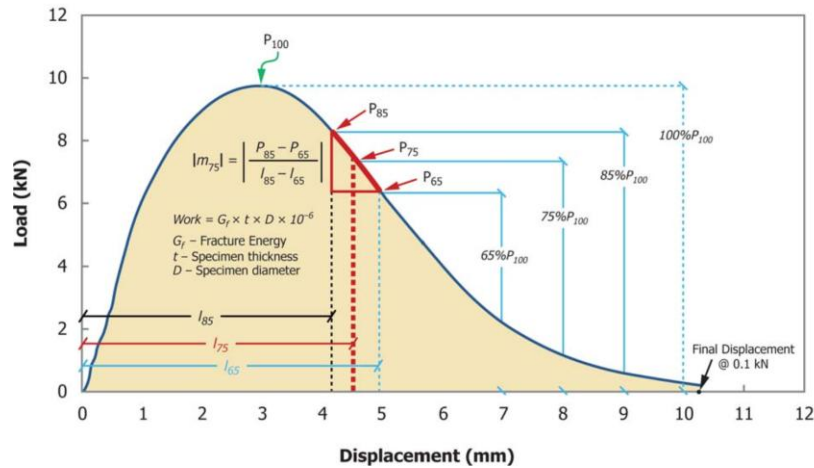


**Figure 14: Load versus Displacement plot of IDEAL-CT**

Field core specimens can be tested with a height of at least 38 mm. The cracking tolerance index can be calculated from the equation, considering the load-displacement curve.

$$CT_{Index} = \frac{t}{62} \times \frac{l_{75}}{D} \times \frac{G_f}{|m_{75}|} \times 10^6 \quad \text{Equation 1}$$

$$G_f = \frac{W_f}{D \times t} \times 10^6 \quad \text{Equation 3}$$

$$m_{75} = \left| \frac{P_{85} - P_{65}}{l_{85} - l_{65}} \right| \times 10^6 \quad \text{Equation 4}$$

$P_{85}, P_{65}$  = 85 and 65 percent of peak load (kN)

$l_{85}, l_{65}$  = displacement occurs at 85 and 65 percent of peak load (mm)

The parameters mentioned above show how the mixture cracks. Every parameter indicates the specific properties of the mixture.  $|m_{75}|$  is the steepness of the load displacement curve, showing how quickly the peak load drops. Lower the  $|m_{75}|$  gentle decline of the peak load and better cracking resistance.  $l_{75}$  is how the specimen deforms at 75 percent of peak load after peak. The greater the  $l_{75}$ , the more deformation occurs after the peak load, up to 75 percent of the peak load, which enhances cracking.

Larger diameter specimens create a more uniform stress distribution, increasing the CT Index, while smaller diameters reduce it. The same applies to the thickness of the specimens.  $G_f$  is the energy required to crack the specimen. Higher  $G_f$  shows more cracking resistance. Figures 15 and 16 show the trend of load versus displacement and displacement versus time plots of a Hveem compacted specimen.

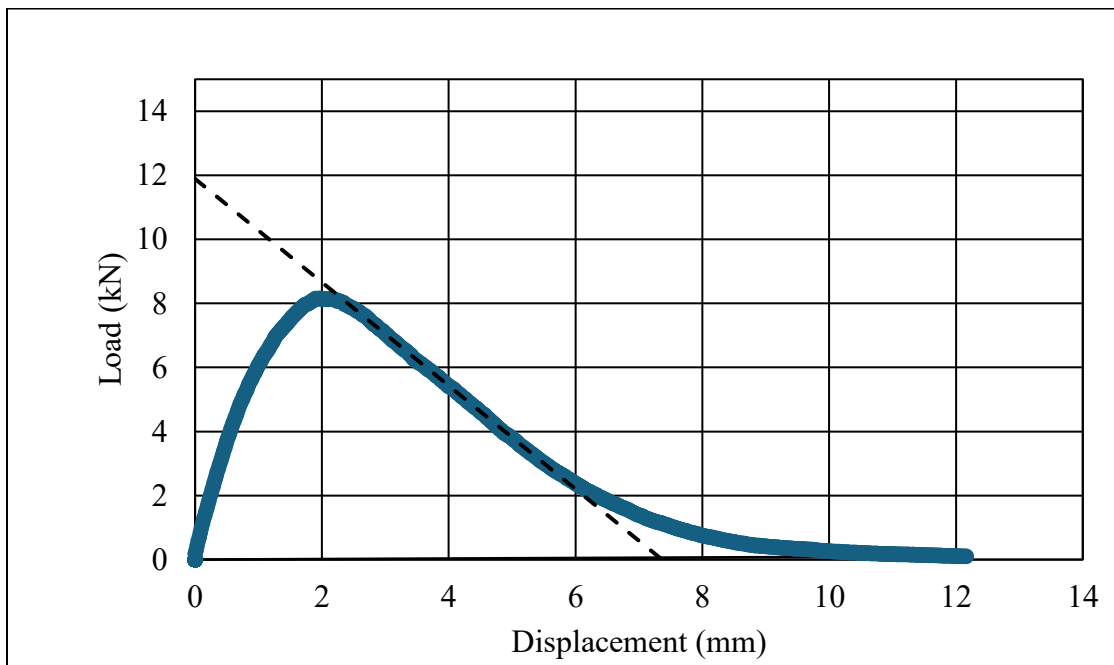


**Figure 15: Load versus displacement plot**

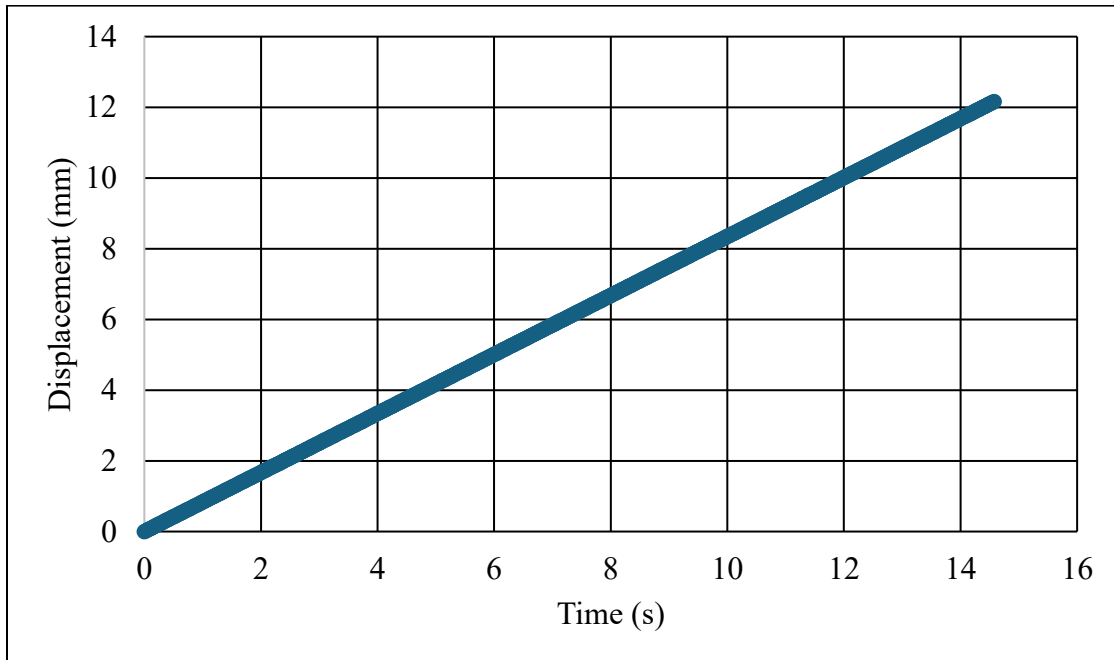


**Figure 16: Displacement versus Time plot**

#### ***4.2.2 Tensile Strength Ratio***

The AASHTO T 283-22 “*Resistance of Compacted Asphalt Mixtures to Moisture-Induced Damage*” [46] evaluates an asphalt mixture’s resistance to moisture damage. Stripping occurs when water causes the bond between asphalt and aggregate to break. This test compares the relative strength of dry-conditioned specimens with that of frozen and thawed specimens. A sample can be prepared from a plant or a lab-produced sample. For this project, the sample was compacted using a kneading compactor and an SGC. For SGC specimens, 150 mm specimens with  $95 \pm 5$  mm height and 100 mm specimens with  $63.5 \pm 2.5$  mm height. The target air voids range for SGC specimens is  $7 \pm 0.5$  percent, and for HV specimens,  $7 \pm 1$  percent.

Two sets of specimens were prepared, one with dry specimens and the other with moisture-conditioned specimens. After the mixture is ready, it is placed inside the oven for  $16 \pm 1$  hours at  $60 \pm 3^\circ\text{C}$ . Then, the temperature increased to the compaction temperature for 2 hours  $\pm$  10 minutes. The compaction temperature for SGC specimens was  $300^\circ\text{F}$ , and HV specimens were at  $230^\circ\text{F}$ .

Dry conditioning keeps compacted specimens on the counter table. For moisture conditioning, specimens were saturated using the vacuum conditioning method to achieve a moisture content of 70 to 80 percent. The specimens were wrapped well with plastic wrap. Then, a specimen was placed inside a Ziplock bag of the appropriate size, and  $10 \pm 0.5$  mL of water was added. The sample was placed inside the freezer at a temperature of  $-18 \pm 3^\circ\text{C}$  for a minimum of 16 hours.

The specimen was transferred into the water bath at  $60 \pm 1^\circ\text{C}$  for  $24 \pm 1$  hours. After that, the sample was moved into the  $25 \pm 0.5^\circ\text{C}$  water bath for 2 hours  $\pm$  10 minutes. As the final step, dry conditioned specimens are also conditioned at a temperature of  $25 \pm 0.5^\circ\text{C}$  before testing using the IDEAL-CT testing machine. Figure 17 shows the vacuum machine used to saturate the specimens.



**Figure 17: Vacuum apparatus for T283**

As this project related to HV compaction working with NDOT, the pan size used for aging specimens was 11” length, 7” width, and 2” deep. For the conditioning, 16 hours, the same as T 283, and placed in compaction temperature for 1.5 hours. Cracked specimens were examined for stripping or breaking of the aggregate to determine how moisture damage affects the bonding between the aggregate and binder. This test takes around 2 to 3 days to complete, and proper care should be taken when vacuuming to avoid oversaturating the specimens.

Tensile strength is calculated according to the equation below.

$$S_t = \frac{2000P}{\pi tD} \quad \text{Equation 5}$$

$S_t$  = Tensile Strength (psi)

$P$  = Peak load (N)

$t$  = specimen thickness (mm)

$D$  = specimen diameter (mm)

Tensile Strength ratio is calculated according to the equation below

$$TSR = \frac{S_2}{S_1} \quad \text{Equation 6}$$

$S_1$  = average tensile strength of the dry conditioned specimens kPa (psi).

$S_2$  = average tensile strength of the wet conditioned specimens, kPa (psi).

#### ***4.2.3 Moisture Induced Sensitivity Tester (MiST)***

AASHTO TP 140-22, “*Moisture Sensitivity Using Hydrostatic Pore Pressure to Determine Cohesion and Adhesion Strength of Compacted Asphalt Mixture Specimens*”

[47], used to evaluate the effect of moisture on the compacted sample by testing tensile strength. This test primarily focuses on rapidly simulating the impact of moisture on asphalt specimens by using high temperatures and high-water pressures. This rapid and repeated conditioning will cause failure of the bond between the asphalt binder and aggregate, as well as within the asphalt binder. Using hydrostatic pressure at high temperatures on the compacted specimen will increase the damage, as occurs in pavements affected by traffic loads in wet conditions.

For HV compacted specimens with a 101.6 mm diameter and  $63.5 \pm 2.5$  mm, and the target air void range of  $7.0 \pm 1$  percent. At least six specimens were made for 100 mm diameter specimens. Two sets are divided according to equal average air voids. One set is conditioned, and the other is control. The conditioning temperature depends on the decision, based on the PG grade of the binder. The conditioning temperature of the test is decided based on the PG Grade of the Binder. The specimen was placed in hot water for 20 hours inside the pressure chamber. Then cyclic hydrostatic pressure at 275 kPa (40 psi) for 3500 cycles. After that, the specimen was placed inside a water bath at  $25 \pm 1^\circ\text{C}$  for 2

to 3 hours before testing using the IDEAL-CT testing machine. Figure 18 shows the picture of the MiST machine.

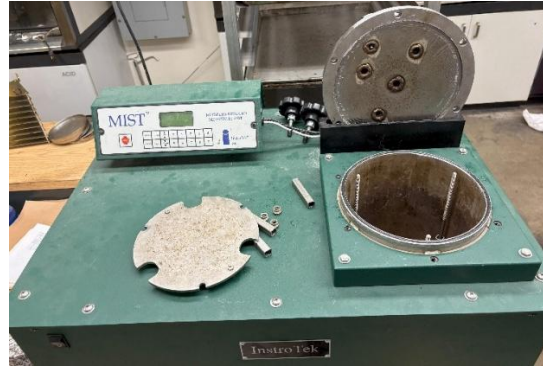


**Figure 18: MiST Machine**

## Chapter 5: Results and Analysis

### 5.1 Phase 1 Evaluation of the Impact of Specimen Size and Compaction

#### Method

##### *5.1.1 IDEAL-CT on Type 2/2C and Type 3 Gradation*

The IDEAL-CT test was conducted on two gradations. Specimens were compacted with the SGC and Hveem compaction methods. The CT Index was determined from the IDEAL-CT test mixtures from Type 2/2C and Type 3, with their air void ranges illustrated in Figure 19. Error bars in the plot indicate a 95 percent confidence interval. Dash and cross points show the maximum, minimum, and average air void of each set of specimens. Generally, a higher CT Index indicates that the mixture has higher cracking resistance. Here, SP represents Superpave compacted specimens and HV represents Hveem compacted specimens. Type 2 gradation exhibits greater variability compared to Type 3 gradation, because of the coarse aggregates in Type 2. When coarse aggregates are packed into a small specimen, it may cause uneven distribution in the specimen, which leads to variability in the CT Index between specimens. In the type 2 mixture, the CT index increases when the specimen diameter reduces from 150 mm to 100/101.6 mm. Diameter plays an important role in the CT Index change. When considering the compaction method, changing from SGC compaction to Hveem compaction, the CT Index increases for the same OBC binder content.

For the Type 3 mix, the CT index decreases when the diameter changes from 150 mm to 100 mm and increases for 101.6 mm. For the compaction effort similar trend was observed

as Type 2, CT Index increases. As an overall comparison for both gradation's Hveem compacted specimens, the CT Index increased with the increase in binder content. This is evident in the CT Index is sensitive to changes in binder content. Overall, based on the observed trend, Type 3 mixture shows a higher CT Index than Type 3, and the Hveem compacted specimens show a higher CT Index than the SGC specimen.

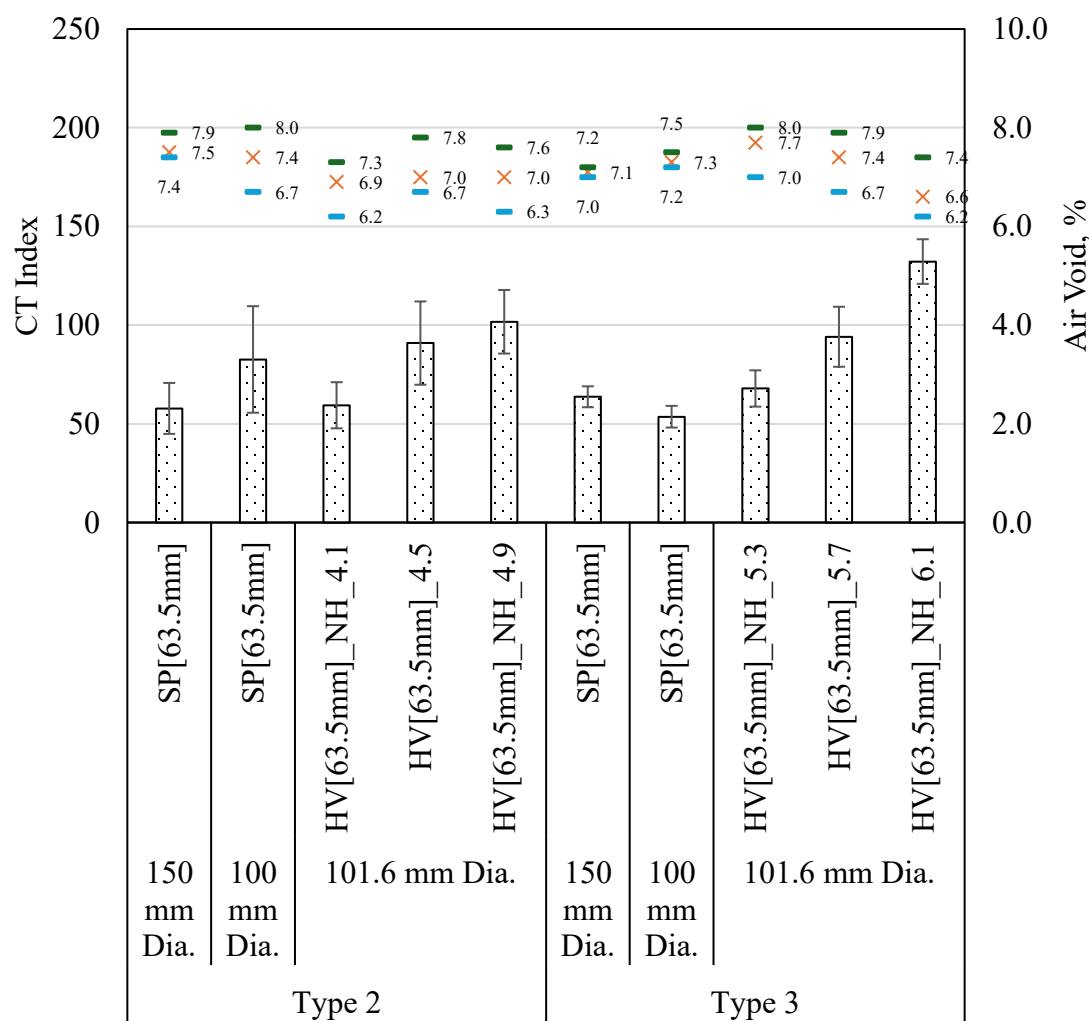


**Figure 19: CT-Index values for the Type 2/2C and Type 3 mixes**

Error bars represent the mean plus or minus the 95% confidence interval.

It is also important to note that there is no threshold value established currently for the Hveem compacted samples available in the standard. Considering only the CT Index is not enough to understand the trend; other parameters involved in the CT Index equation also need to be compared. Figure 20 describes the  $m_{75}$  value of each mixture. The  $m$  value represents the slope of the 75 percent post-peak load in the load versus displacement curve. A lower  $m$  value signifies a more ductile behavior, whereas a higher  $m$  value, a more brittle behavior. Type 2 mixture showed a decreasing trend in the CT Index when the diameter was reduced from 150 mm to 100/101.6 mm. Conversely, for the Type 3 mixture, with the diameter reduction, the CT Index increases. When considering the type of compaction, changing from SGC to Hveem compacted specimen, the  $m$  value decreases. Both gradations exhibit a decreasing trend in  $m$  value with an increase in binder content for Hveem compacted samples, which explains sensitivity to binder content.

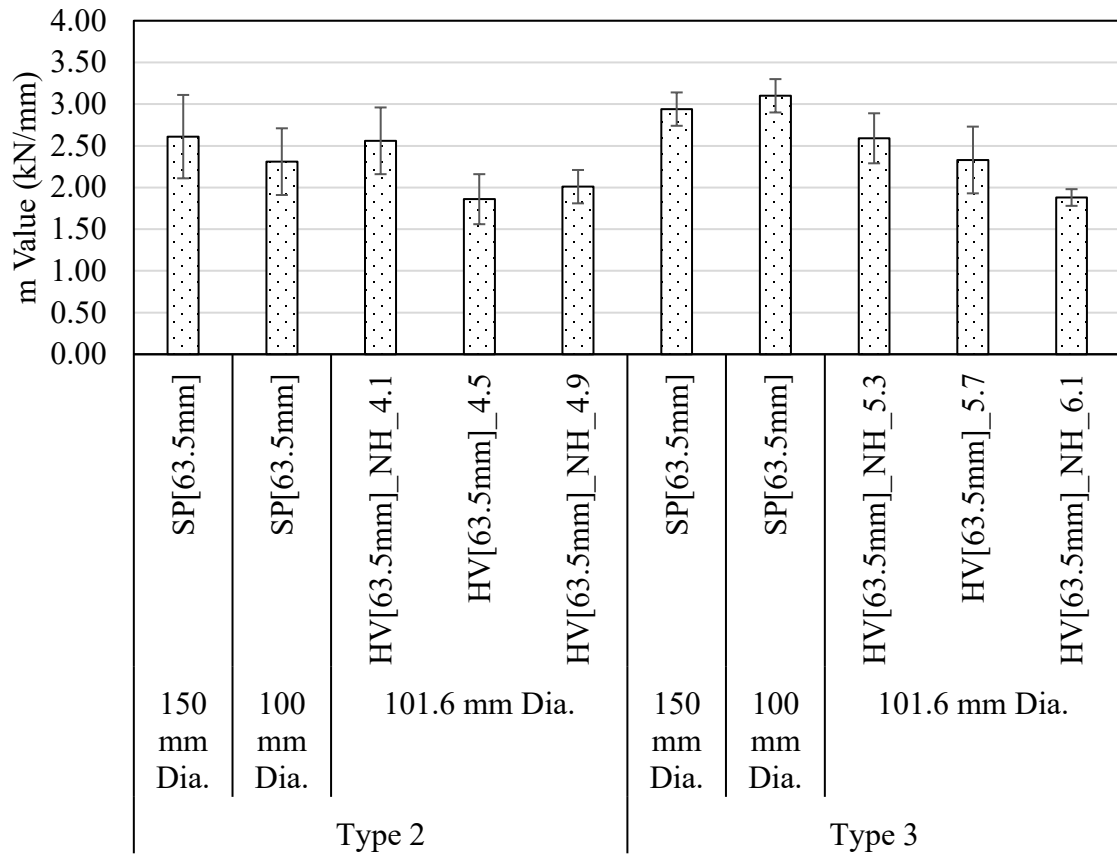


**Figure 20:  $m_{75}$  values for the Type 2/2C and Type 3 mixtures**

Error bars represent the mean plus or minus the 95% confidence interval.

Figure 21 represents the  $l_{75}$  value of the CT Index test. The  $l_{75}$  value represents the amount of deformation the specimen can endure to reach 75 percent of its peak load. The higher the  $l_{75}$  value, the more deformation a sample can take before failure. With the reduction in the diameter from 150 mm to 100 mm. Type 2 mixture exhibited a decrease in  $l$  value, and Type 3 shows an increase. This change could be because of the gradation effect. Considering the compaction method, for both gradation  $l$  value decreases when changing from SGC to Hveem Compaction. Both gradations exhibit an increasing trend in  $m$  value with an

increase in binder content for Hveem compacted samples, which explains sensitivity to binder content.

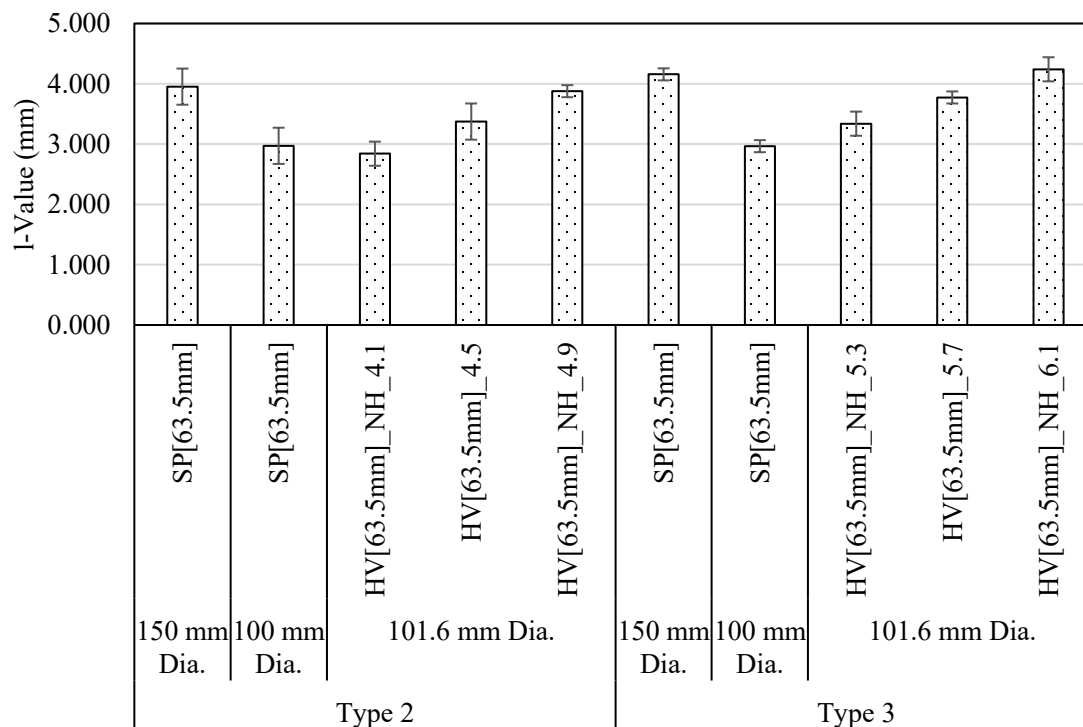


**Figure 21:  $l_{75}$  values for the Type 2/2C and Type 3**

Error bars represent the mean plus or minus the 95% confidence interval.

Figure 22 illustrates the  $l_{75}/m_{75}$  CT Index test. The higher  $l_{75}/m_{75}$  in a specimen indicates a greater strength. For both gradations, when the diameter was reduced from 150 mm to 100 mm, the  $l/m$  value reduced. When considering the compaction method changing from SGC to Hveem compaction, the  $l/m$  value increases. An increasing trend was observed for the  $l/m$  value with the increase in binder content.

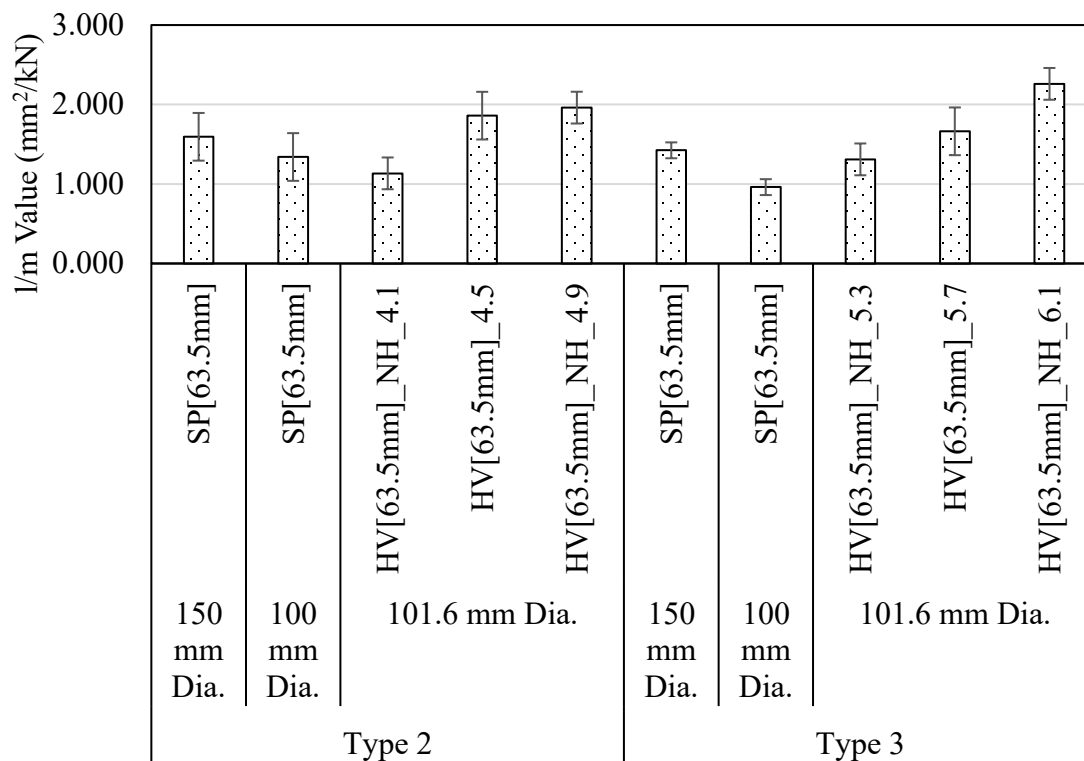


**Figure 22:  $I_{75}/m_{75}$  values for the Type 2/2C and Type 3 mixtures**

Error bars represent the mean plus or minus the 95% confidence interval.

Peak load represents the maximum load an asphalt specimen can withstand before crack initiation. A higher peak load, which diminishes load gradually, suggests greater resistance to cracking. Figure 23 illustrates the changes in peak load values with different mixtures. For both gradations, with the diameter change from 150 mm to 100 mm, the peak load reduces. When considering the compaction method, the peak load decreases when changing from SGC to Hveem compaction. Peak load decreases with binder content increase for both gradations. Type 3 generally exhibits a higher peak load than Type 2 under similar testing conditions.

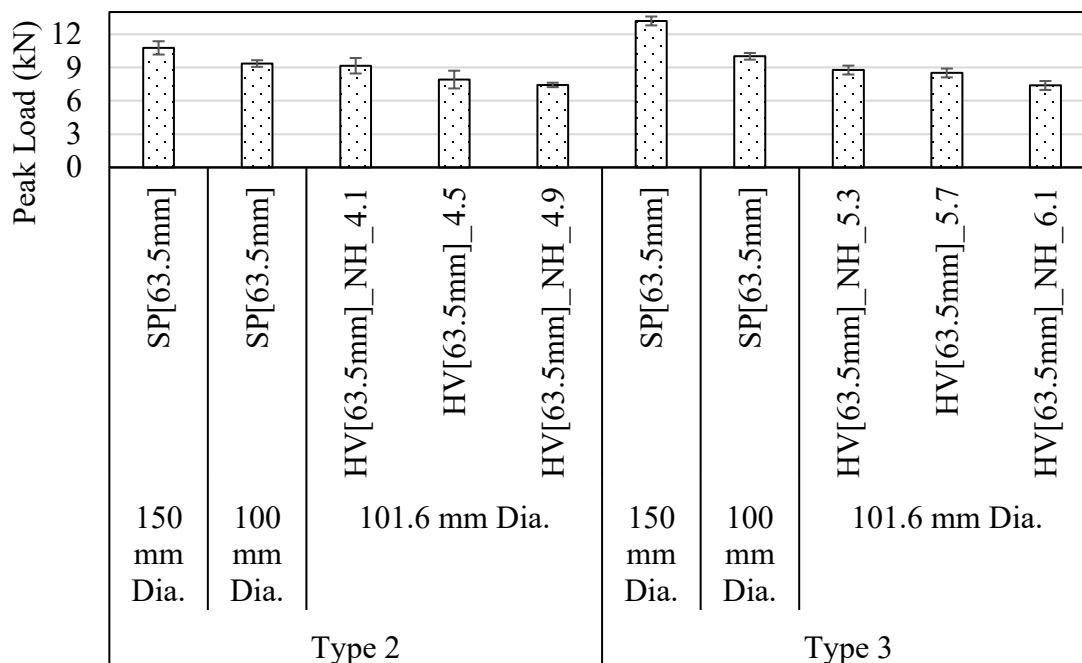


**Figure 23: Peak Load values for the Type 2/2C and Type 3 mixture**

Error bars represent the mean plus or minus the 95% confidence interval.

Fracture energy is the energy per unit area required to propagate a crack through an asphalt specimen. Figure 24 shows the Fracture Energy of the CT Index. For the Type 2 mixture, when the diameter changes from 150 mm to 100 mm, fracture energy increases. Conversely, for the Type 3 mixture, fracture energy decreases with a reduction in diameter. When considering the compaction method, the fracture energy didn't change much when changing from SGC to Hveem compaction for both gradations. Hveem compacted samples were not sensitive to binder content for both gradations. The diameter of the sample has a greater impact on the fracture energy, regardless of the different gradations.

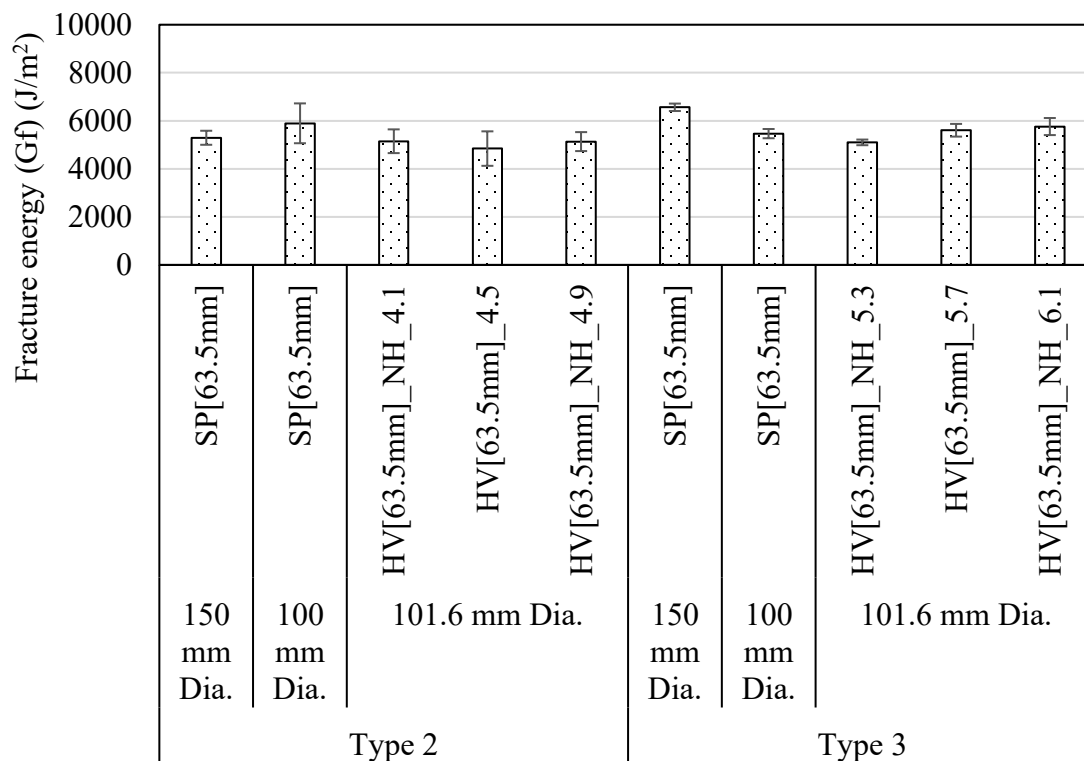


**Figure 24: Fracture Energy for the Type 2/2C and Type 3 mixture**

Error bars represent the mean plus or minus the 95% confidence interval.

Figure 25 shows the Tensile Strength from the CT Index for the mixture. Tensile strength is an indication of an asphalt mixture's ability to sustain higher tensile stress before cracking. For both gradations, the tensile strength increases with a change in diameter from 150 mm to 100 mm. When the compaction method changes from SGC to the Hveem compaction method, the tensile strength decreases. Tensile strength decreases with an increase in binder content. As an overall comparison, a similar trend was observed for Type 2 and Type 3 gradations. The diameter of the sample plays an important role in tensile strength change.

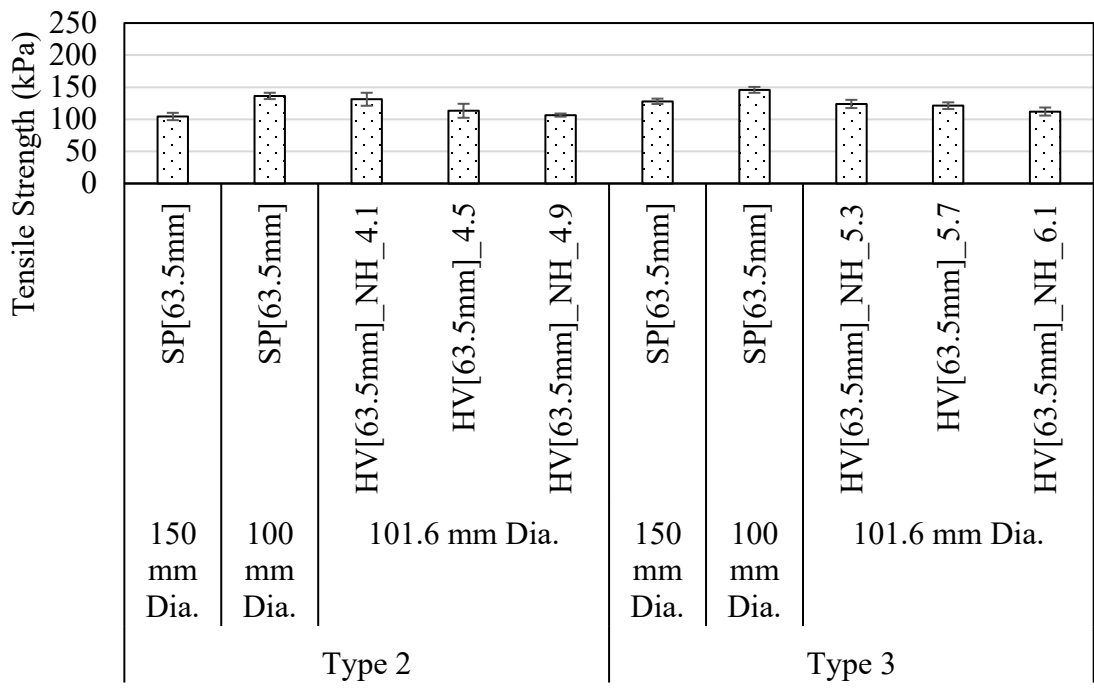


**Figure 25: Tensile Strength for the Type 2/2C and Type 3 mixtures**

Error bars represent the mean plus or minus the 95% confidence interval.

The air void in the specimen plays a crucial role in IDEAL-CT testing. For the SGC sample, the air void range is  $7 \pm 0.5$  percent, and for the Hveem compacted sample, due to variability, the range is  $7 \pm 1$  percent. Figure 26 states the average air voids of the mixtures.

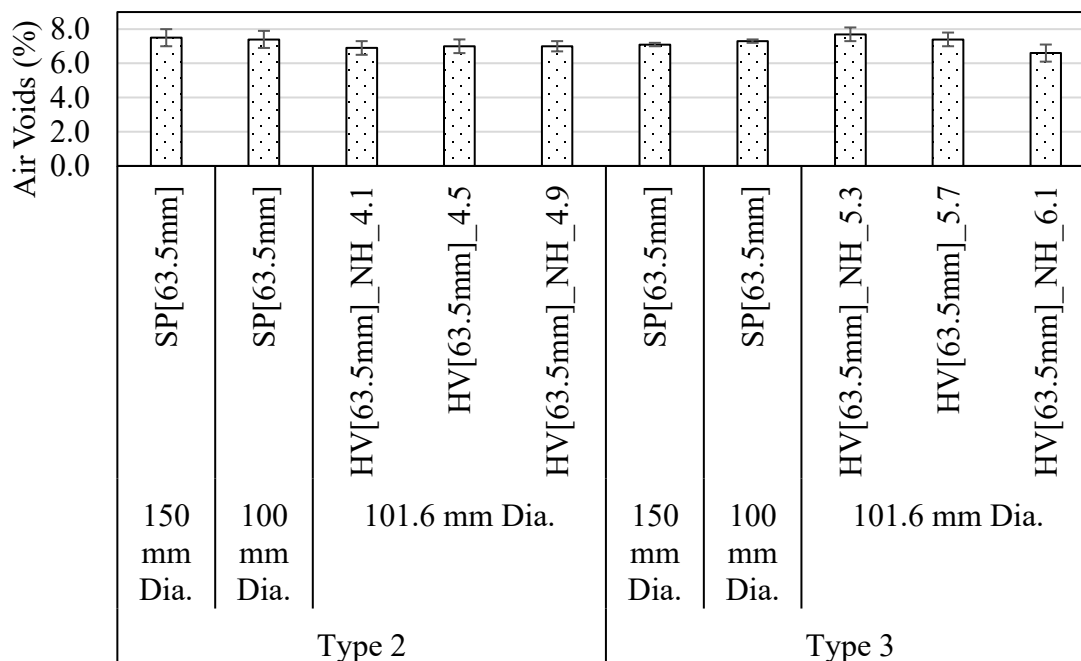


**Figure 26: Air void percent for the Type 2/2C and Type 3 mixtures**

Error bars represent the mean plus or minus the 95% confidence interval.

Statistical analysis was done for the IDEAL-CT population mean for different diameter samples and compaction methods. The F-test is used to check whether the population of each set has equal variance, and the t-test was performed to assess the significance of the difference between the CT Index population means. The significance level used for this testing was 0.05. The null hypothesis ( $H_0$ ) of this t-test checks whether the population means of two sets of specimens are significantly different. Table 5 states the summary of the significance of Type 2 mixture samples. When the diameter changes from 150 mm to 100 mm, the SGC specimen shows no significant difference in the population mean. This explains the SGC specimen; the CT Index can be related to diameter change. For the compaction method, SGC 100 mm and Hveem 101.6 mm specimens show no significant difference in the population mean. Overall, for SGC compaction, diameter change did not

affect the CT Index population mean, and SGC and Hveem with similar diameters exhibit similar effects.

**Table 5: Type 2/2C mixture Significance difference in population mean**

Significantly different (SD)/ Not Significantly Different (NSD) (Significance level: 0.05)					
	150 mm SP	100 mm SP	101.6 mm HV	101.6 mm HV 4.1	101.6 mm HV 4.9
150 mm SP		NSD	SD	NSD	SD
100 mm SP	NSD		NSD	NSD	NSD
101.6 mm HV	SD	NSD		SD	NSD
101.6 mm HV 4.1	NSD	NSD	SD		SD
101.6 mm HV 4.9	SD	NSD	NSD	SD	

Table 6 states the significant difference between the Type 3 mixture population mean. Except for the 150 mm SP and 101.6 mm HV with 5.3 percent binder content, other population sets show a significant difference in mean. Diameter change or compaction method for the Type 3 mixture showed no significant difference in the population mean and cannot be related.

**Table 6: Type 3 mixture Significance difference in population mean**

Significantly different (SD)/ Not Significantly Different (NSD) (Significance level: 0.05)					
	150 mm SP	100 mm SP	101.6 mm HV	101.6 mm HV 5.3	101.6 mm HV 6.1
150 mm SP		SD	SD	NSD	SD
100 mm SP	SD		SD	SD	SD
101.6 mm HV	SD	SD		SD	SD
101.6 mm HV 5.3	NSD	SD	SD		SD
101.6 mm HV 6.1	SD	SD	SD	SD	

## 5.2 Phase 2: Evaluation of Moisture Damage

### 5.2.1 Tensile Strength Ratio (TSR) (AASHTO T 283)

The minimum requirements of the Nevada DOT Standard Specification for the TSR test are 70 percent, and the minimum unconditioned tensile strength of 65 psi [28]. Figure 27 states the TSR percentage for the Type 2 and Type 3 specimens compacted using the Hveem method. Both gradations have passed the minimum requirement of 74 percent for Type 2 and 70 percent for Type 3. Figure 28 illustrates the wet and dry tensile strength of both mixtures, and the error bar indicates 95 percent confidence interval.

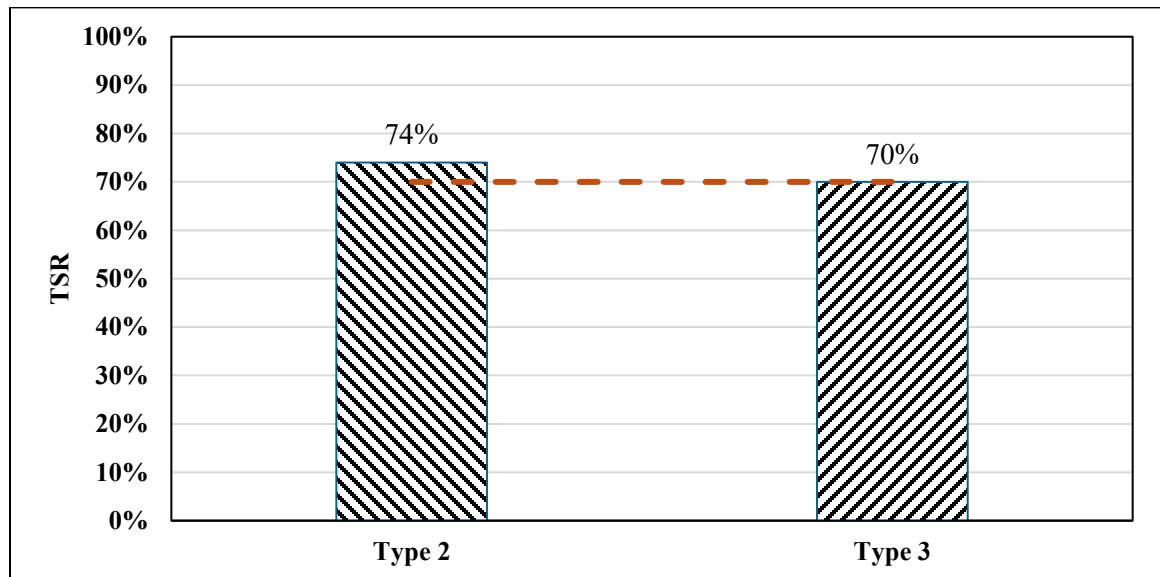


**Figure 27: TSR for Hveem compacted specimens**

Because the lime-marinated aggregates are stored for about 48 hours, and the compaction method can influence the TSR percentage, there is a noticeable resistance to stripping. The same conditioning procedure was followed as specified in AASHTO T 283 [46].

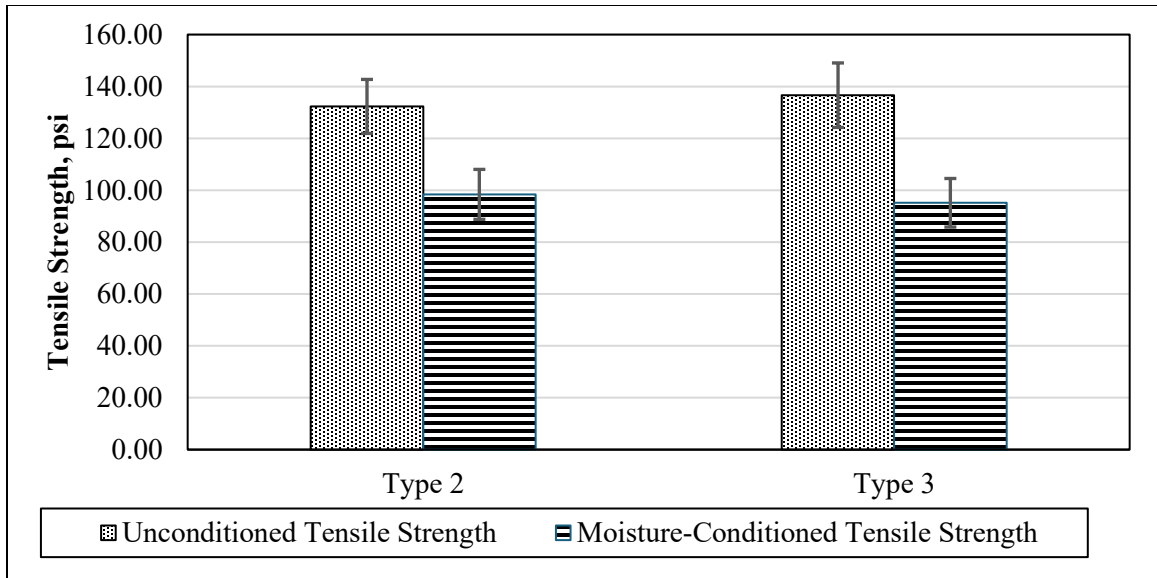


**Figure 28: Tensile strength values of Type 2 and Type 3 mixtures**

Error bars represent the mean plus or minus the 95% confidence interval.

### ***5.2.2 MiST Test for the Hveem Compacted Specimens***

The MiST test is used to evaluate the moisture susceptibility of the asphalt mixture. This test was performed for Hveem compacted specimens. Specimens were prepared under the same conditions as those specified in AASHTO T 283. Figure 29 presents the moisture-conditioned tensile strength of the MiST-tested samples. The Type 2 mixture exhibits higher tensile strength than the Type 3 mixture.

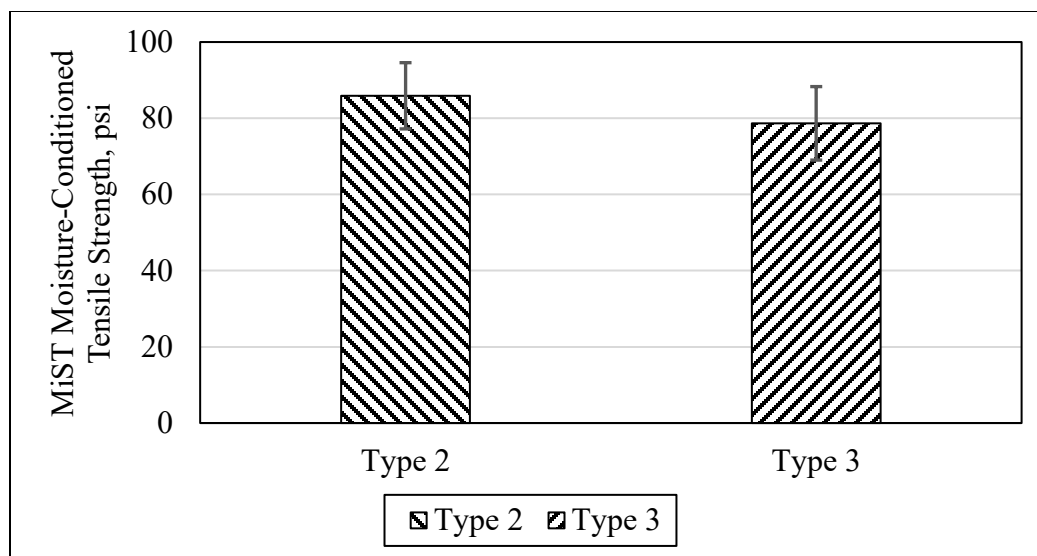


**Figure 29: MiST tensile strength values of Type 2 and Type 3 mixtures**

Error bars represent the mean plus or minus the 95% confidence interval.

### ***5.2.3 Comparison of Tensile Strength Values***

One of the key aspects of moisture sensitivity is comparing the relationship between different tensile strengths in various tests. Hveem compacted samples are compared for their IDEAL-CT tensile strength, moisture-conditioned and unconditioned tensile strengths from T 283, and moisture-conditioned MiST tensile strengths. Figure 30 illustrates the different tensile strengths among the different sets of samples. The unconditioned tensile strength of T 283 has become the highest among both the gradations due to the aging effect of conditioning before compaction. Both Type 2 and Type 3 exhibit similar trends across various tensile strengths. For the MiST moisture-conditioned specimens, the tensile strength reduced after 3500 cycles at 40 psi and 60°C temperature. Type 2 should be considered for use in wet conditions in the field for improved performance.

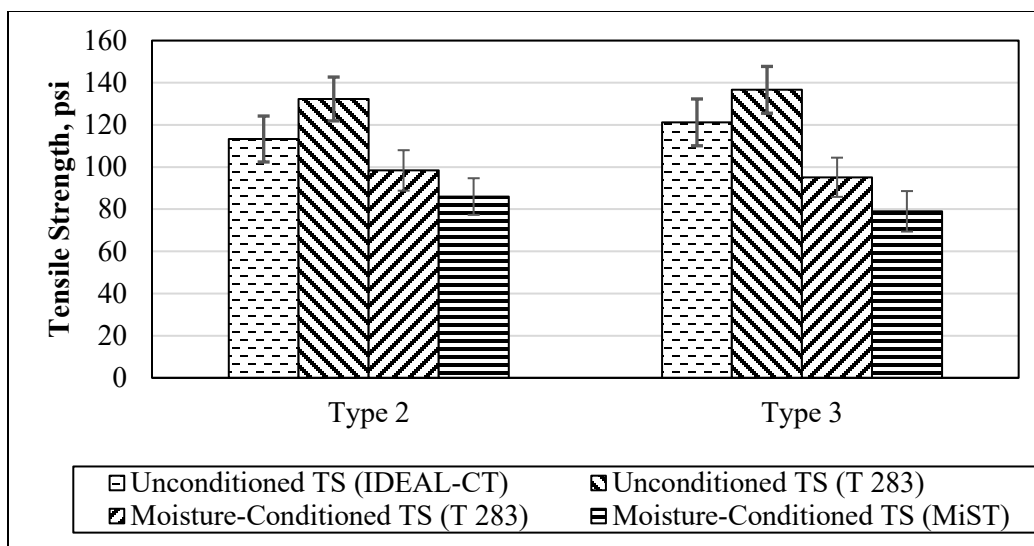


**Figure 30: Comparison of tensile strength values of Type 2 and Type 3 mixtures**

Error bars represent the mean plus or minus the 95% confidence interval.

For IDEAL-CT specimens, the loose mixture was aged for 2 hours at 230°F before compaction, and for the T 283 and MiST specimens, the loose mixture was aged for 16 hours at 140°F before compaction.

As a part of the comparison, statistical analysis was carried out for the different tensile strengths mentioned above. The t-test was done to check the significant difference between the population means of unconditioned IDEAL-CT, unconditioned T 283, moisture-conditioned T 283, and moisture-conditioned MiST tensile strengths. Tables 7 and 8 illustrate the summary of the analysis of Type 2 and Type 3 mixtures. The results showed that there is no significant difference between the population's means of moisture-conditioned T 283 and moisture-conditioned MiST tensile strength. There is a significant difference in the population means of unconditioned IDEAL-CT, unconditioned T 283.

**Table 7: Type 2/2C mixture Significance difference in population mean of tensile strength**

Significantly different (SD)/ Not Significantly Different (NSD) (Significance level: 0.05)				
	Unconditioned TS (IDEAL- CT)	Unconditioned TS (T 283)	Moisture- Conditioned TS (T 283)	Moisture- Conditioned TS (MiST)
Unconditioned TS (IDEAL- CT)		SD	NSD	SD
Unconditioned TS (T 283)	SD		SD	SD
Moisture- Conditioned TS (T 283)	NSD	SD		NSD
Moisture- Conditioned TS (MiST)	SD	SD	NSD	

**Table 8: Type 3 mixture Significance difference in population mean of tensile strength**

Significantly different (SD)/ Not Significantly Different (NSD) (Significance level: 0.05)				
	Unconditioned TS (IDEAL- CT)	Unconditioned TS (T 283)	Moisture- Conditioned TS (T 283)	Moisture- Conditioned TS (MiST)
Unconditioned TS (IDEAL- CT)		SD	SD	SD
Unconditioned TS (T 283)	SD		SD	SD
Moisture- Conditioned TS (T 283)	SD	SD		NSD
Moisture- Conditioned TS (MiST)	SD	SD	NSD	

This is because of the difference in the aging condition of IDEAL-CT and the T283 before the compaction. Unconditioned IDEAL-CT cannot be used to calculate TSR.

Figure 31 illustrates the TSR calculated for T 283 and MiST. TSR percentage for T 283 meets the minimum requirement established by NDOT. Type 2 mix performs well in both scenarios. Moisture damage done by the MiST is greater than the T 283 (1 freeze-thaw cycle). The number of cycles used for the MiST should be adjusted to match the effect with T 283.

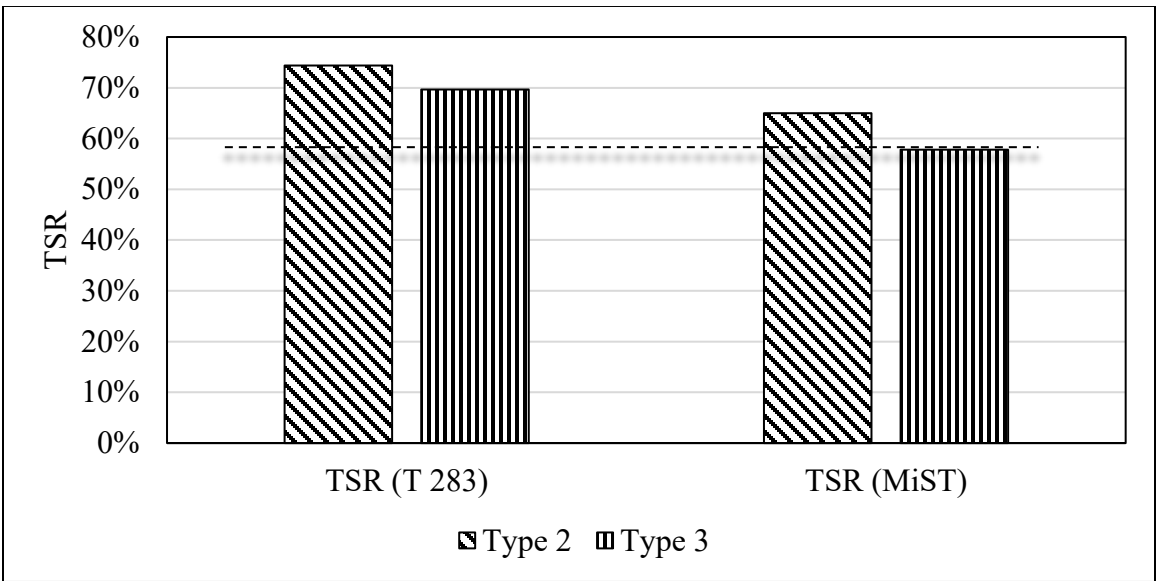


**Figure 31: Comparison of TSR**

### **5.3 Phase 3: Preliminary Validation of the CT Index**

#### ***5.3.1 IDEAL-CT Results for the Field Cores***

Field cores obtained from SPS-10 project, for 12 months ( $T_{12}$ ) and 23 months ( $T_{23}$ ), were cut from the top layer with a thickness of approximately 50 mm. The bulk specific gravity of these specimens was measured to determine the air void percentage of the cores. The IDEAL-CT test was performed on the cores to assess their cracking tolerance for each period. Figure 32 states the CT Index of each mixture field core. The error bar represents a 95 percent confidence interval.

Some of the cores exhibit higher variability among the mixtures. A common trend can be observed in most of the mixtures, where the CT Index reduces from 12 to 23 months. Foam, Advera, and Advera-NVTR showed an opposite trend of the CT Index. This might be because of the unevenness between the field cores, field compaction, and the location of the field core. There is a chance that WMA additives enhance the performance of the mixtures. Evotherm and Sonne mixtures showed a lesser reduction in the CT Index from 12 to 23 months. This explains why both mixes perform well. HMA mixture with an open-grade overlay showed a higher CT Index compared to the HMA mixture, which explains open-grade overlay protects the underlying layer from aging and absorption of binder by aggregates.

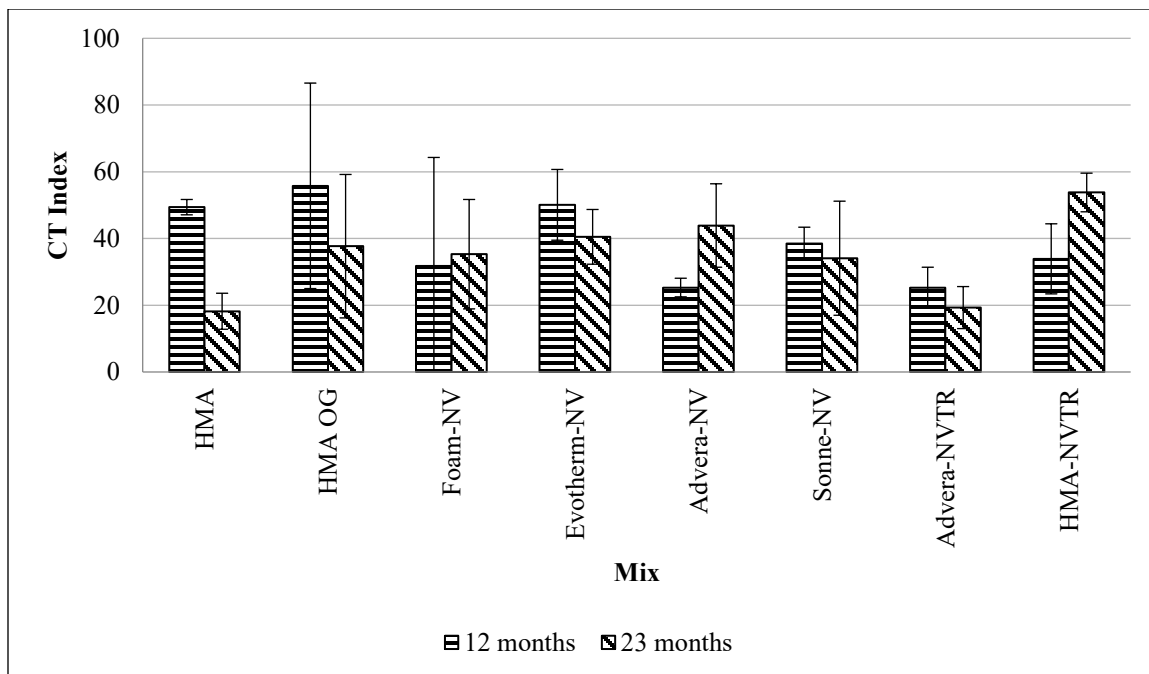


**Figure 32: CT Index values Field Cores from SPS-10**

Error bars represent the mean plus or minus the 95% confidence interval.

After testing for the IDEAL-CT, core samples were heated and loosened and tested for  $G_{mm}$  using AASHTO T 209 [35]. Air voids are calculated according to the  $G_{mm}$  obtained. Figure 32 states the air void trend of cores obtained at  $T_0$ ,  $T_6$ ,  $T_{12}$ , and  $T_{23}$  months. Error bars indicate a 95 percent confidence interval. Air voids of  $T_0$  and  $T_6$  were obtained from the previous project [33]. Error bars are not available for  $T_0$  and  $T_6$  months. Air voids observed for these mixtures with different set periods exhibit irregular trends; each mixture shows a distinct trend compared to the others. This could be because of the variability that occurred during the process of  $G_{mm}$  for getting the Air voids.

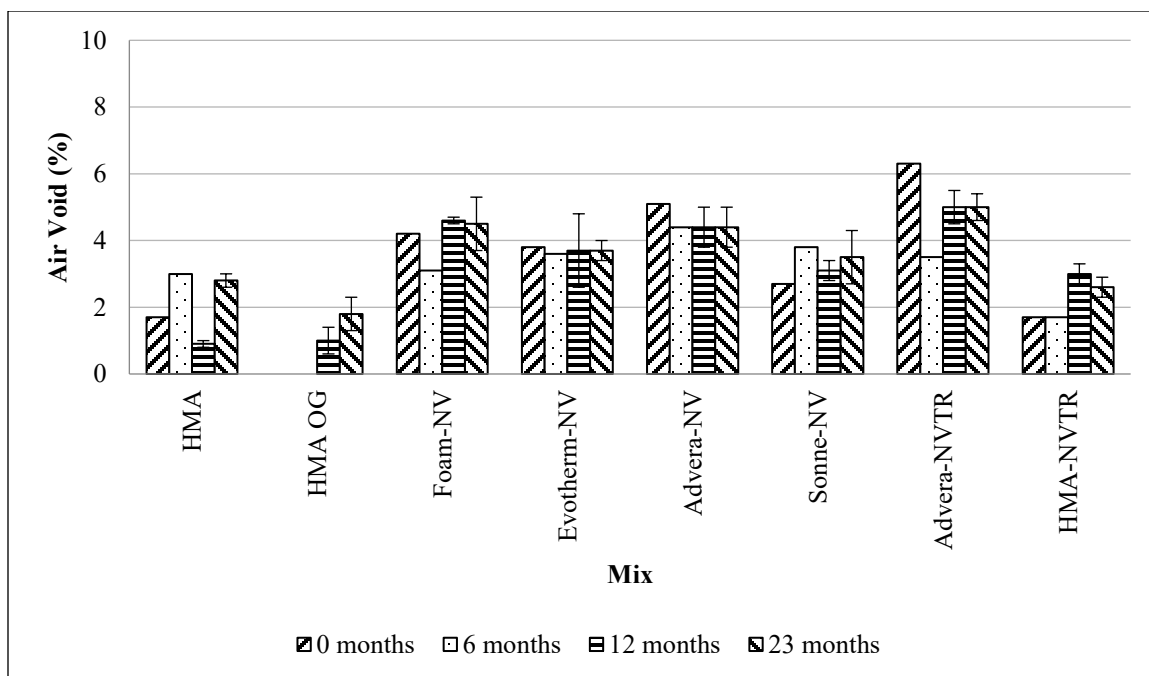


**Figure 33: Air void values field cores from SPS-10**

Error bars represent the mean plus or minus the 95% confidence interval.

Evotherm and Advera mixtures show stable air voids over time, indicating good resistance to environmental effects and traffic load. The lowest air voids were observed in HMA and HMA OG, showing high compaction due to traffic load.

Table 9 states the  $G_{mm}$  of cores along with field mixture data. When determining the  $G_{mm}$  for the field cores, all the cut aggregates from the cores were removed before starting the test. This removal could cause the  $G_{mm}$  values not to align with the field mixture data. Most of the mixtures showed a slight difference between them.

**Table 9: Gmm values for Field cores and Field mixture**

<b>Mixture</b>	<b>Average G<sub>mm</sub> from the cores</b>	<b>G<sub>mm</sub> from plant mixtures</b>
HMA	2.516	2.529
Foam-NV	2.515	2.521
Evotherm-NV	2.501	2.512
HMA Open grade Overlay	2.507	2.529
Sonne-NV	2.509	2.545
Advera-NV	2.515	2.522
Advera-NVTR	2.522	2.523
HMA-NVTR	2.518	2.526

### ***5.3.2 Reheated Plant Mix Lab Compacted (RPLMC) for SPS-10***

The plant mix obtained from the LTPP storage is used for making SGC and Hveem compacted specimens, targeting  $7\pm 0.5$  percent and  $7\pm 1$  percent air voids, respectively. Both types of compactions were also targeted with in place air voids, matching with field core air voids. Figure 34 illustrates CT Index values of SGC and Hveem specimens.

The CT Index of SGC specimens was lower than that of Hveem compacted specimens. This difference occurred because of the compaction method and the change in diameter. In the Foam mixture, a steep drop of CT index is observed for the SGC specimen when the air void decreases, but for the Hveem specimen drop is less. This explains that the CT index is less sensitive to changes in the air voids for Hveem compacted specimens. The lowest CT index was observed for Advera-NVTR SGC samples, which indicates low cracking performance. For all the mixes, SGC specimens, with 7 percent exhibit a similar visible CT index.

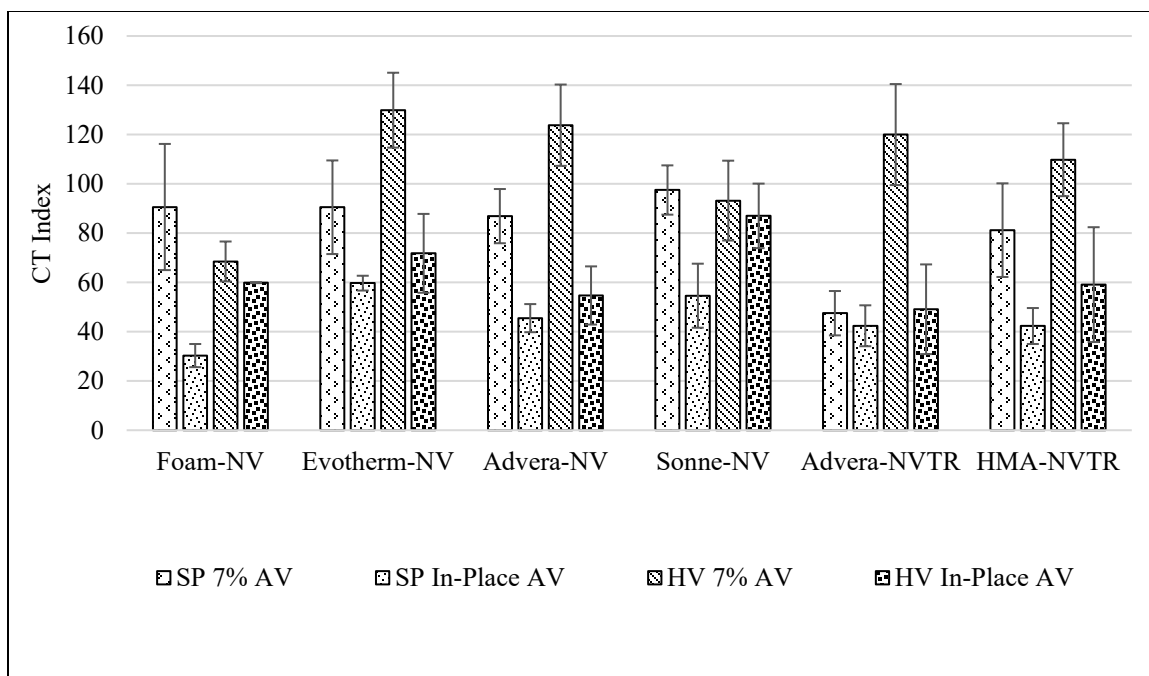


**Figure 34: RPLC CT Index for SGC and Hveem-compacted specimens**

Error bars represent the mean plus or minus the 95% confidence interval.

### 5.3.3 Analysis of Field Distress data for SPS-10

The SPS-10 project, which was constructed in 2016, has been actively monitored throughout time. Distress data have been recorded, measured, and updated yearly in the LTPP InfoPave database. This data has been collected to study how different WMA mixtures perform over service life. One of the distresses that was measured is Non-Wheel Path Longitudinal Crack (NWP), categorized into low, medium, and high severity according to the database. Figure 35 shows the combination of all severities in the NWP longitudinal crack. During 2016, distress surveys were collected before the overlay construction. The low-severity distress began appearing in 2018 among the mixtures, with the foam mixture exhibiting higher distress compared to the other mixtures. Medium-severity cracks began to appear in 2022, and Evotherm began showing higher low-severity

cracks among the mixtures. High-severity cracks began to appear recently in 2024. Higher distress was found for Evotherm, Foam, Sonne, and Advera-NVTR.

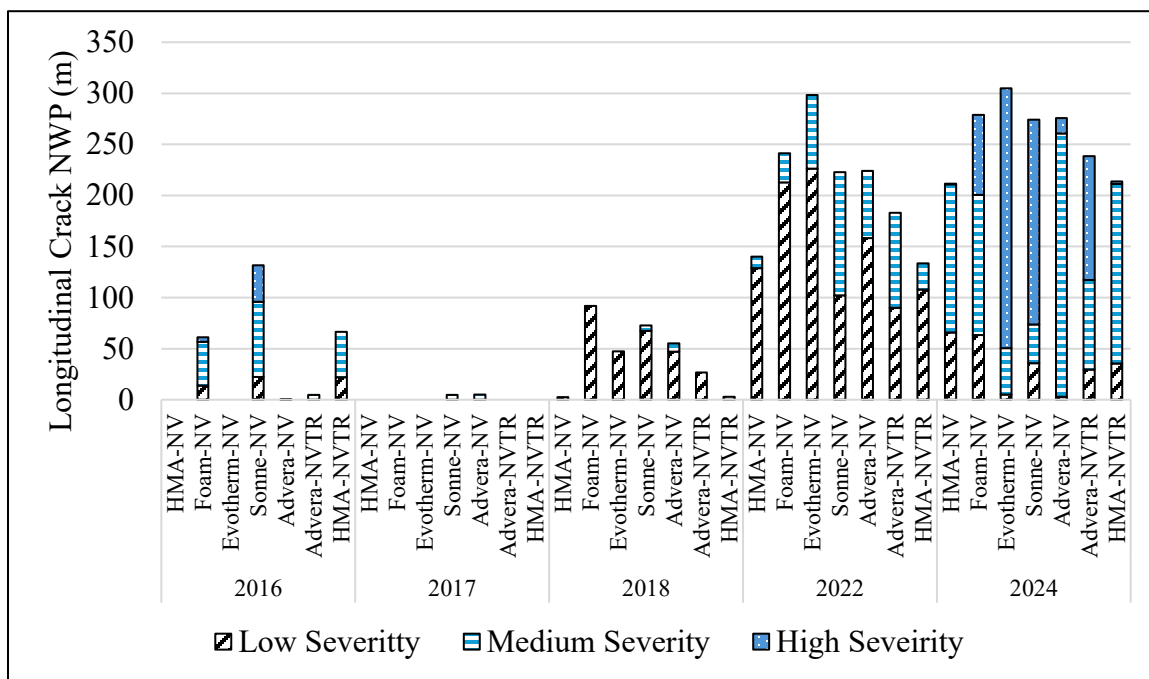


**Figure 35: Longitudinal Crack NWP combination**

The next distress considered is the wheel path crack length. Figure 35 states a cracked wheel path throughout service life. Before the construction, higher crack lengths were observed on Advera and Advera-NVTR. During 2017 and 2018, no distress was observed. Higher distress was observed for Advera in 2022; other mixtures didn't show much distress. Advera continues to exhibit higher crack lengths than other mixtures in 2024, and HMA also begins to show a certain amount of crack length. Advera and Advera-NVTR mixtures were influenced by cracks from the underlying layer before the construction, which continued throughout their service life.

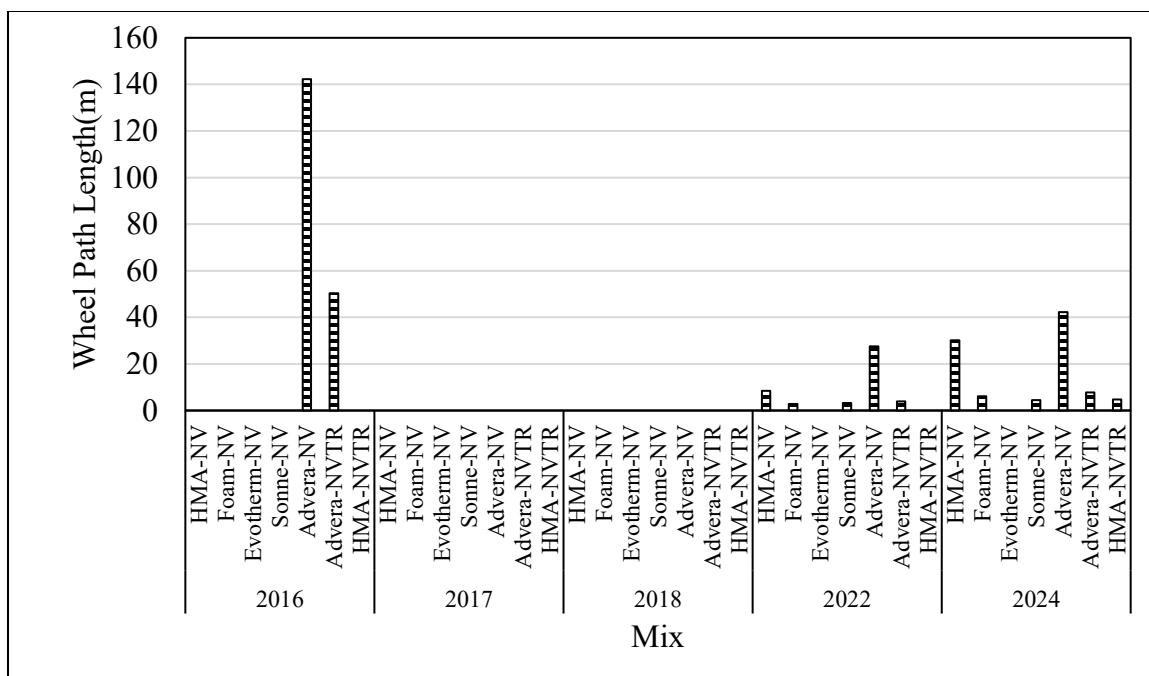


**Figure 36: Wheel path length cracks during service life**

Alligator (fatigue) cracking is another type of distress that occurs on the wheel path, measured in square meters. Figure 37 depicts Alligator cracks observed from test sections. Like wheel path cracks, Alligator cracks also showed distress on the Advera and Advera-NVTR test sections before the 2016 construction. In 2017 and 2018, no cracking was observed. Advera and Advera-NVTR exhibit a similar trend in 2022, and high-severity cracks are observed for both mixtures in 2024. These cracks are transferred from the already available layer before construction to the overlay, as observed from wheel path crack length. HMA starts showing the low-severity and high-severity cracks in 2024.

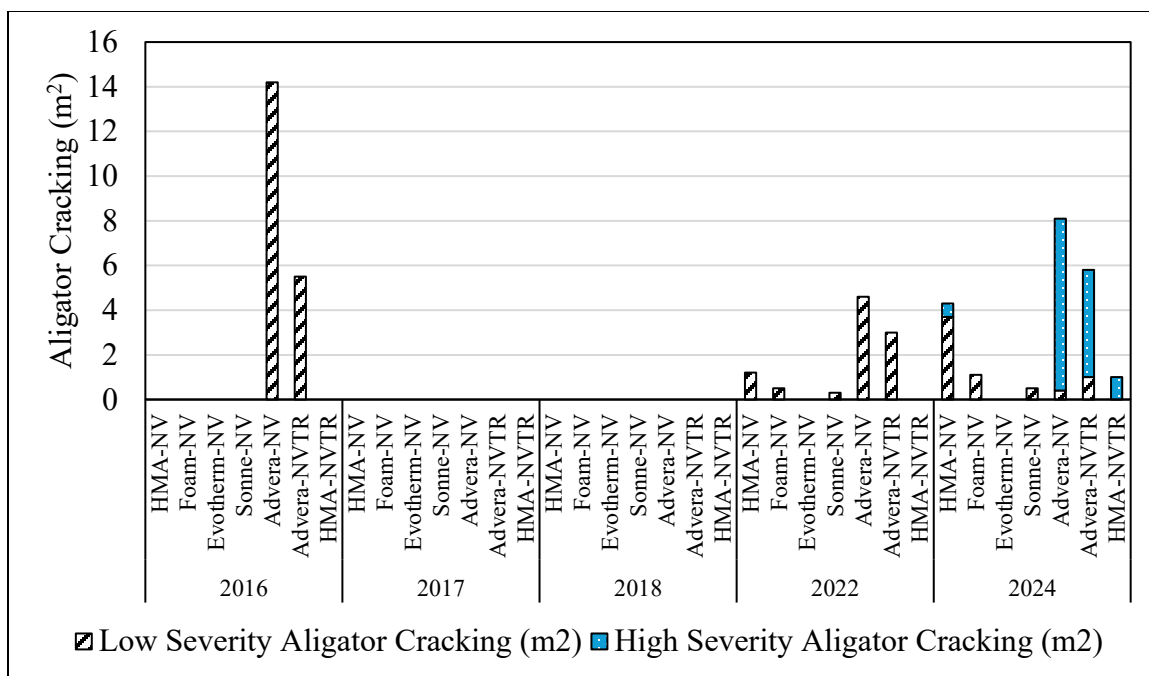


**Figure 37: Alligator cracking during the service life**

IDEAL-CT results of field cores obtained in 2017 and 2018 as of T<sub>12</sub> and T<sub>23</sub>. Distresses observed were too small during the period to compare, and no relationship could be found between field stress and CT Index. RPMLC mixtures were plotted with the field distress mentioned above, resulting in all the mixture points being dispersed across the plot. No relationship could be found between them.

#### **5.3.4 Comparison of CT Index Results with Field Performance**

As part of the validation process, RPMLC and PMFC specimens were compared with the field distress, such as longitudinal NWP crack, Wheel path crack, and alligator crack. CT index was plotted against distress. Comparison was done between the RPMLC CT Index of SP and Hveem compacted specimens and PMFC 12- and 23-month field cores CT Index with the wheel path crack length through the service years. Figures 39 and 40 illustrate

RPMLC Hveem CT index comparison with NWP longitudinal crack. Other plots are included in the Appendix of the thesis.

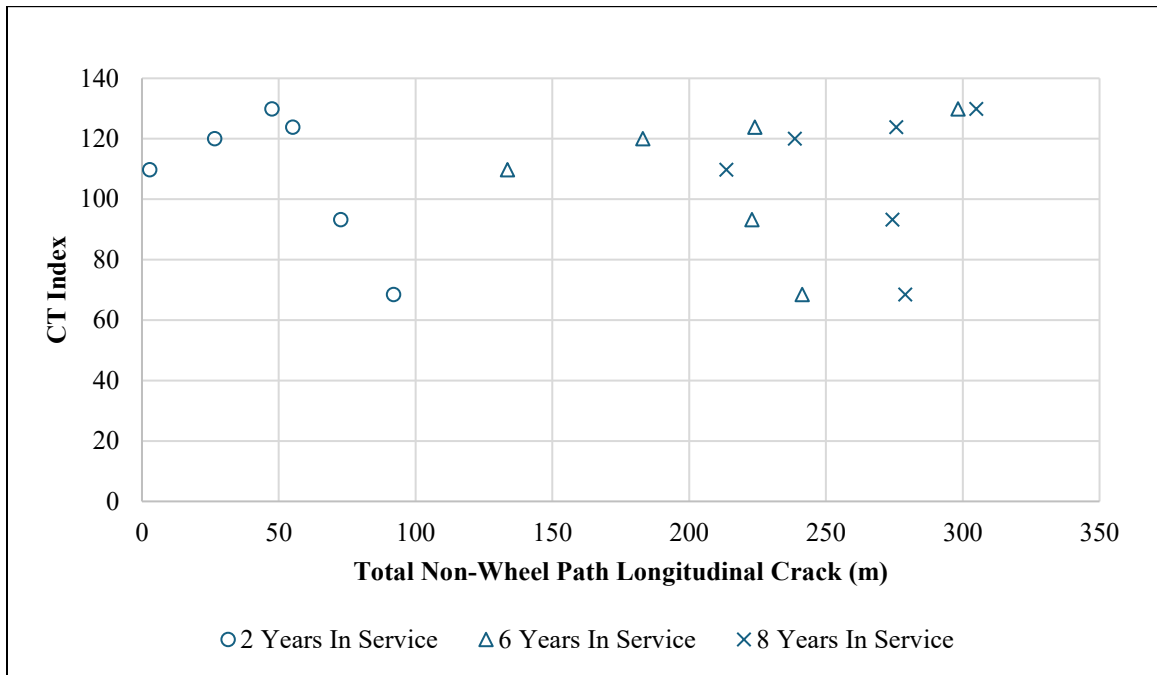


**Figure 38: Comparison of RPMLC HV with 7% AV CT Index and NWP longitudinal crack throughout the service years**

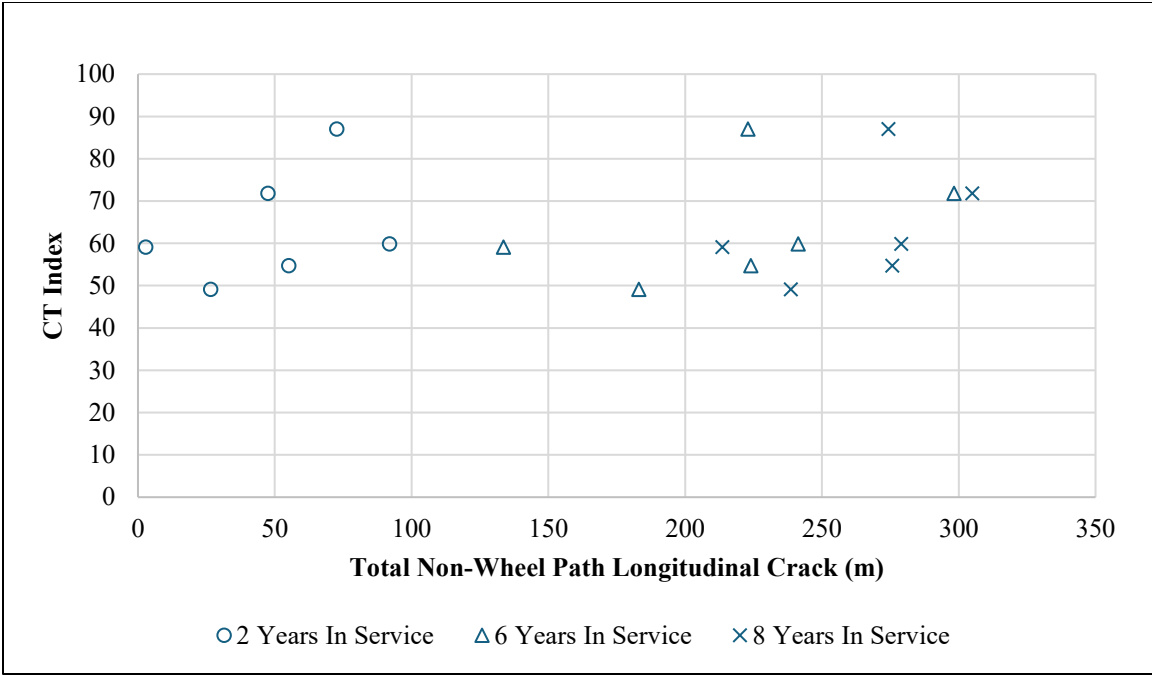


**Figure 39: Comparison of RPMLC HV with In-Place AV CT Index and NWP longitudinal crack throughout service years.**

In general, no clear relationship was found between the CT Index and the NWP path longitudinal cracks. A slight trend was observed for the Hveem compacted specimens with 7 percent air void and the NWP longitudinal cracking after 2 years of service.

Figures 41 and 42 show the RPMLC CT Index of the Hveem compacted specimens as a function of the wheel path crack length at the various service years. There is no relationship found between the CT Index values and the associated wheel path crack data.

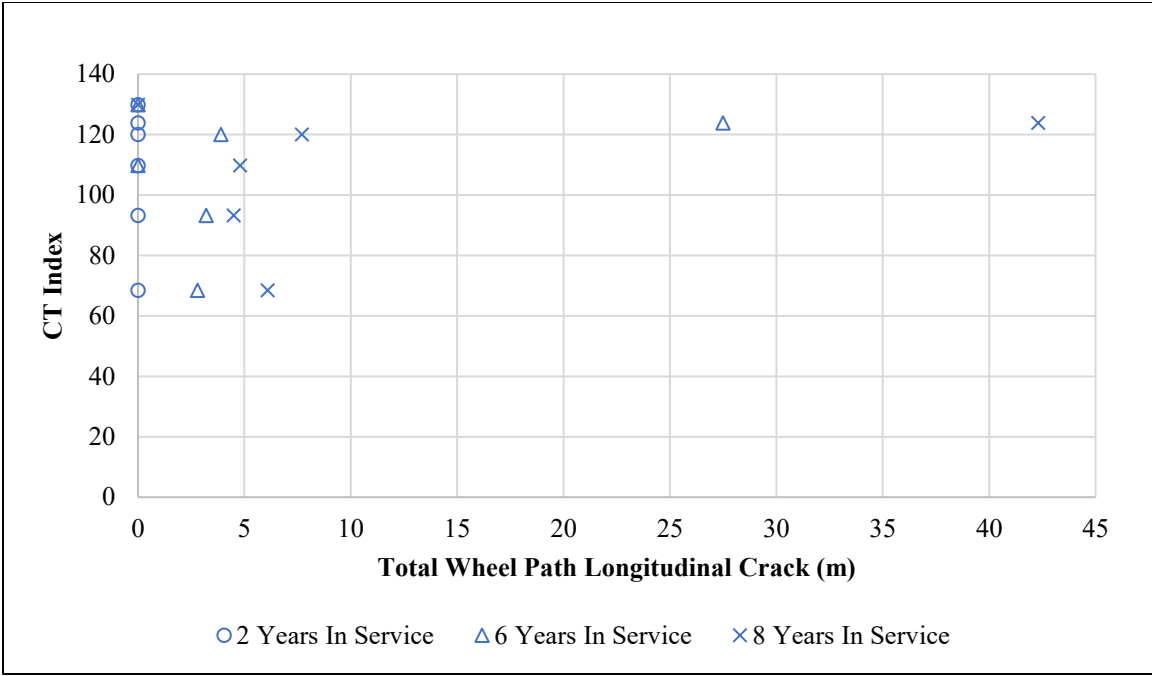


Figure 40: Comparison of RPMLC HV with 7% AV CT Index and Wheel path crack length throughout service years.

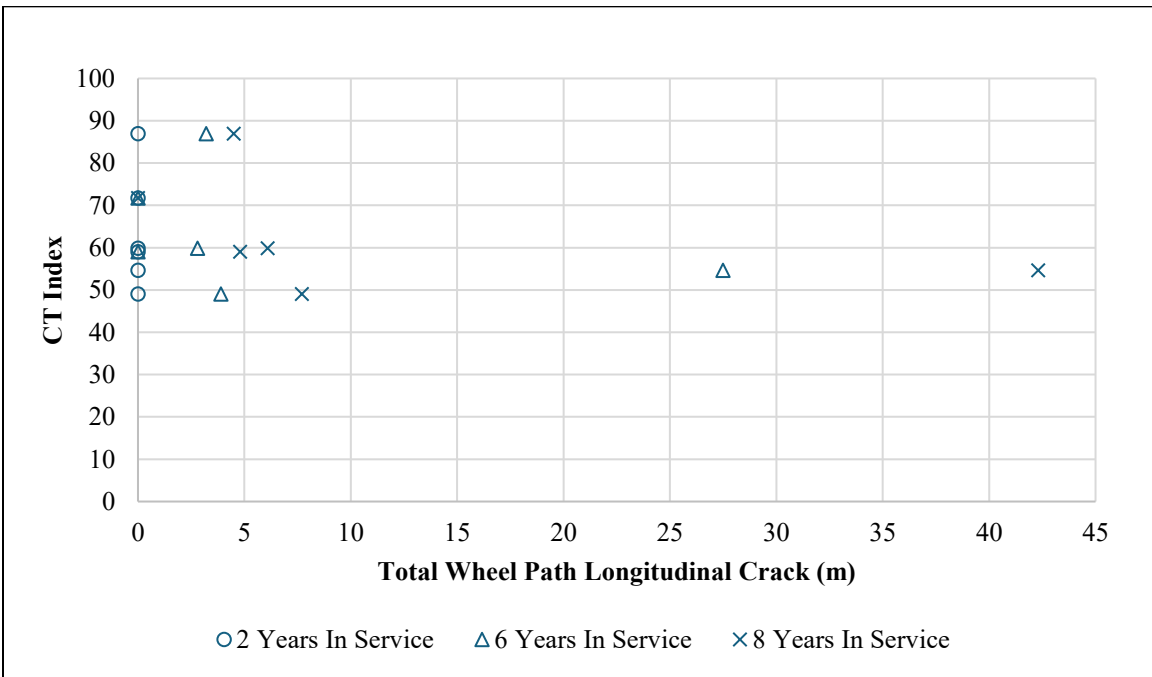
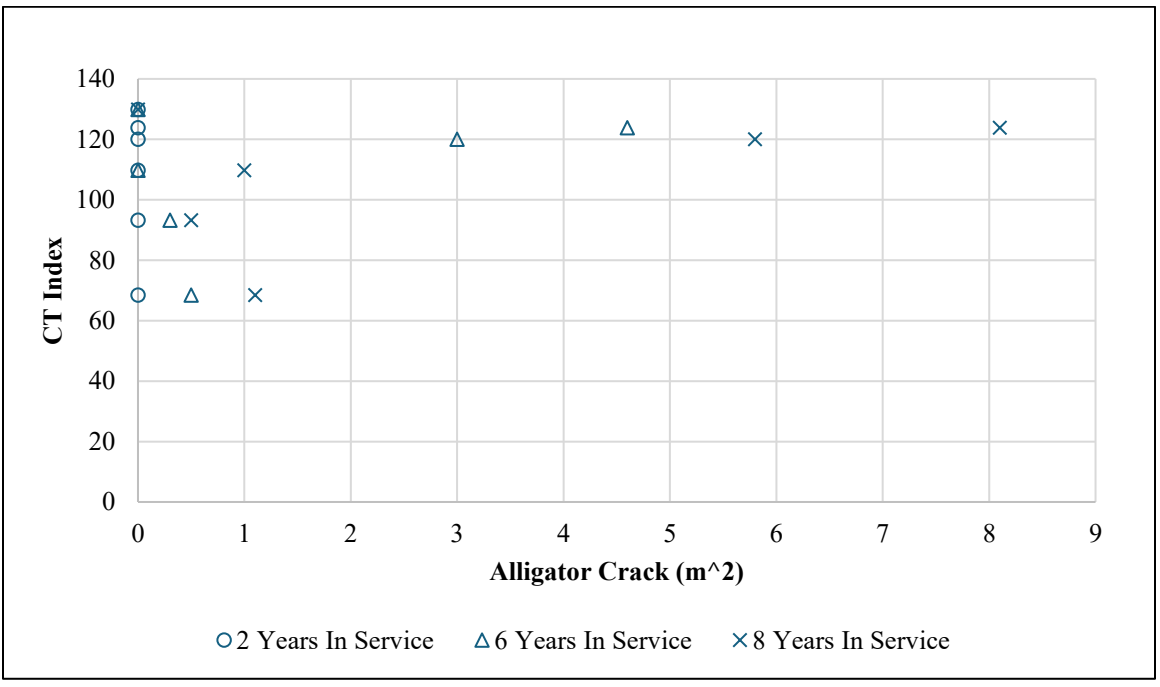
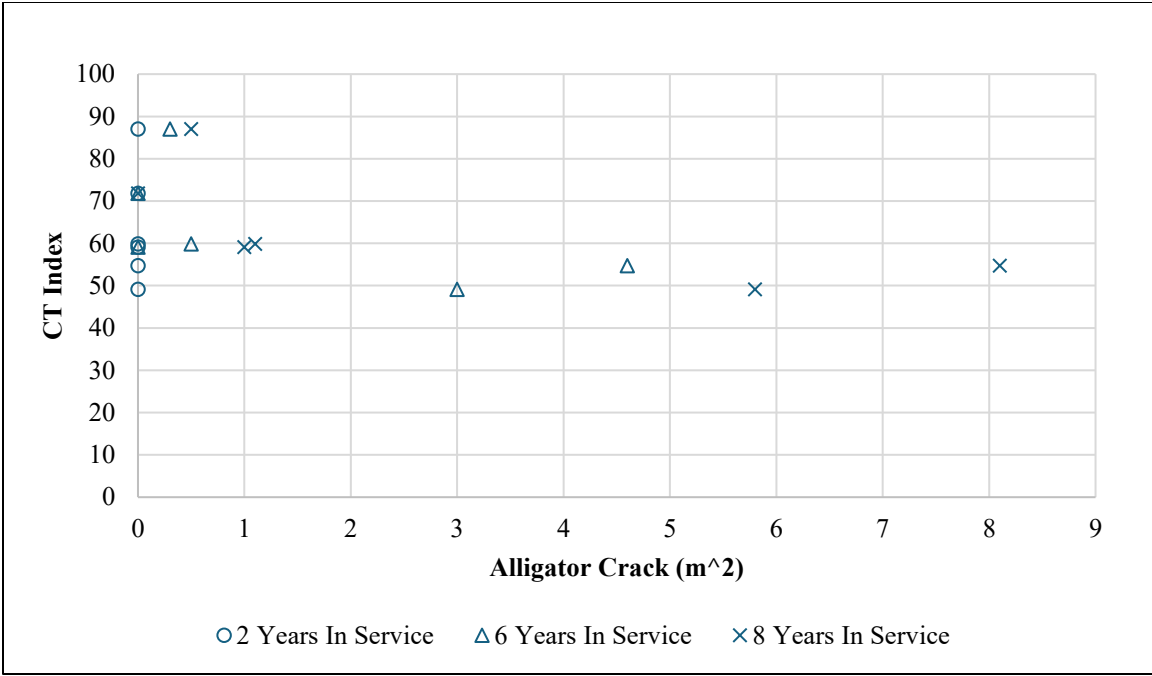


Figure 41: Comparison of RPMLC HV with In-place AV CT Index and Wheel path crack length throughout service years

Figures 42 and 43 illustrate the RPMLC CT Index of the Hveem compacted specimens as a function of the alligator crack at the various service years. There is no relationship found between the CT Index values and the associated alligator crack.



**Figure 42: Comparison of RPMLC HV with 7% AV CT Index and Alligator crack throughout service years**



**Figure 43: Comparison of RPMLC HV with In-Place AV CT Index and Alligator crack throughout service years**

Overall, no clear relationship was observed between RPMLC SP and Hveem-compacted specimens and PMFC field cores in relation to field distresses over the service years. This may be attributed to the fact that the Advera and Advera-NVTR mixture sections had already exhibited cracking prior to the overlay construction, which is reflected in the current distress conditions.

## Chapter 6: Conclusions, Findings, and Recommendations

The purpose of this study was to evaluate the IDEAL-CT test on Hveem-compacted asphalt mixture specimens from Nevada and compare the results to those from SGC-compacted specimens. The research also examined the effects of specimen diameter and compaction method on IDEAL-CT values. Additionally, it analyzed the cracking performance of WMA test sections based on both plant mixtures and field cores over time in relation to field distress, to determine whether a potential correlation exists between IDEAL-CT results and observed field distress.

### 6.1 Conclusion

**IDEAL-CT Applicability to Hveem Compacted Samples:** IDEAL-CT can be effectively modified to test Hveem compacted specimens, demonstrating its suitability for more general use in NDOT's mix design method. Required adjustments in loading strip thickness, height, and curvature played a key role in obtaining consistent results on smaller diameter samples.

**Influence of Compaction Method and Sample Diameter:** IDEAL-CT parameters, such as CT Index,  $m_{75}$ ,  $l_{75}$ , peak load, and fracture energy, show notable differences between SGC and Hveem compacted specimens. Diameters of 150 mm and 100 mm/101.6 mm also affect the CT Index parameters.

For Type 2 Gradation, the CT Index tends to increase when moving from a 150 mm to a 100 mm SGC specimen and continues to increase for Hveem compacted samples. Type 3 gradation exhibits a larger CT Index and fractured energy than Type 2, indicating better

cracking resistance. Specimens with smaller diameters exhibit higher tensile strength due to their dimensions, while larger diameter samples allow for higher deformation before failure.

**Sensitivity of CT Index to Mix Design Parameters:** IDEAL-CT was found to be sensitive to variations in asphalt mixture composition, such as binder content and gradations. Increasing and reducing the binder content tend to produce higher and lower CT Index values, respectively, suggesting that CT index of Hveem compacted specimens was sensitive to binder content.

**Moisture Sensitivity:** The TSR (T 283) for Type 2 and Type 3 gradation meets the Nevada DOT's requirement for moisture resistance ( $TSR \geq 70$  percent). Interestingly, the reduction in the tensile strength caused by one freeze-thaw cycle in the AASHTO T 283 test was not significantly different from the decrease in tensile strength in the MiST test after 3500 cycles, which implies identical moisture damage. The unconditioned IDEAL-CT tensile strength population means is significantly different from the unconditioned T 283 tensile strength because of different aging effects.

**Laboratory Performance of SPS-10 Mixtures:** The Field Core tested for IDEAL-CT indicated different trends in the CT Index over time. Most mixtures exhibit a decreasing trend from  $T_{12}$  and  $T_{23}$ , indicating an anticipated aging effect. There were mixtures, such as Foam, Advera, and HMA-NVTR, that showed an irregular trend of increasing CT Index due to mixture variability and the effect of WMA additives. RPMLC mix Hveem compacted specimens show higher CT Index than SP compacted specimens.

**Comparison Between CT Index and Field Performance:** RPMLC SP and Hveem compacted, and PMFC field cores CT Index didn't show any relationship between field distress throughout the service life.

## 6.2 Findings

- The effective modification of the IDEAL-CT testing machine to accommodate 100 mm and 101.6 mm diameter samples plays a vital role in improving the repeatability and reproducibility of the CT Index.
- Hveem-compacted specimens tend to exhibit different cracking performance compared to SGC-compacted specimens, even when using the same aggregate gradation and binder. The kneading action of the California Kneading Compactor alters the internal aggregate structure differently from the SGC, which subsequently affects the mixture's cracking performance.
- The increasing trend in CT Index with higher binder content for Hveem-compacted specimens highlights the significant influence of binder content on the cracking resistance of the mixture.
- While lime-treated aggregates typically perform well with TSR values approaching 100%, the TSR of Hveem-compacted samples is closer to the minimum requirements set by the Nevada DOT. This suggests that the compaction method can influence the results of moisture sensitivity testing.
- The CT Index decreases with field aging and as air voids are reduced.
- No clear relationship was observed between the CT Index of RPMLC and PMFC samples and the actual field distresses.

### 6.3 Recommendation

- Due to the unique characteristics of Hveem-compacted samples, it is recommended that the Nevada DOT develop a dedicated IDEAL-CT test method and establish specific acceptance criteria or thresholds. This will support the full integration of IDEAL-CT into the mix design requirements for Hveem-compacted mixtures.
- Further research is needed to investigate the microstructure and aggregate–binder interactions in SGC- and Hveem-compacted specimens. This may involve advanced image analysis techniques during or after testing.
- Continued refinement of the loading strip design for 100 mm and 101.6 mm diameter samples is necessary to ensure proper stress distribution, taking into account mixture type and gradation.
- Ongoing monitoring of the LTPP SPS-10 test sections is crucial. Long-term field distress data should continue to be collected, and additional field cores should be extracted and tested for the CT Index to help establish a correlation between lab-measured CT Index values and actual field performance.

## References

- [1] American Association of State Highway and Transportation Officials. (2022). AASHTO T 245-22: Resistance to plastic flow of bituminous mixtures using Marshall apparatus. Washington, DC: AASHTO.
- [2] Nevada Department of Transportation. (n.d.). T303D: Method of Test for Stabilometer Value of Bituminous Paving Mixtures. In Materials Test Manual. Carson City, NV: Nevada Department of Transportation.
- [3] Federal Highway Administration. (n.d.). The history and future challenges of gyratory compaction 1939 to present [Online]. U.S. Department of Transportation. Retrieved June 8, 2025, from <https://www.fhwa.dot.gov/publications/research/infrastructure/pavements/asphalt/labs/mixtures/hisofgyratory/index.cfm>
- [4] American Association of State Highway and Transportation Officials. (2022). *Standard specification for Superpave volumetric mix design (AASHTO M 323-22)*. Washington, DC: AASHTO.
- [5] Nevada Department of Transportation. (2014). Standard specifications for road and bridge construction (Test Method Nev. T303D). Carson City, NV: Nevada Department of Transportation. <https://www.dot.nv.gov>
- [6] West, R., Rodezno, C., & Taylor, A. (2018). A Proposed Framework for Balanced Mix Design (BMD). National Center for Asphalt Technology (NCAT) Report 18-06.

- [7] ASTM International. (2019). ASTM D8225-19 Standard Test Method for Indirect Tensile Asphalt Cracking Test (IDEAL-CT) of Asphalt Mixtures. West Conshohocken, PA: ASTM International.
- [8] National Asphalt Pavement Association. (n.d.). Implementation efforts. In *Balanced Mix Design Resource Guide*. Retrieved August 8, 2025, from <https://www.asphaltpavement.org/expertise/engineering/resources/bmd-resource-guide/implementation-efforts>
- [9] Airey, G. D., & Collop, A. C. (2014). Mechanical and structural assessment of laboratory- and field-compacted asphalt mixtures. *Journal of Materials in Civil Engineering*, 26(5), 04014029.
- [10] State of Nevada Department of Transportation, Materials Division. (2005). *Method of Test for Resistance of Compacted Bituminous Mixture to Moisture-Induced Damage (Lottman) (Test Method Nev. T341D)*. Carson City, NV.
- [11] National Cooperative Highway Research Program. (2004). NCHRP Report 530: Evaluation of indirect tensile test to identify asphalt concrete performance criteria. Transportation Research Board.
- [12] Federal Highway Administration. (n.d.). LTPP InfoPave. In *Long-Term Pavement Performance (LTPP) program*. Retrieved August 13, 2025, from <https://infopave.fhwa.dot.gov/>
- [13] Zhou, F., & West, K. (2023, May–June). Indirect tension asphalt cracking test: Ensuring asphalt mix designs for durable pavements. *TR News*, (345), 32–34.

[14] Gavadakatla, V., Dangi, J., & Singh, D. (2024). Rutting and cracking performance of asphalt mixtures for 150 mm and 100 mm diameter samples using simple performance tests. *Journal of Materials in Civil Engineering*, 36(10), 04024307. <https://doi.org/10.1061/JMCEE7.MTENG-17802>.

[15] ASTM International. (2017). ASTM D6931-17: Standard Test Method for Indirect Tensile (IDT) Strength of Bituminous Mixtures. West Conshohocken, PA: ASTM International.

[16] ASTM International. (2022). ASTM D8360-22: Standard Test Method for Indirect Tensile Asphalt Layer-Rutting Test (IDEAL-RT) of Asphalt Mixtures. West Conshohocken, PA: ASTM International.

[17] Brown, E. R., & Bassett, C. E. (1990). Effects of maximum aggregate size on rutting potential and other properties of asphalt-aggregate mixtures. *Transportation Research Record*, 1259, 107–119.

[18] Kandhal, P. S., & Brown, E. R. (1990). *Comparative evaluation of 4-inch and 6-inch diameter specimens for testing large stone asphalt mixes* (Tech. Rep. rep90-05). National Center for Asphalt Technology. <https://doi.org/10.21949/1404492>

[19] Montañez, J., Martin, A. E., & Arámbula-Mercado, E. (2023). Development and verification of CT Index correction methods to normalize air void content and thickness of field cores. *Transportation Research Record*, 2677(9), 478–488. <https://doi.org/10.1177/03611981231159402>.

- [20] Zhou, F., Im, S., & Hu, S. (2019). Development and validation of the IDEAL cracking test. In *Transportation Research Circular E-C251: Relationship Between Laboratory Cracking Tests and Field Performance of Asphalt Mixtures* (pp. 1–21). Transportation Research Board. <https://onlinepubs.trb.org/onlinepubs/circulars/ec251.pdf>
- [21] Golalipour, A., Veginati, V., & Mensching, D. J. (2021). Evaluation of asphalt mixture performance using cracking and durability tests at a full-scale pavement facility. *Transportation Research Record: Journal of the Transportation Research Board*, 2675(11), 226–236. <https://doi.org/10.1177/03611981211021856>
- [22] Boz, I., Habbouche, J., Bilgic, Y., & others. (2022). Precision estimates and statements for performance indices from the indirect tensile cracking test at intermediate temperature. *Transportation Research Record*, 2676(5), 505–518. <https://doi.org/10.1177/03611981211061129>
- [23] Zhou, F., Im, S., Sun, L., & Scullion, T. (2017). Development of an IDEAL cracking test for asphalt mix design and QC/QA. *Road Materials and Pavement Design*, 18(suppl. 4), 405–427. <https://doi.org/10.1080/14680629.2017.1389082>
- [24] Zhou, F. (2021). Implementation of the IDEAL Cracking Test for asphalt mix design and QC/QA (NCHRP Project 20-44(16)). National Cooperative Highway Research Program, Transportation Research Board, National Academies of Sciences, Engineering, and Medicine. <https://doi.org/10.17226/26445>
- [25] Romero-Zambrana, P. (2023). Variability of the IDEAL-CT test for pavement cracking to achieve a balanced asphalt mix design (MPC 23-492). Mountain-Plains Consortium. <https://www.ugpti.org/resources/reports/downloads/mpc23-492.pdf>

- [26] Leavitt, N. Z., Tran, N., Arambula, E., & Martin, A. E. (2024). Model for evaluating cracking performance of asphalt pavements with field aging based on IDEAL-CT. Transportation Research Record. <https://doi.org/10.1177/03611981241252521>
- [27] Chen, C., & Rodezno, C. (2025). Differences in lab-prepared vs. plant-produced asphalt mixtures using IDEAL-CT. National Center for Asphalt Technology. Retrieved from NCAT website.
- [28] Zhou, F., Hu, S., & Newcomb, D. (2023). Ruggedness of laboratory tests to assess cracking resistance of asphalt mixtures (NCHRP Web-Only Document 389). Transportation Research Board, National Academies of Sciences, Engineering, and Medicine. <https://doi.org/10.17226/27421>
- [29] Badreddine, N. (2024). Analysis of fine asphalt concrete mixture gradations from various sources to enhance durability (Master's thesis, University of Nevada, Reno). University of Nevada, Reno.
- [30] Nevada Department of Transportation "Standard Specifications for Road and Bridge Construction", 2014.
- [31] National Asphalt Pavement Association. (2024). Asphalt pavement industry survey on recycled materials and warm-mix asphalt usage: 2023 construction season (Information Series No. 138). National Asphalt Pavement Association. Retrieved August 8, 2025, from <https://go.asphaltpavement.org/is-138>
- [32] Texas Department of Transportation. (2019). Tex-248-F: Overlay test (Effective July 2019 – June 2021) [Test procedure]. Texas Department of Transportation, from [https://ftp.dot.state.tx.us/pub/txdot-info/cst/TMS/200-F\\_series/archives/248-0719.pdf](https://ftp.dot.state.tx.us/pub/txdot-info/cst/TMS/200-F_series/archives/248-0719.pdf)

- [33] ASTM International. (2020). ASTM D8303-20: Standard test method for determining thermal cracking properties of asphalt mixtures through measurement of thermally induced stress and strain. ASTM International. <https://doi.org/10.1520/D8303-20>
- [34] Nimeri, M. A., Morian, N. E., Hand, A. J. T., Hajj, E. Y., & Sebaaly, P. E. (2017). Evaluation of mixtures from LTPP SPS-10 warm mix asphalt (WMA) sections: NDOT contract no. 3598 – Project no. STP-580-1(032) (Final report). Western Regional Superpave Center, Department of Civil & Environmental Engineering, University of Nevada, Reno.
- [35] “Test method Nev. T303D-Method of test for Stabilometer value of Bituminous Paving Mixtures,” 2005, Nevada Department of Transportation.
- [36] American Association of State Highway and Transportation Officials. (2022). AASHTO T 247: Standard Method of Test for Preparation of Test Specimens of Hot Mix Asphalt (HMA) by Means of California Kneading Compactor. Washington, DC: AASHTO.
- [37] Brown, E. R., & Buckman, M. S. (1998). NCHRP Report 9-9: Evaluation of the Superpave Gyrotory Compaction Procedure. National Cooperative Highway Research Program, Transportation Research Board.
- [38] ASTM International. (2023). ASTM D6925-23: Standard test method for preparation and determination of the relative density of asphalt mix specimens by means of the Superpave gyrotory compactor. ASTM International. <https://doi.org/10.1520/D6925-23>

[39] American Association of State Highway and Transportation Officials (AASHTO T209), "Standard Method of Test for Theoretical Maximum Specific Gravity (Gmm) and Density of Asphalt Mixtures," Washington, DC, 2020.

[40] American Association of State Highway and Transportation Officials. (2019). AASHTO R 47: Standard Practice for Reducing Samples of Hot Mix Asphalt (HMA) to Testing Size by Means of Mechanical Splitting and Quartering. Washington, DC: AASHTO.

[41] American Association of State Highway and Transportation Officials. (2024). AASHTO T 164-24: Quantitative extraction of asphalt binder from hot mix asphalt. Washington, DC: AASHTO.

[42] American Association of State Highway and Transportation Officials. (2023). AASHTO T 319-22: Standard method of test for quantitative extraction and recovery of asphalt binder from asphalt mixtures using accelerated solvent extraction. Washington, DC: AASHTO.

[43] American Association of State Highway and Transportation Officials. (2023). AASHTO T 27-24: Standard method of test for sieve analysis of fine and coarse aggregates. Washington, DC: AASHTO.

[44] American Association of State Highway and Transportation Officials. (2024). Standard method of test for mechanical analysis of extracted aggregate (AASHTO T 30-24). Washington, DC: AASHTO.

[45] American Association of State Highway and Transportation Officials. (2024). Standard method of test for determining the rheological properties of asphalt binder using a dynamic shear rheometer (DSR) (AASHTO T 315-24). Washington, DC: AASHTO.

[46] American Association of State Highway and Transportation Officials. (2022). Standard method of test for resistance of compacted asphalt mixtures to moisture-induced damage (AASHTO T 283-22). Washington, DC: AASHTO.

[47] American Association of State Highway and Transportation Officials. (2024). Standard method of test for moisture sensitivity using hydrostatic pore pressure to determine cohesion and adhesion strength of compacted asphalt mixture specimens (AASHTO Designation: TP 140-22). Washington, D.C.: AASHTO.

## Appendix

**Table A- 1: Gradation for Gradation 1**

<b>Gradation-01</b>				
<b>Sieve size</b>			<b>Passing %</b>	<b>Retained %</b>
<b>0.45 power</b>	<b>US</b>	<b>SI (mm)</b>		
4.3	1"	25	100.0	0.0
3.8	3/4"	19	91.9	8.4
3.1	1/2"	12.5	72.5	25.2
2.8	3/8"	9.5	64.1	8.3
2.0	#4	4.75	54.0	6
1.5	#8	2.36	39.6	14.2
1.4	#10	2	36.2	4.6
1.1	#16	1.18	27.6	9.3
0.8	#30	0.6	18.7	10.3
0.7	#40	0.425	14.9	4.2
0.6	#50	0.3	11.7	3.9
0.4	#100	0.15	7.2	2.6
0.3	#200	0.075	5.0	1.3
0.0	Pan	0	0.0	1.7

**Table A- 2: Gradation of Gradation 04**

<b>Gradation-04</b>				
<b>Sieve size</b>			<b>Passing %</b>	<b>Retained %</b>
<b>0.45 power</b>	<b>US</b>	<b>SI (mm)</b>		
4.257	1"	25	100.0	0
3.762	3/4"	19	100.0	0
3.116	1/2"	12.5	100.0	0
2.754	3/8"	9.5	96.1	4.6
2.016	#4	4.75	72.3	22.2
1.472	#8	2.36	53.9	18.2
1.366	#10	2	49.5	5.3
1.077	#16	1.18	37.5	14.6
0.795	#30	0.6	24.6	13.5
0.68	#40	0.425	19.0	6.4
0.582	#50	0.3	14.2	6.2
0.426	#100	0.15	8.0	7.4
0.312	#200	0.075	5.3	1.2
0	Pan	0	0.0	0.4

**Table A- 3: Superpave Gyrotory 100 mm diameter and 63.5 mm height CT Index**

Sample ID	Air Voids (%)	CT Index (Machine)	CT Index (Calculation)	Average CT Index (Calculation)	STD CT Index (Calculation)	COV CT Index (Calculation)	95% CI CT Index (Calculation)
<b>T2/T2C (1st trial)</b>							
T21(1)_S4_63.5_NH	6.9	117.3	119.5	<b>82.6</b>	<b>30.83</b>	<b>37.3</b>	<b>27.0</b>
T22(1)_S4_63.5_NH	7.7	105.1	102.9				
T23(1)_S4_63.5_NH	7.5	38.6	39.0				
T24(1)_S4_63.5_NH	6.7	81.6	80.3				
T25(1)_S4_63.5_NH	8.0	73.0	71.5				
<b>T3</b>							
T31(1)_S4_63.5_NH	7.3	52.0	51.2	<b>53.6</b>	<b>6.27</b>	<b>11.7</b>	<b>5.5</b>
T32(1)_S4_63.5_NH	7.3	47.7	47.1				
T33(1)_S4_63.5_NH	7.5	49.7	49.7				
T34(1)_S4_63.5_NH	7.2	58.4	57.9				
T35(1)_S4_63.5_NH	7.4	60.7	62.3				

**Table A- 4: Superpave Gyrotory 100 mm diameter and 63.5 mm height m value**

Sample ID	Air Voids (%)	CT Index (Calculation)	m Value (kN/mm)	Average	STD	COV	95%
<b>T2/T2C (1st trial)</b>							
T21(1)_S4_63.5_NH	6.9	119.5	2.05	<b>2.31</b>	<b>0.44</b>	<b>18.9</b>	<b>0.4</b>
T22(1)_S4_63.5_NH	7.7	102.9	1.85				
T23(1)_S4_63.5_NH	7.5	39.0	2.92				
T24(1)_S4_63.5_NH	6.7	80.3	2.13				
T25(1)_S4_63.5_NH	8.0	71.5	2.58				
<b>T3</b>							
T31(1)_S4_63.5_NH	7.3	51.2	3.17	<b>3.10</b>	<b>0.25</b>	<b>8.0</b>	<b>0.2</b>
T32(1)_S4_63.5_NH	7.3	47.1	3.36				
T33(1)_S4_63.5_NH	7.5	49.7	3.28				
T34(1)_S4_63.5_NH	7.2	57.9	2.93				
T35(1)_S4_63.5_NH	7.4	62.3	2.77				

**Table A- 5: Superpave Gyratory 100 mm diameter and 63.5 mm height I value**

Sample ID	Air Voids (%)	CT Index (Calculation)	I-value (mm)	Average	STD	COV	95 % CI
<b>T2/T2C (1st trial)</b>							
T21(1)_S4_63.5_NH	6.9	119.5	3.332	<b>2.972</b>	<b>0.33</b>	<b>11.0</b>	<b>0.3</b>
T22(1)_S4_63.5_NH	7.7	102.9	3.118				
T23(1)_S4_63.5_NH	7.5	39.0	2.457				
T24(1)_S4_63.5_NH	6.7	80.3	2.901				
T25(1)_S4_63.5_NH	8.0	71.5	3.053				
<b>T3</b>							
T31(1)_S4_63.5_NH	7.3	51.2	2.821	<b>2.966</b>	<b>0.09</b>	<b>3.0</b>	<b>0.1</b>
T32(1)_S4_63.5_NH	7.3	47.1	3.023				
T33(1)_S4_63.5_NH	7.5	49.7	2.990				
T34(1)_S4_63.5_NH	7.2	57.9	2.946				
T35(1)_S4_63.5_NH	7.4	62.3	3.052				

**Table A- 6: Superpave Gyrotory 100 mm diameter and 63.5 mm height I/m value**

Sample ID	Air Voids (%)	CT Index (Calculation)	I/m value (mm <sup>2</sup> /kN)	Average	STD	COV	95% CI
<b>T2/T2C (1st trial)</b>							
T21(1)_S4_63.5_NH	6.9	119.5	1.625	<b>1.340</b>	<b>0.35</b>	<b>25.7</b>	<b>0.3</b>
T22(1)_S4_63.5_NH	7.7	102.9	1.689				
T23(1)_S4_63.5_NH	7.5	39.0	0.842				
T24(1)_S4_63.5_NH	6.7	80.3	1.361				
T25(1)_S4_63.5_NH	8.0	71.5	1.183				
<b>T3</b>							
T31(1)_S4_63.5_NH	7.3	51.2	0.889	<b>0.961</b>	<b>0.09</b>	<b>9.5</b>	<b>0.1</b>
T32(1)_S4_63.5_NH	7.3	47.1	0.899				
T33(1)_S4_63.5_NH	7.5	49.7	0.910				
T34(1)_S4_63.5_NH	7.2	57.9	1.006				
T35(1)_S4_63.5_NH	7.4	62.3	1.102				

**Table A- 7: Superpave Gyratory 100 mm diameter and 63.5 mm height Peak Load**

Sample ID	Air Voids (%)	CT Index (Calculation )	Peak Load (kN)	Average	STD	COV	95 % CI
<b>T2/T2C (1st trial)</b>							
T21(1)_S4_63.5 NH	6.9	119.5	9.866	<b>9.361</b>	<b>0.38</b>	<b>4.1</b>	<b>0.3</b>
T22(1)_S4_63.5 NH	7.7	102.9	8.900				
T23(1)_S4_63.5 NH	7.5	39.0	9.200				
T24(1)_S4_63.5 NH	6.7	80.3	9.625				
T25(1)_S4_63.5 NH	8.0	71.5	9.213				
<b>T3</b>							
T31(1)_S4_63.5 NH	7.3	51.2	10.409	<b>10.012</b>	<b>0.36</b>	<b>3.6</b>	<b>0.3</b>
T32(1)_S4_63.5 NH	7.3	47.1	9.631				
T33(1)_S4_63.5 NH	7.5	49.7	9.999				
T34(1)_S4_63.5 NH	7.2	57.9	10.331				
T35(1)_S4_63.5 NH	7.4	62.3	9.690				

**Table A- 8: Superpave Gyrotory 100 mm diameter and 63.5 mm height Fracture Energy**

Sample ID	Air Voids (%)	CT Index (Calculation)	Fracture energy (Gf) (J/m <sup>2</sup> )	Average	STD	COV	95 % CI
<b>T2/T2C (1st trial)</b>							
T21(1)_S4_63.5_NH	6.9	119.5	7214.3	<b>5895</b>	<b>945.85</b>	<b>16.0</b>	<b>829.1</b>
T22(1)_S4_63.5_NH	7.7	102.9	5977.8				
T23(1)_S4_63.5_NH	7.5	39.0	4546.4				
T24(1)_S4_63.5_NH	6.7	80.3	5794.0				
T25(1)_S4_63.5_NH	8.0	71.5	5941.3				
<b>T3</b>							
T31(1)_S4_63.5_NH	7.3	51.2	5651.2	<b>5466</b>	<b>219.90</b>	<b>4.0</b>	<b>192.7</b>
T32(1)_S4_63.5_NH	7.3	47.1	5134.5				
T33(1)_S4_63.5_NH	7.5	49.7	5357.7				
T34(1)_S4_63.5_NH	7.2	57.9	5643.1				
T35(1)_S4_63.5_NH	7.4	62.3	5544.5				

**Table A- 9: Superpave Gyrotory 100 mm diameter and 63.5 mm height Tensile Strength**

Sample ID	Air Voids (%)	CT Index (Calculation)	Tensile Strength (kPa)	Average	STD	COV	95% CI
<b>T2/T2C (1st trial)</b>							
T21(1)_S4_63.5 NH	6.9	119.5	992.2	<b>940.9</b>	<b>38.77</b>	<b>4.1</b>	<b>34.0</b>
T22(1)_S4_63.5 NH	7.7	102.9	894.2				
T23(1)_S4_63.5 NH	7.5	39.0	924.2				
T24(1)_S4_63.5 NH	6.7	80.3	967.5				
T25(1)_S4_63.5 NH	8.0	71.5	926.3				
<b>T3</b>							
T31(1)_S4_63.5 NH	7.3	51.2	1046.5	<b>1005.7</b>	<b>36.21</b>	<b>3.6</b>	<b>31.7</b>
T32(1)_S4_63.5 NH	7.3	47.1	966.9				
T33(1)_S4_63.5 NH	7.5	49.7	1003.9				
T34(1)_S4_63.5 NH	7.2	57.9	1037.9				
T35(1)_S4_63.5 NH	7.4	62.3	973.5				

**Table A- 10: Superpave Gyrotory 150 mm diameter and 63.5 mm height CT Index**

Sample ID	Air Voids (%)	CT Index (Machine)	CT Index (Calculation)	Average CT Index (Calculation)	STD CT Index (Calculation)	COV CT Index (Calculation)	95% CI CT Index (Calculation)
<b>T2/T2C</b>							
T21(2)_S 6 63.5	8.3	59.4	63.5	<b>57.8</b>	<b>16.10</b>	<b>27.8</b>	<b>12.9</b>
T22(2)_S 6 63.5	6.3	57.0	55.3				
T23(2)_S 6 63.5	7.4	73.1	72.1				
T24(2)_S 6 63.5	7.7	72.2	71.9				
T25(2)_S 6 63.5	7.9	45.2	43.5				
T2T1(2)_ S6 63.5	7.9	33.9	34.5				
T2T2(2)_ S6 63.5	7.9	69.8	69.6				
<b>T3</b>							
T31(1)_S 6 63.5	7.1	61.1	58.8	<b>63.7</b>	<b>6.02</b>	<b>9.5</b>	<b>5.3</b>
T32(1)_S 6 63.5	7.1	63.6	63.4				
T33(1)_S 6 63.5	7.0	72.2	73.6				
T34(1)_S 6 63.5	7.1	57.8	58.9				
T35(1)_S 6 63.5	7.2	64.3	63.7				

**Table A- 11: Superpave Gyrotory 150 mm diameter and 63.5 mm height m Value**

Sample ID	Air Voids (%)	m value (kN/mm)	Average	STD	COV	95% CI
<b>T2/T2C</b>						
T21(2) S6 63.5	8.3	1.74	<b>2.61</b>	<b>0.64</b>	<b>24.6</b>	<b>0.5</b>
T22(2) S6 63.5	6.3	2.52				
T23(2) S6 63.5	7.4	2.20				
T24(2) S6 63.5	7.7	2.07				
T25(2) S6 63.5	7.9	2.94				
T2T1(2) S6 63.5	7.9	3.75				
T2T2(2) S6 63.5	7.9	2.19				
<b>T3</b>						
T31(1) S6 63.5	7.1	3.05	<b>2.94</b>	<b>0.25</b>	<b>8.6</b>	<b>0.2</b>
T32(1) S6 63.5	7.1	2.99				
T33(1) S6 63.5	7.0	2.58				
T34(1) S6 63.5	7.1	3.26				
T35(1) S6 63.5	7.2	2.83				

**Table A- 12: Superpave Gyrotory 150 mm diameter and 63.5 mm height I Value**

Sample ID	Air Voids (%)	I-value (mm)	Average	STD	COV	95% CI
<b>T2/T2C</b>						
T21(2) S6 63.5	8.3	3.505	<b>3.953</b>	<b>0.31</b>	<b>8.0</b>	<b>0.3</b>
T22(2) S6 63.5	6.3	3.523				
T23(2) S6 63.5	7.4	4.080				
T24(2) S6 63.5	7.7	4.143				
T25(2) S6 63.5	7.9	3.819				
T2T1(2) S6 63.5	7.9	3.755				
T2T2(2) S6 63.5	7.9	4.401				
<b>T3</b>						
T31(1) S6 63.5	7.1	3.966	<b>4.157</b>	<b>0.12</b>	<b>2.8</b>	<b>0.1</b>
T32(1) S6 63.5	7.1	4.133				
T33(1) S6 63.5	7.0	4.249				
T34(1) S6 63.5	7.1	4.228				
T35(1) S6 63.5	7.2	4.208				

**Table A- 13: Superpave Gyrotory 150 mm diameter and 63.5 mm height I/m Value**

Sample ID	Air Voids (%)	I/m value (mm <sup>2</sup> /kN)	Average	STD	COV	95% CI
<b>T2/T2C</b>						
T21(2) S6 63.5	8.3	2.012	<b>1.594</b>	<b>0.42</b>	<b>26.4</b>	<b>0.3</b>
T22(2) S6 63.5	6.3	1.399				
T23(2) S6 63.5	7.4	1.855				
T24(2) S6 63.5	7.7	2.003				
T25(2) S6 63.5	7.9	1.301				
T2T1(2) S6 63.5	7.9	1.000				
T2T2(2) S6 63.5	7.9	2.008				
<b>T3</b>						
T31(1) S6 63.5	7.1	1.302	<b>1.424</b>	<b>0.15</b>	<b>10.4</b>	<b>0.1</b>
T32(1) S6 63.5	7.1	1.381				
T33(1) S6 63.5	7.0	1.649				
T34(1) S6 63.5	7.1	1.299				
T35(1) S6 63.5	7.2	1.488				

**Table A- 14: Superpave Gyrotory 150 mm diameter and 63.5 mm height Peak Load**

Sample ID	Air Voids (%)	Peak load (kN)	Average	STD	COV	95% CI
<b>T2/T2C</b>						
T21(2) S6 63.5	8.3	9.980	<b>10.770</b>	<b>0.73</b>	<b>6.8</b>	<b>0.6</b>
T22(2) S6 63.5	6.3	11.807				
T23(2) S6 63.5	7.4	11.013				
T24(2) S6 63.5	7.7	10.247				
T25(2) S6 63.5	7.9	10.268				
T2T1(2) S6 63.5	7.9	11.345				
T2T2(2) S6 63.5	7.9	9.938				
<b>T3</b>						
T31(1) S6 63.5	7.1	13.271	<b>13.198</b>	<b>0.49</b>	<b>3.7</b>	<b>0.4</b>
T32(1) S6 63.5	7.1	13.603				
T33(1) S6 63.5	7.0	12.871				
T34(1) S6 63.5	7.1	13.698				
T35(1) S6 63.5	7.2	12.549				

**Table A- 15: Superpave Gyrotory 150 mm diameter and 63.5 mm height Fracture Energy**

Sample ID	Air Voids (%)	Fracture energy (Gf)	Average	STD	COV	95% CI
<b>T2/T2C</b>						
T21(2) S6 63.5	8.3	4620.7	<b>5293</b>	<b>364.95</b>	<b>6.9</b>	<b>292.0</b>
T22(2) S6 63.5	6.3	5787.7				
T23(2) S6 63.5	7.4	5690.7				
T24(2) S6 63.5	7.7	5255.5				
T25(2) S6 63.5	7.9	4899.8				
T2T1(2)_S6_63.5	7.9	5049.5				
T2T2(2)_S6_63.5	7.9	5074.5				
<b>T3</b>						
T31(1) S6 63.5	7.1	6614.3	<b>6562</b>	<b>176.67</b>	<b>2.7</b>	<b>154.9</b>
T32(1) S6 63.5	7.1	6730.9				
T33(1) S6 63.5	7.0	6547.1				
T34(1) S6 63.5	7.1	6646.8				
T35(1) S6 63.5	7.2	6268.5				

**Table A- 16: Superpave Gyrotory 150 mm diameter and 63.5 mm height Tensile Strength**

Sample ID	Air Voids (%)	Tensile strength	Average	STD	COV	95% CI
<b>T2/T2C</b>						
T21(2) S6 63.5	8.3	96.7	<b>104.4</b>	<b>7.10</b>	<b>6.8</b>	<b>5.7</b>
T22(2) S6 63.5	6.3	114.5				
T23(2) S6 63.5	7.4	106.8				
T24(2) S6 63.5	7.7	99.3				
T25(2) S6 63.5	7.9	99.5				
T2T1(2) S6 63.5	7.9	110.0				
T2T2(2) S6 63.5	7.9	96.3				
<b>T3</b>						
T31(1) S6 63.5	7.1	128.8	<b>128.0</b>	<b>4.75</b>	<b>3.7</b>	<b>4.2</b>
T32(1) S6 63.5	7.1	132.0				
T33(1) S6 63.5	7.0	124.9				
T34(1) S6 63.5	7.1	132.9				
T35(1) S6 63.5	7.2	121.7				

**Table A- 17: Hveem Compacted 101.6 mm diameter and 63.5 mm height CT Index**

Sample ID	Air Voids (%)	CT Index (Machine)	CT Index (Calculation)	Average CT Index (Calculation)	STD CT Index (Calculation)	COV CT Index (Calculation)	95% CI CT Index (Calculation)
<b>T2/T2C</b>							
T21(1)_HV NH	6.9	127.4	126.1	<b>90.9</b>	<b>24.13</b>	<b>26.6</b>	<b>21.1</b>
T22(1)_HV NH	6.7	84.3	84.3				
T23(1)_HV NH	6.9	81.7	80.3				
T24(1)_HV NH	6.9	104.8	101.4				
T25(1)_HV NH	7.8	67.0	62.2				
<b>T3</b>							
T31(1)_HV NH	7.5	93.7	94.1	<b>94.1</b>	<b>17.32</b>	<b>18.4</b>	<b>15.2</b>
T32(1)_HV NH	6.7	95.9	95.1				
T33(1)_HV NH	7.5	75.6	72.2				
T34(1)_HV NH	7.3	92.1	88.9				
T35(1)_HV NH	7.9	118.1	120.4				

**Table A- 18: Hveem Compacted 101.6 mm diameter and 63.5 mm height m Value**

Sample ID	Air Voids (%)	m value (kN/mm)	Average	STD	COV	95% CI
<b>T2/T2C</b>						
T21(1) HV NH	6.9	1.61	<b>1.86</b>	<b>0.37</b>	<b>20.0</b>	<b>0.3</b>
T22(1) HV NH	6.7	2.41				
T23(1) HV NH	6.9	2.05				
T24(1) HV NH	6.9	1.51				
T25(1) HV NH	7.8	1.69				
<b>T3</b>						
T31(1) HV NH	7.5	2.00	<b>2.33</b>	<b>0.42</b>	<b>18.0</b>	<b>0.4</b>
T32(1) HV NH	6.7	2.43				
T33(1) HV NH	7.5	2.93				
T34(1) HV NH	7.3	2.42				
T35(1) HV NH	7.9	1.87				

**Table A- 19: Hveem Compacted 101.6 mm diameter and 63.5 mm height I Value**

Sample ID	Air Voids (%)	I-value (mm)	Average	STD	COV	95% CI
<b>T2/T2C</b>						
T21(1) HV NH	6.9	3.561	<b>3.374</b>	<b>0.32</b>	<b>9.5</b>	<b>0.3</b>
T22(1) HV NH	6.7	3.728				
T23(1) HV NH	6.9	3.330				
T24(1) HV NH	6.9	3.378				
T25(1) HV NH	7.8	2.872				
<b>T3</b>						
T31(1) HV NH	7.5	3.631	<b>3.774</b>	<b>0.11</b>	<b>2.9</b>	<b>0.1</b>
T32(1) HV NH	6.7	3.886				
T33(1) HV NH	7.5	3.692				
T34(1) HV NH	7.3	3.810				
T35(1) HV NH	7.9	3.854				

**Table A- 20: Hveem Compacted 101.6 mm diameter and 63.5 mm height I/m Value**

Sample ID	Air Voids (%)	I/m value (mm <sup>2</sup> /kN)	Average	STD	COV	95% CI
<b>T2/T2C</b>						
T21(1) HV NH	6.9	2.206	<b>1.860</b>	<b>0.33</b>	<b>17.8</b>	<b>0.3</b>
T22(1) HV NH	6.7	1.544				
T23(1) HV NH	6.9	1.622				
T24(1) HV NH	6.9	2.231				
T25(1) HV NH	7.8	1.699				
<b>T3</b>						
T31(1) HV NH	7.5	1.819	<b>1.663</b>	<b>0.30</b>	<b>17.9</b>	<b>0.3</b>
T32(1) HV NH	6.7	1.602				
T33(1) HV NH	7.5	1.260				
T34(1) HV NH	7.3	1.573				
T35(1) HV NH	7.9	2.061				

**Table A- 21: Hveem Compacted 101.6 mm diameter and 63.5 mm height Peak Load**

Sample ID	Air Voids (%)	Peak load (kN)	Average	STD	COV	95% CI
<b>T2/T2C</b>						
T21(1) HV NH	6.9	8.152	<b>7.916</b>	<b>0.86</b>	<b>10.9</b>	<b>0.8</b>
T22(1) HV NH	6.7	8.661				
T23(1) HV NH	6.9	8.656				
T24(1) HV NH	6.9	7.457				
T25(1) HV NH	7.8	6.653				
<b>T3</b>						
T31(1) HV NH	7.5	7.914	<b>8.513</b>	<b>0.40</b>	<b>4.7</b>	<b>0.4</b>
T32(1) HV NH	6.7	8.986				
T33(1) HV NH	7.5	8.551				
T34(1) HV NH	7.3	8.730				
T35(1) HV NH	7.9	8.386				

**Table A- 22: Hveem Compacted 101.6 mm diameter and 63.5 mm height Fracture Energy**

Sample ID	Air Voids (%)	Fracture energy (Gf)	Average	STD	COV	95% CI
<b>T2/T2C</b>						
T21(1)_HV_N H	6.9	5693.4	<b>4843</b>	<b>818.69</b>	<b>16.9</b>	<b>717.6</b>
T22(1)_HV_N H	6.7	5454.6				
T23(1)_HV_N H	6.9	4901.2				
T24(1)_HV_N H	6.9	4545.1				
T25(1)_HV_N H	7.8	3621.7				
<b>T3</b>						
T31(1)_HV_N H	7.5	5106.2	<b>5606</b>	<b>301.35</b>	<b>5.4</b>	<b>264.1</b>
T32(1)_HV_N H	6.7	5896.2				
T33(1)_HV_N H	7.5	5663.3				
T34(1)_HV_N H	7.3	5598.7				
T35(1)_HV_N H	7.9	5766.9				

**Table A- 23: Hveem Compacted 101.6 mm diameter and 63.5 mm height Tensile Strength**

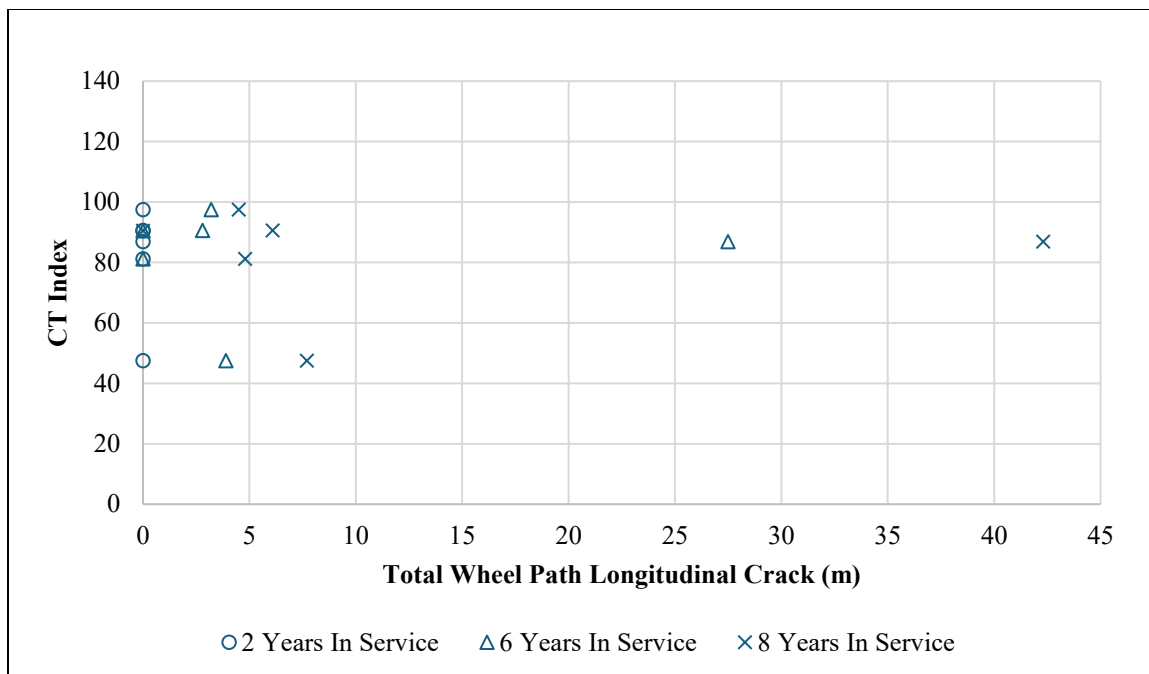
Sample ID	Air Voids (%)	Tensile strength	Average	STD	COV	95% CI
<b>T2/T2C</b>						
T21(1) HV NH	6.9	116.9	<b>113.3</b>	<b>12.48</b>	<b>11.0</b>	<b>10.9</b>
T22(1) HV NH	6.7	124.4				
T23(1) HV NH	6.9	123.3				
T24(1) HV NH	6.9	107.2				
T25(1) HV NH	7.8	94.6				
<b>T3</b>						
T31(1) HV NH	7.5	112.5	<b>121.2</b>	<b>5.99</b>	<b>4.9</b>	<b>5.2</b>
T32(1) HV NH	6.7	128.4				
T33(1) HV NH	7.5	121.8				
T34(1) HV NH	7.3	124.4				
T35(1) HV NH	7.9	119.1				

Table A- 24: Type 2 mix summary results

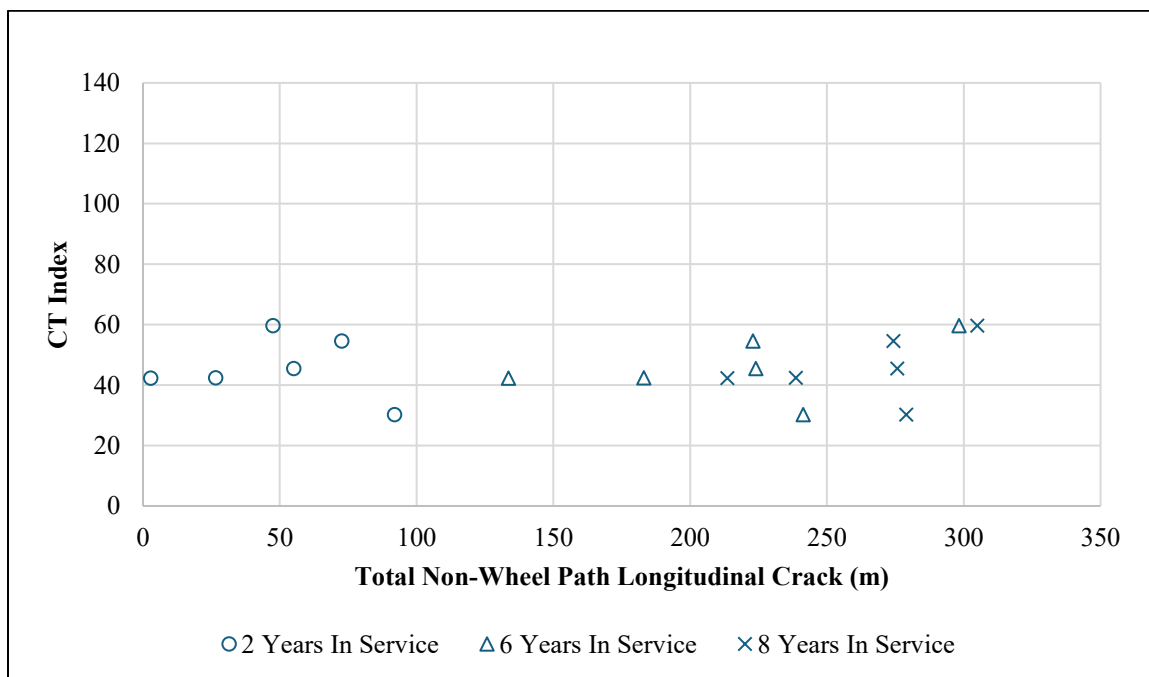
		Type 2				
		150 mm Dia.	100 mm Dia.	101.6 mm Dia.		
		SP(2)[63.5mm]	SP[63.5 mm] NH	HV[63.5m m] NH 4.1	HV[63.5 mm] NH	HV(2)[63.5m m] NH 4.9
CT	Ave rage	57.8	82.6	59.4	90.9	101.7
	95% CI	12.9	27.0	11.7	21.1	16.1
m-Value (kN/mm)	Ave rage	2.61	2.31	2.56	1.86	2.01
	95% CI	0.5	0.4	0.4	0.3	0.2
I-Value (mm)	Ave rage	3.953	2.972	2.841	3.374	3.878
	95% CI	0.3	0.3	0.2	0.3	0.1
I/m Value (mm <sup>2</sup> /kN)	Ave rage	1.594	1.340	1.134	1.860	1.961
	95% CI	0.3	0.3	0.2	0.3	0.2
Peak Load (kN)	Ave rage	10.770	9.361	9.161	7.916	7.433
	95% CI	0.6	0.3	0.7	0.8	0.2
Fracture Energy (Gf) (J/m <sup>2</sup> )	Ave rage	5293	5895	5149	4843	5134
	95% CI	292.0	829.1	493.5	717.6	394.2
Tensile Strength (kPa)	Ave rage	104.4	136.5	131.2	113.3	106.6
	95% CI	39.2	34.0	69.3	10.9	16.5
Air Void (%)	Ave rage	7.5	7.4	6.9	7.0	7.0
	95% CI	0.5	0.5	0.4	0.4	0.3
Air Void (%)	Min	7.4	6.7	6.2	6.7	6.3
	Max	7.9	8.0	7.3	7.8	7.6
	Ave rage	7.5	7.4	6.9	7.0	7.0

Table A- 25: Type 3 mix summary results

	Type 3				
	150 mm Dia.	100 mm Dia.	101.6 mm Dia.		
	SP[63.5 mm]	SP[63.5m m] NH	HV[63.5mm] NH 5.3	HV[63.5m m] NH	HV[63.5mm] NH 6.1
CT	63.7	53.6	67.9	94.1	132.2
	5.3	5.5	9.2	15.2	11.3
m-Value (kN/mm)	2.94	3.10	2.59	2.33	1.88
	0.2	0.2	0.3	0.4	0.1
I-Value (mm)	4.157	2.966	3.339	3.774	4.241
	0.1	0.1	0.2	0.1	0.2
I/m Value (mm <sup>2</sup> /kN)	1.424	0.961	1.310	1.663	2.260
	0.1	0.1	0.2	0.3	0.2
Peak Load (kN)	13.198	10.012	8.774	8.513	7.384
	0.4	0.3	0.4	0.4	0.4
Fracture Energy (Gf) (J/m <sup>2</sup> )	6562	5466	5101	5606	5761
	154.9	192.7	117.7	264.1	355.2
Tensile Strength (kPa)	128.0	145.9	123.9	121.2	112.1
	28.7	31.7	43.8	5.2	43.5
Air Void (%)	7.1	7.3	7.7	7.4	6.6
	0.1	0.1	0.4	0.4	0.5
Air Void (%)	7.0	7.2	7.0	6.7	6.2
	7.2	7.5	8.0	7.9	7.4
	7.1	7.3	7.7	7.4	6.6



**Figure A- 1: Comparison of RPMLC SP with 7% AV CT Index and NWP longitudinal crack through the service year.**



**Figure A- 2: Comparison of RPMLC SP with In-Place AV CT Index and NWP longitudinal crack through the service year**

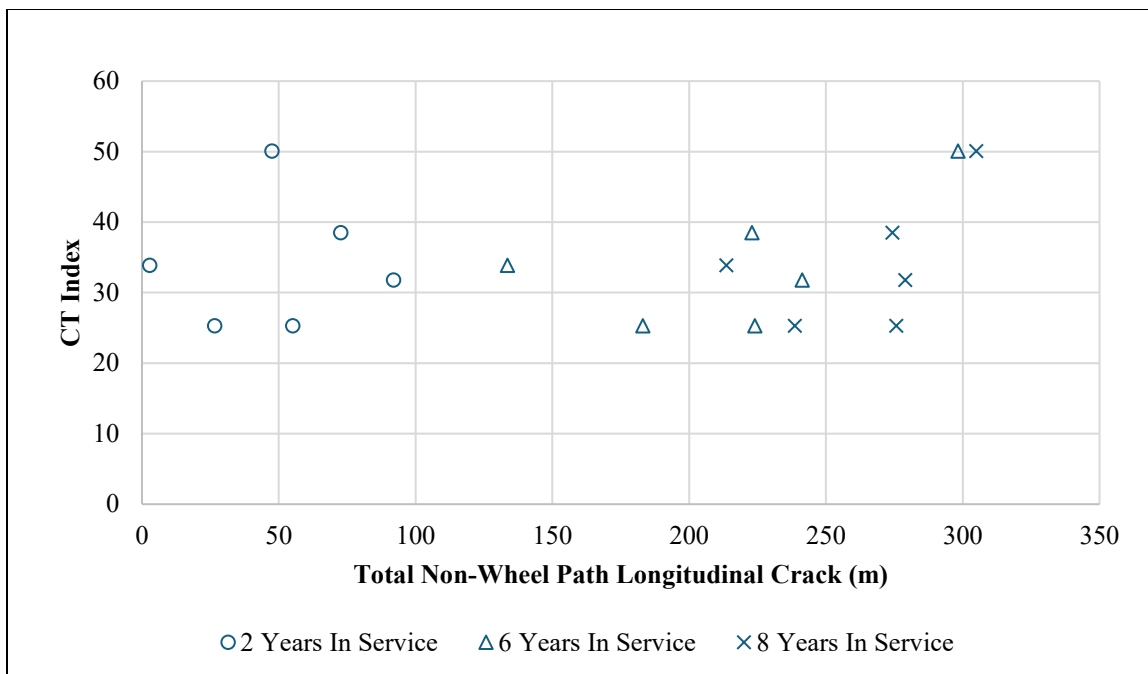


**Figure A- 3: Comparison of PMFC 12-month field core CT Index and NWP longitudinal crack through the service year**

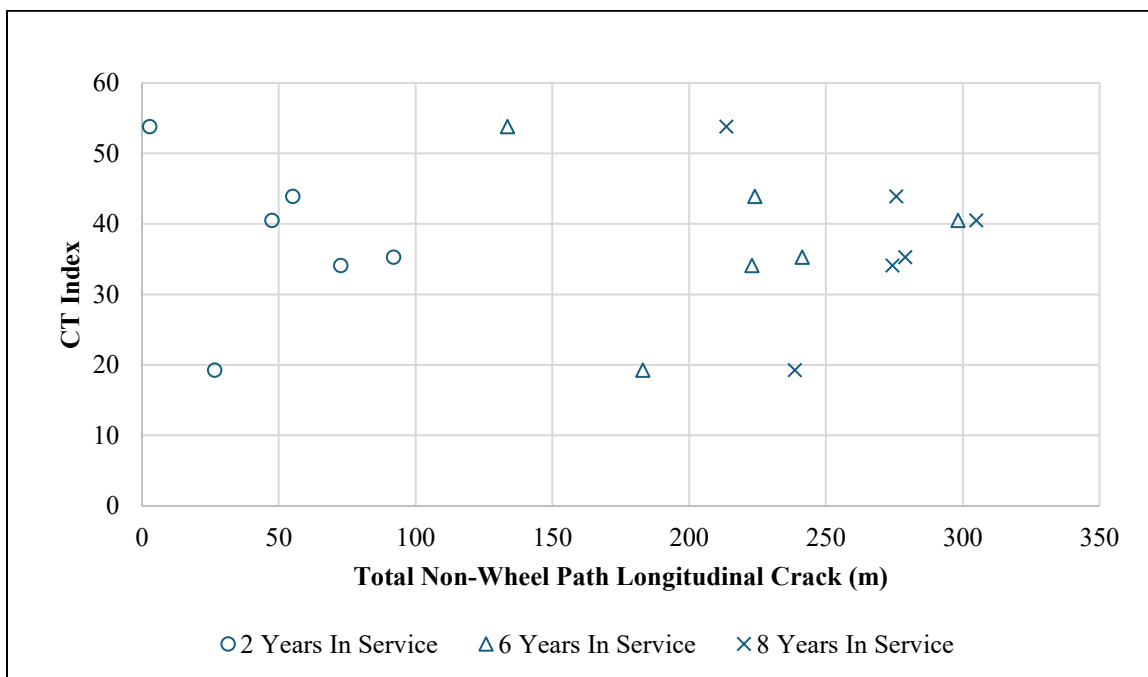


**Figure A- 4: Comparison of PMFC 23-month field core CT Index and NWP longitudinal crack through the service year**

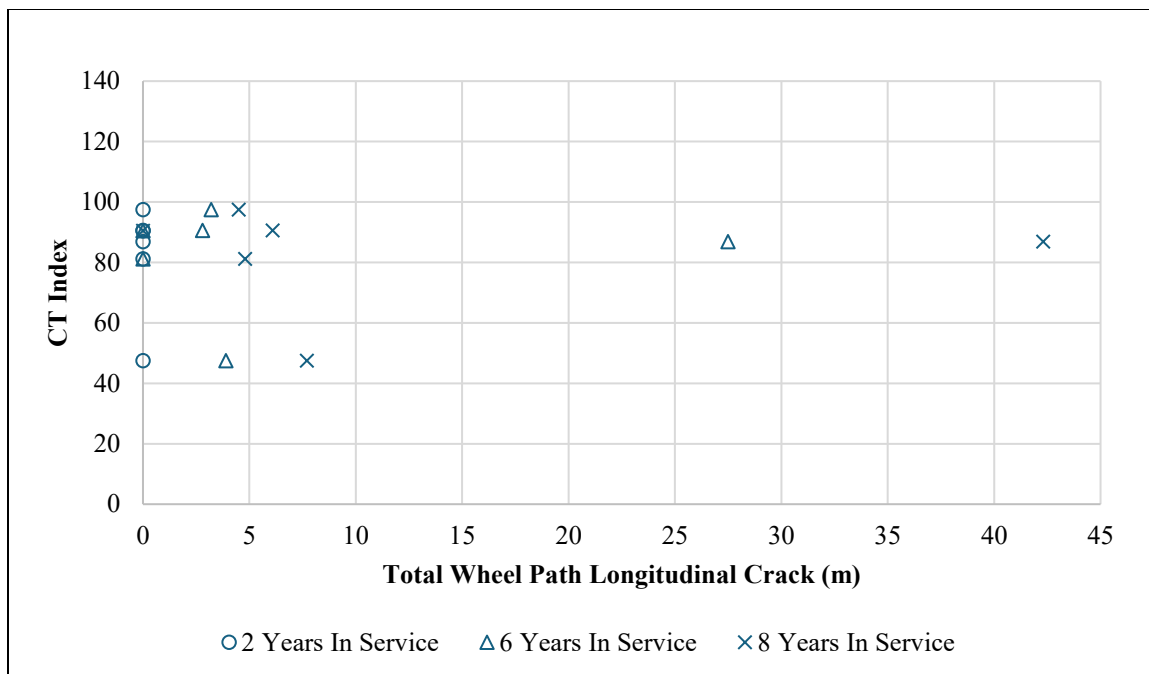


**Figure A- 5: Comparison of RPMLC SP with 7% AV CT Index and Wheel path crack length throughout service years.**

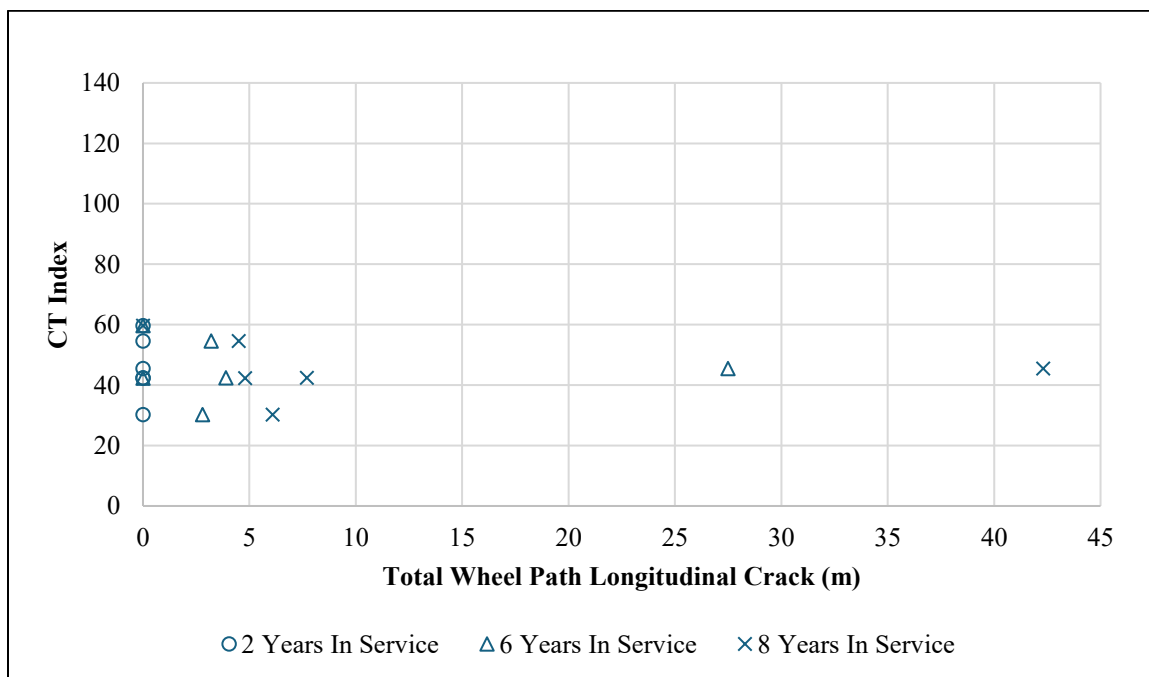


**Figure A- 6: Comparison of RPMLC SP with In-Place AV CT Index and Wheel path crack length throughout service years.**

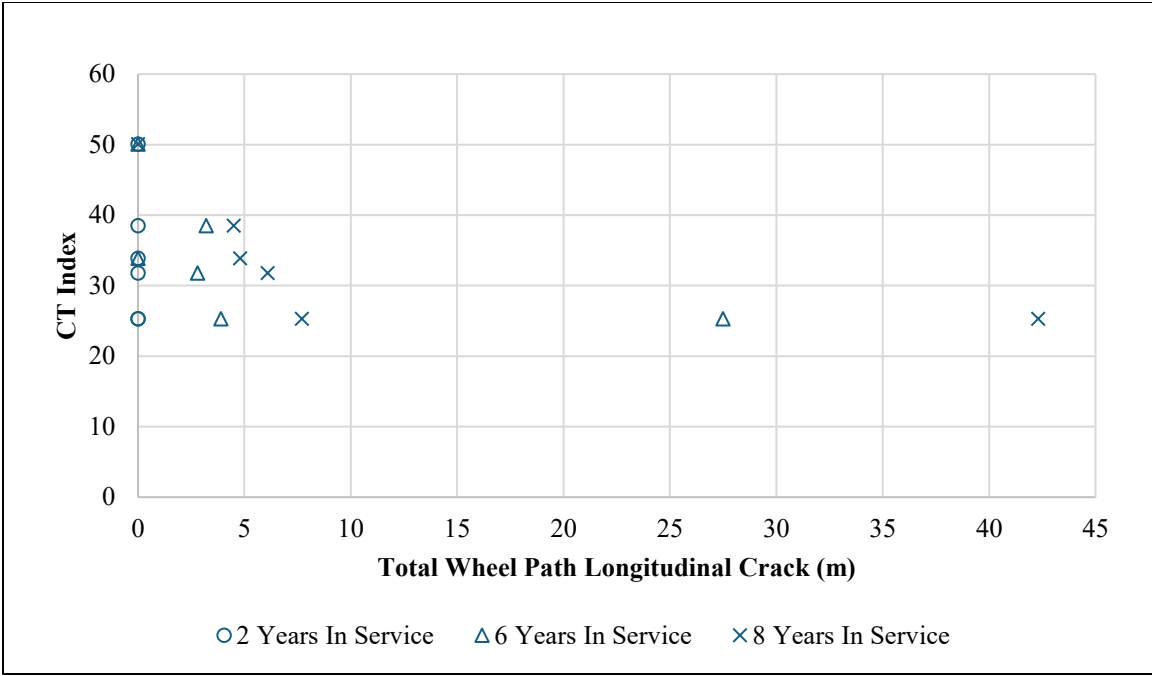


Figure A- 7: Comparison of PMFC 12-month field core CT Index and Wheel path crack length throughout the service year

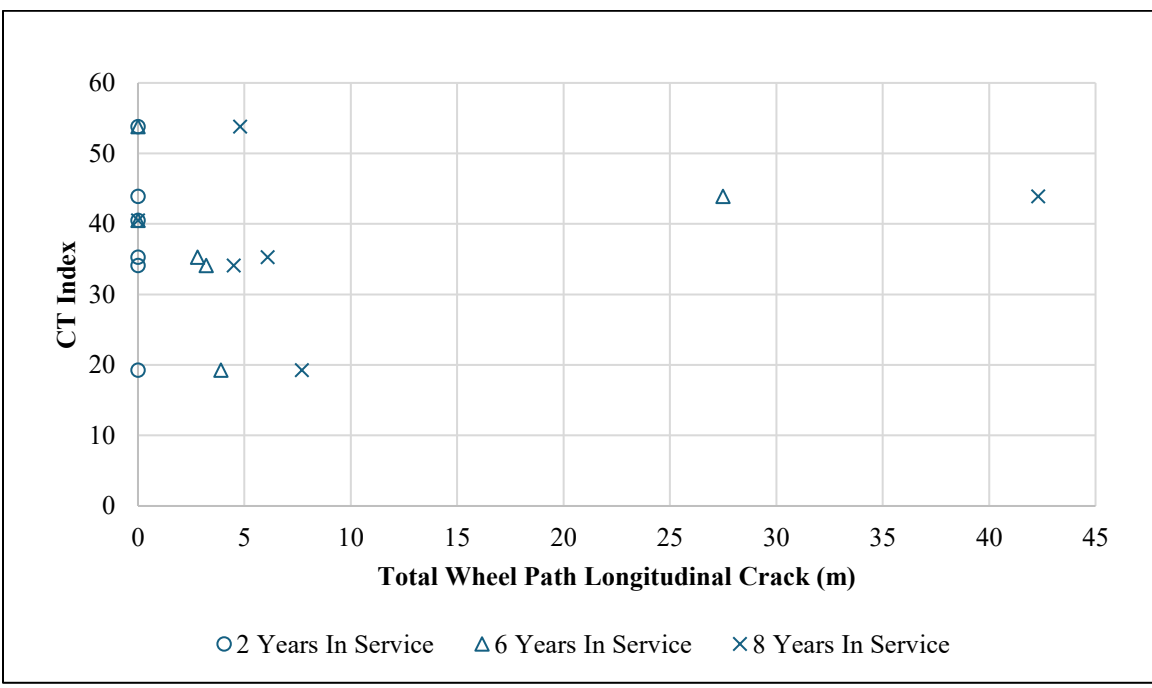
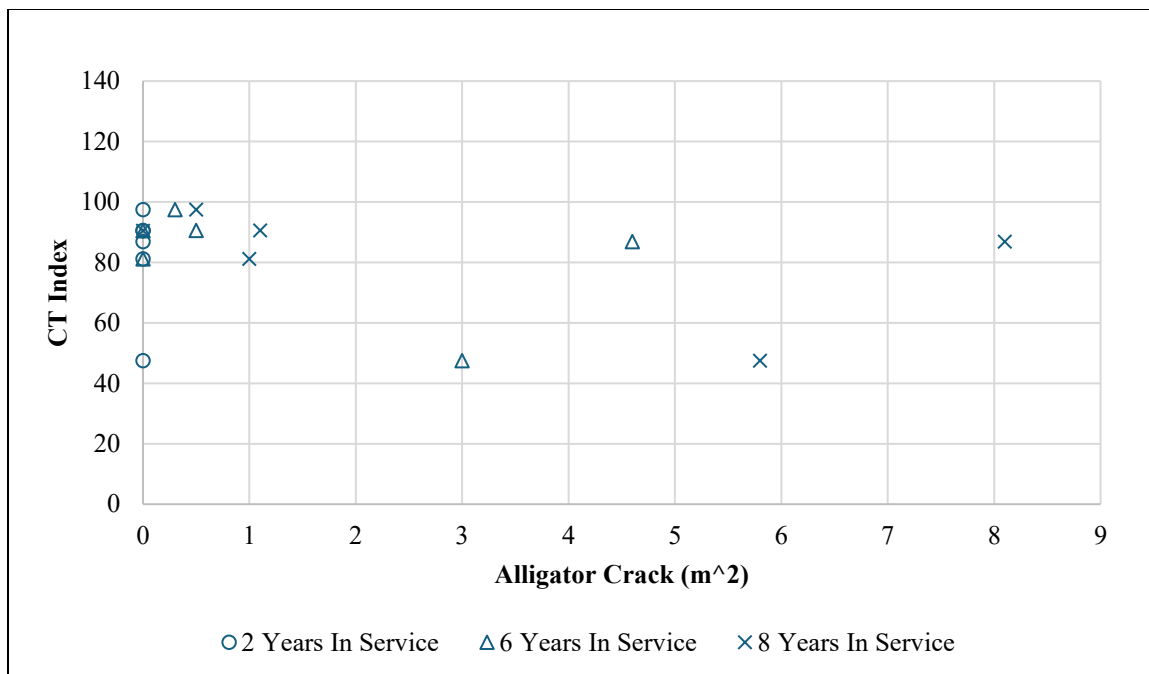
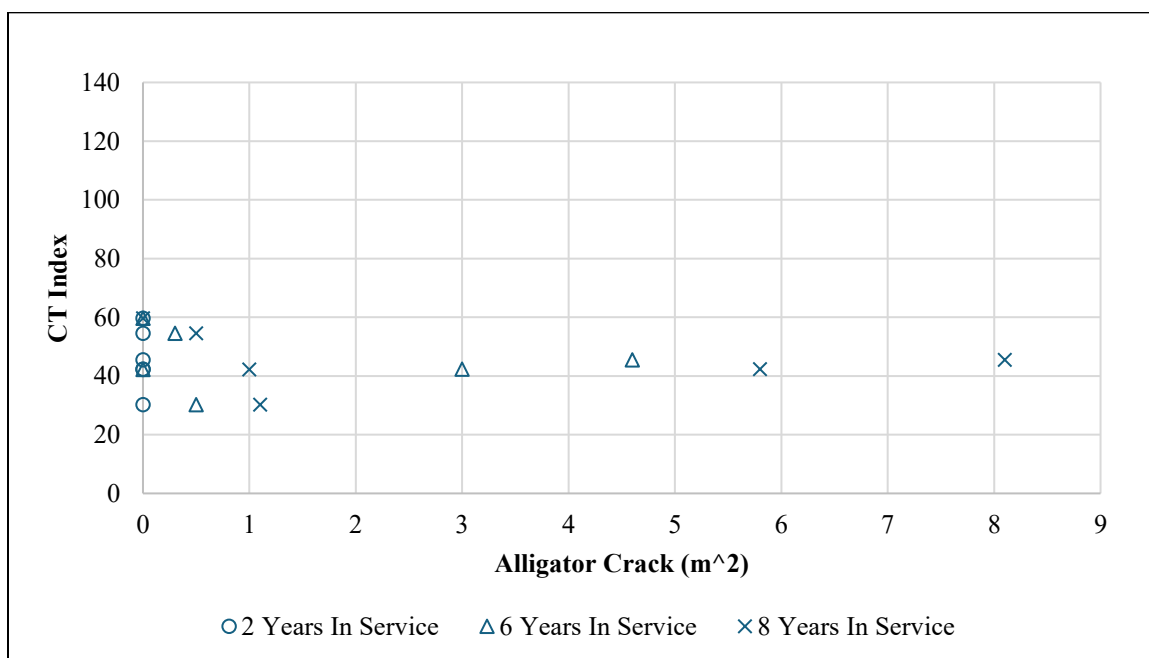


Figure A- 8: Comparison of PMFC 23-month field core CT Index and Wheel path crack length throughout the service year



**Figure A- 9: Comparison of RPMLC SP with 7% AV CT Index and Alligator crack throughout service years.**



**Figure A- 10: Comparison of RPMLC SP with In-Place AV CT Index and Alligator crack throughout service years.**

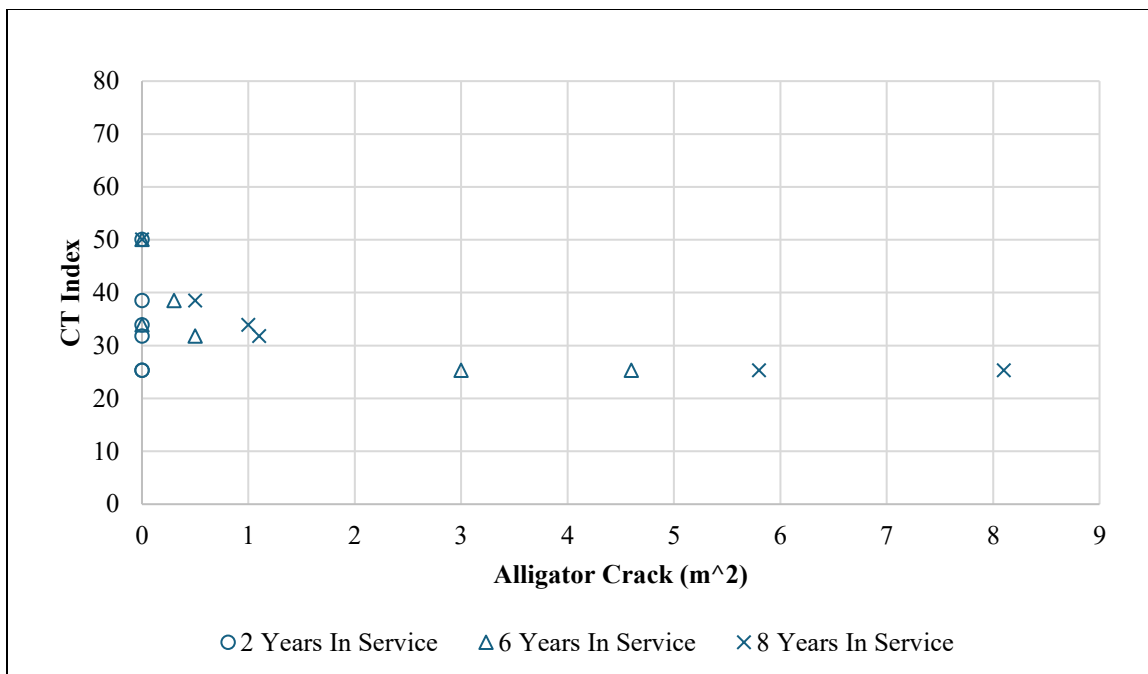


**Figure A- 11: Comparison of PMFC 12-month field core CT Index and Alligator crack throughout the service year**

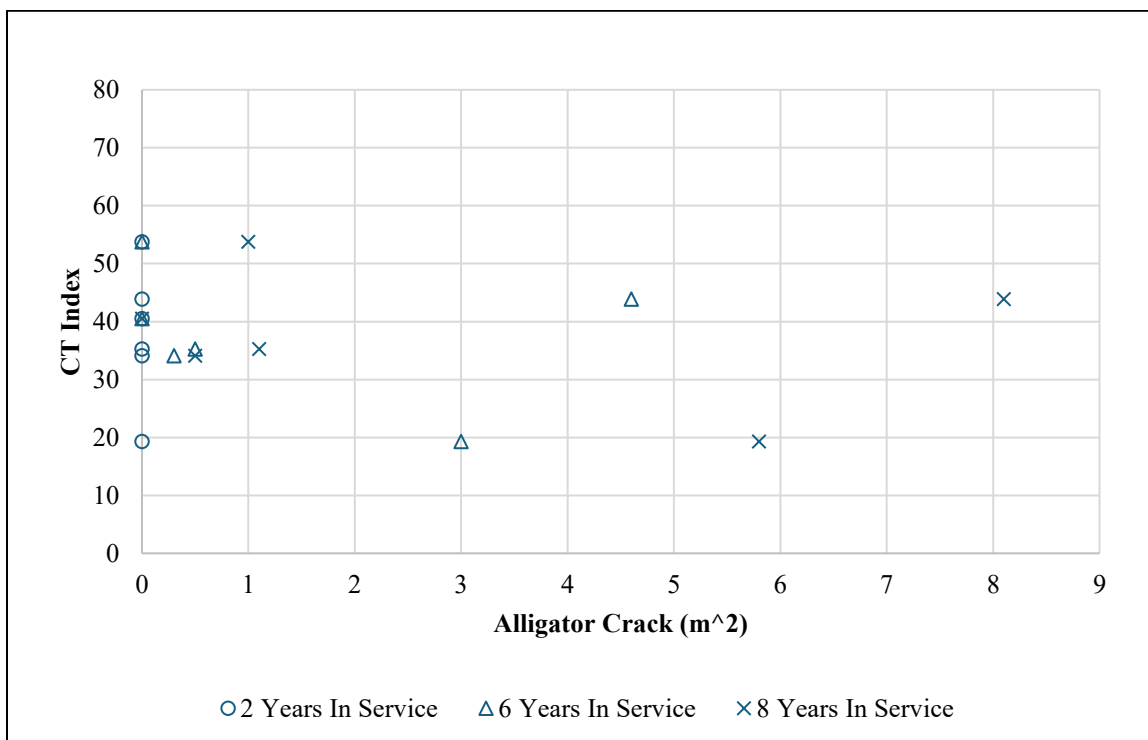


**Figure A- 12: Comparison of PMFC 23-month field core CT Index and Alligator crack throughout the service year**